

On Stripe Correlations in Cuprate Superconductors

O.Y. Osman Ibrahim

09 FEB. 2001

BIBLIOTHEEK
GORLAEUS LABORATORIA

Postbus 9502
2300 RA LEIDEN
Tel.: 071 - 527 43 66 / 67

Universiteit Leiden



1 369 351 5

**On Stripe Correlations
in Cuprate Superconductors**

in *Europe's* *Reproductive*
in *Europe's* *Reproductive*

On Stripe Correlations in Cuprate Superconductors

PROEFSCHRIFT

ter verkrijging van
de graad van Doctor aan de Universiteit Leiden,
op gezag van de Rector Magnificus Dr. W.A. Wagenaar,
hoogleraar in de faculteit der Sociale Wetenschappen,
volgens besluit van het College voor Promoties
te verdedigen op woensdag 4 oktober 2000
te klokke 14.15 uur

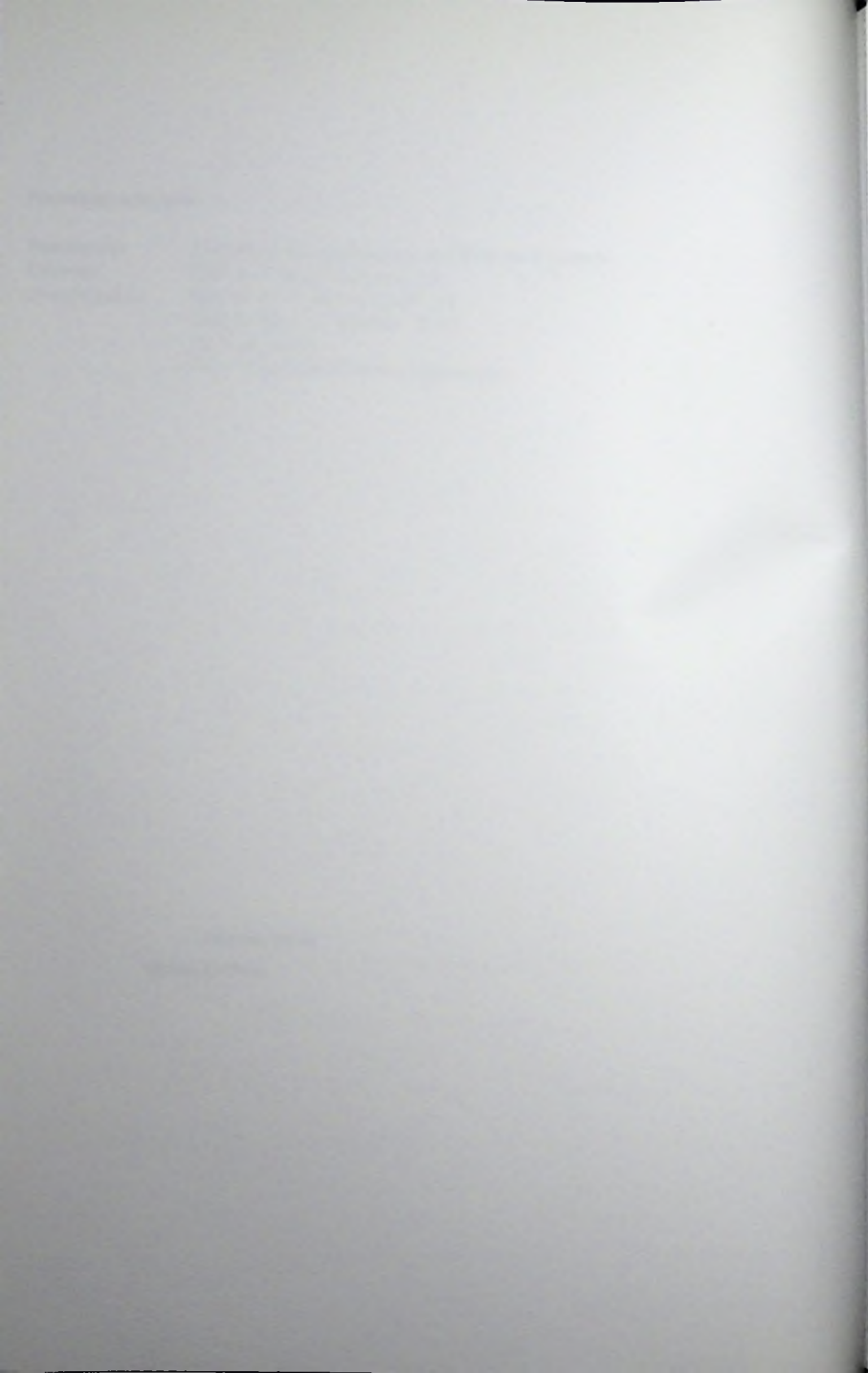
door

Osman Yousif Osman Ibrahim

geboren te Khartoum (SUDAN)
in 1966

Promotiecommissie:

Promotoren: Prof. dr. ir. W. van Saarloos and Prof. dr. J Zaanen
Referent: Prof. dr. J. M. J. van Leeuwen
Overige leden: Prof. dr. G. A. Sawatzky (RUG)
Prof. dr. M. A. J. Michels (TUE)
Dr. H. B. Brom
Dr. J. Tworzydło (Warsaw University)



Contents

1	Introduction	7
1.1	overview	7
1.2	Models for the High T_c cuprates.	9
1.3	Two dimensional quantum antiferromagnets	11
1.4	The Quantum non Linear Sigma Model.	12
1.5	Stripes as generic feature of doped antiferromagnets.	15
1.6	Stripes in High T_c Cuprate superconductors	16
1.7	Organization of the thesis	18
2	Numerical techniques in strongly correlated electron systems	19
2.1	Introduction	19
2.2	Exact diagonalization techniques	19
2.2.1	Lanczos Technique	20
2.3	Quantum Monte-Carlo	21
2.3.1	The Suzuki-Trotter path-integral transformation	23
2.3.2	World-line algorithm	24
2.3.3	The Loop cluster Algorithm	26
3	The single stripe problem	29
3.1	Introduction	29
3.2	Model: The meandering lattice string	32
3.3	Relation to RSOS-like surface models	37
3.4	Spontaneous orientation of the quantum lattice string.	39
3.5	Directedness at low but finite temperature	42
3.6	Directed strings and the spin-1 chain	48
3.7	The phases ($E=0$)	50
3.8	The full phase diagram	54
3.9	Discussion and conclusions	59
3.10	APPENDIX	62

3.10.1	Transfer matrix formalism	62
3.10.2	Global Monte-Carlo moves	65
4	Metallic stripes: Separation of spin, charge and string fluctuations	67
4.1	Introduction	67
4.2	Construction	68
4.3	The Model	72
4.4	Discussion	73
4.5	Conclusion	75
5	Quantum magnetism of the static stripe phase	77
5.1	QNLSM description of the static stripe phase	77
5.2	The coupled spin ladders model	78
5.3	Comparison with renormalization group analysis	84
5.4	Conclusions	85
6	Dynamical stripes in an antiferromagnetic spin background	87
6.1	Introduction	87
6.2	The Quantum string gas	87
6.3	Hidden order in the stripe phase	91
6.4	A Model for dynamical stripes in an antiferromagnetic background	96
6.5	The phase diagram	99
6.6	Discussion of the Phase Diagram	101
	Bibliography	107
	Samenvatting	117
	List of publications	121
	Curriculum Vitae	122
	Acknowledgement	123

1 Introduction

1.1 overview

The experimental discovery of the stripe phase in insulating nickelates and high T_c superconducting cuprates has sparked a new momentum for the race towards understanding the mechanism of high T_c superconductivity. Although the theoretical prediction of this phase was made only few years after the discovery of the high T_c superconducting cuprates, it is only recently that it has been considered for extensive studies. Many groups working in this field believe that the stripe phase will play a central role in our understanding of the mechanism for high T_c superconductivity. Some theories explaining high T_c superconductivity depending on the existence of the stripe phase, have already been put forward [37]. Even those who do not possess this view believe that this stripe phase deserves to be studied extensively, as it competes and, most probably, coexists with the superconducting phase. In this thesis I will address some of the physics of the stripe phase in the cuprate superconductors, the physics of a single stripe and the role both the static and dynamical stripe phase play in the quantum magnetism of these materials.

Superconductivity is the disappearance of electrical resistivity below a critical temperature T_c . Below this temperature the material also acquires special magnetic properties. This phenomenon was first discovered by Kamerlingh-Onnes in the beginning of this century in metallic materials (conventional superconductors). The critical temperature T_c of these materials is usually a few kelvins above the absolute zero. High T_c Superconductivity was discovered in the mid eighties of the last century by Bednorz and Müller. As the name suggests, T_c for the high T_c materials is much higher. Typically one to two orders of magnitude higher than that of the conventional materials, and could reach up to $\simeq 160K$. These temperatures are temptingly high and raises hopes that one day we may be able to manufacture materials that superconduct at room temperature. Consequently a great amount of research was and is being done on the cuprates materials.

The mechanism of superconductivity for the conventional superconductors is essentially the phonon mediated attractive interaction between the quasi particles charge carriers, or electrons in this case. The BCS theory, which describes the superconducting instability of the Fermi liquid in the presence of a small attractive interaction between quasi-particles, proves to be quite successful for the conventional superconductors. The critical temperature depend linearly on the phonons Debye frequency of the material. However for the high T_c superconductors the BCS theory is inapplicable and fails to explain the physics of these materials specifically the large critical superconducting temperature. In fact the normal state of these materials is itself quite anomalous. A strong case can be made that the behavior of some physical properties, like the resistivity, shows that an approach based on the existence of quasi-particles is inapplicable[1]. This rules out any approach based on

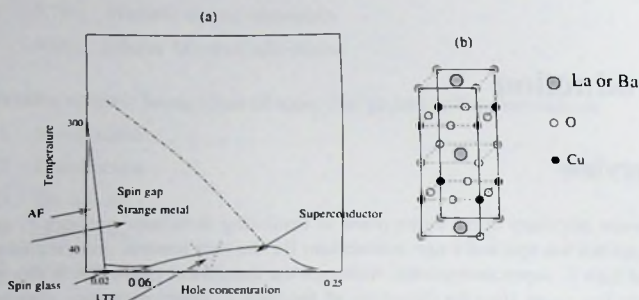


Figure 1-1. (a) Typical phase diagram of High- T_c superconductor. (b) Crystal structure of $\text{La}_{2-x}\text{Ba}_x\text{CuO}_4$.

Landau-Fermi liquid theory. Furthermore it can actually be argued that in this case strong interactions play a central role. In addition, since these materials are layered with a quasi two-dimensional structure and have a low density of charge carriers, fluctuations play a much more important role. This rules out the BCS theory as a possible explanation for the high T_c superconductivity.

The cuprates are a group of ceramic compounds having in common stacks of CuO_2 planes. The other elements forming these materials are mainly rare-earth elements. These elements together with oxygen and sometimes copper atoms occupy the interstitial regions between the planes. A typical example of a high T_c compound, and the first to be discovered, is the "214" La_2CuO_4 material. In figure 1-1 (b) we depict the chemical structure of this compound. The CuO_2 planes have a square lattice structure, where the Cu atoms occupy the sites of the lattice. Band structure calculations showed that the states close to the Fermi surface are related to the CuO_2 planes[6]. This fact suggests a quasi two-dimensional description of the material. In fact the couplings in the CuO_2 planes are much larger than those between the planes.

The $\text{La}_{2-x}\text{Sr}_x\text{CuO}_4$ material is an insulator with a rather large band gap ($\approx 2\text{eV}$). Superconductivity arises upon replacing some of the trivalent La atoms by atoms of divalent elements such as Ba or Sr. This amounts to doping the material with holes and one gets the doped compound $\text{La}_{2-x}\text{Sr}_x\text{CuO}_4$. The undoped material has a half-filled Cu-band, equivalent to one electron per Cu-site in the planes. From the band structure one would expect a metallic behavior. However, due to the strong interactions between the electrons inside the planes a charge gap opens at the Fermi surface and the material is insulator. Such interaction-induced insulators are known as Mott insulators.

In figure 1-1 (a) we show the phase diagram of this $\text{La}_{2-x}\text{Sr}_x\text{CuO}_4$ material as a function of doping x and temperature T . This phase diagram is quite general for all the cuprate high T_c materials. At zero-doping the material is an antiferromagnetically ordered insulator with a rather large Néel temperature. Upon doping the magnetic order disappears rapidly

and at low temperatures the material enters a region with properties associated with spin-glass behavior. A spin-gap or pseudo-gap has also been observed in this region and at a high temperature $T^*(x)$ (depending on the doping) this gap disappears. At a higher doping ($x \approx 0.06$) the material enters the superconducting phase. The critical temperature is maximum at the so called optimal doping ($x \approx 0.15 - 0.2$). At dopings higher than this the superconducting region is called overdoped. The underdoped region lies between the onset of superconductivity and the optimal doping. Due to doping, the region with a pseudo-gap have a nonzero conductivity, however the physics of this region is quite different than normal metals which are well described by the Fermi liquid theory. Experiment suggests that this pseudo-gap and the superconducting gap originate from the same physics, both gaps have a d-wave symmetry and evolve continuously into each other[2]

An anomalous suppression of superconductivity occurs at a range of dopings around $x = \frac{1}{8}$ where the material turns into insulator. This occurs when partially substituting a rare earth element like Neodymium (Nd) or Europium (Eu) for La. A structural transition also takes place, where the crystal structure is changed from the Low Temperature Orthogonal (LTO) phase to the Low Temperature tetragonal (LTT) one and a buckling in the CuO_2 planes occurs. The suppression of superconductivity is due to the stabilization of the static stripes phase, where the stripes get pinned by the LTT structural change.

The stripe phase is a novel collective phase whose basic ingredient is a many-particle bound state: a charge domain wall where the charges (holes) bind together and form anti-phase charged magnetic domain walls in the 2-dimensional antiferromagnetic spin background. Microscopically these domain walls, in two dimensions, consist of holes bound in a linear string-like fashion, separating antiferromagnetically ordered regions. Across a domain wall the antiferromagnetically ordered spins point in opposite directions. Figure 1-2 is a cartoon picture of an ordered stripe phase.

The stripes need not be static. In fact inelastic neutron scattering data revealed that strong dynamical stripe correlations persist in the metallic and superconducting phase for a number of High T_c cuprate materials[25, 26, 27, 28, 30]. The doping $x = \frac{1}{8}$ is not singular, but in fact static stripes can be stabilized by the LTT buckling along all dopings up to the end of the superconducting concentration[27, 28].

This thesis is entirely devoted to the study of aspects of this stripe phase. In the following sections of this introductory chapter I will review first the physics of the antiferromagnets, then show that stripes are a generic feature of doped antiferromagnets. The experimental status of the stripe phase in the High T_c cuprates will be discussed in the last section.

1.2 Models for the High T_c cuprates.

The Model that is believed to capture the physics of the CuO_2 planes is the single band Hubbard model. This is one of the simplest models designed to reach beyond the independent electron approximation and it was designed to study the effects of electron correlations

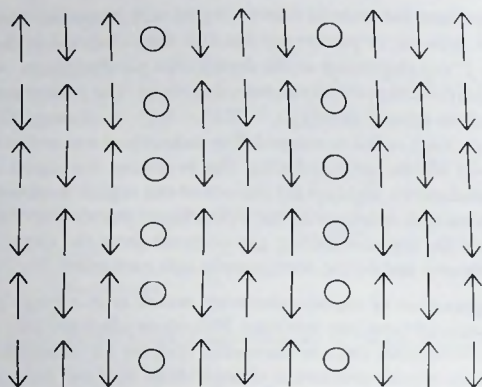


Figure 1-2. An ordered stripe state.

in such narrow-band systems and Mott insulators. Although the Hubbard model in two dimensions is easily written down, however despite a long lasting immense effort nobody has succeeded to arrive at a general solution for this problem. The Hamiltonian of the Model reads;

$$\mathcal{H} = t \sum_{\langle i,j \rangle} \sum_{\sigma=\uparrow\downarrow} (c_{i\sigma}^\dagger c_{j\sigma} + c_{j\sigma}^\dagger c_{i\sigma}) + U \sum_i n_{i\uparrow} n_{i\downarrow} - \mu \sum_i (n_{i\uparrow} + n_{i\downarrow}), \quad (1.2.1)$$

where the summation $\sum_{\langle i,j \rangle}$ runs over all nearest neighbor sites i, j of a square lattice. The fermion-operators $c_{i\sigma}^\dagger$ create an electron with spin σ at the Cu-site i . They satisfy the anticommutation relations

$$\begin{aligned} \{c_{i\sigma}, c_{j\tau}^\dagger\} &= \delta_{ij} \delta_{\sigma\tau}, \\ \{c_{i\sigma}, c_{j\tau}\} &= 0. \end{aligned} \quad (1.2.2)$$

The number operator $n_{i\sigma} = c_{i\sigma}^\dagger c_{i\sigma}$ measures the number of electrons in site i with spin σ . The first term in H describe the kinetic energy due to the overlap of electron orbitals of the Cu-atoms (bandwidth). The second term is an on-site Coulomb interaction: a doubly occupied site costs an energy U .

At half filling and for large U ($U \gg t$) doubly occupied sites are expensive. Therefore, in the ground state every site is singly occupied and the electrons are localized on the lattice sites. The kinetic term gives rise to virtual excitations, where doubly occupied sites are present with an energy cost U . A gap of order U towards charge excitations will open up

and the system becomes an insulator of the Mott-Hubbard kind. This leaves the spins of the localized electrons as the only low-energy degrees of the system. The effective Hamiltonian of the remaining spin system is the antiferromagnetic Heisenberg Model

$$\mathcal{H} = J \sum_{\langle i, j \rangle} \vec{S}_i \cdot \vec{S}_j. \quad (1.2.3)$$

The superexchange integral J is related to the parameters of the Hubbard model by $J = 4t^2/U$. A constant term is left out. The spin operators \vec{S} read

$$S^\alpha = \frac{1}{2}(c_\uparrow^\dagger, c_\downarrow^\dagger) \sigma_\alpha \begin{pmatrix} c_\uparrow \\ c_\downarrow \end{pmatrix}, \quad (1.2.4)$$

where σ_α is a Pauli spin-matrix.

$$\sigma_x = \begin{pmatrix} 0 & 1 \\ 1 & 0 \end{pmatrix}; \quad \sigma_y = \begin{pmatrix} 0 & -i \\ i & 0 \end{pmatrix}; \quad \sigma_z = \begin{pmatrix} 1 & 0 \\ 0 & -1 \end{pmatrix}. \quad (1.2.5)$$

Away from half filling, electrons can move without causing doubly occupied sites. The Hubbard model in this case transforms into the much studied $t - J$ model, with a Hamiltonian given by;

$$\begin{aligned} \mathcal{H}_{t-J} = & t \sum_{\langle i, j \rangle} \sum_{\sigma=\pm\frac{1}{2}} \left((1 - n_{i, -\sigma}) c_{i, \sigma}^\dagger c_{j, \sigma} + (1 - n_{j, -\sigma}) c_{j, \sigma}^\dagger c_{i, \sigma} \right) \\ & + J \sum_{\langle i, j \rangle} \vec{S}_i \cdot \vec{S}_j. \end{aligned} \quad (1.2.6)$$

The operator $(1 - n_{i, -\sigma})$ in the first term projects out doubly occupied sites. The exact derivation of this Hamiltonian from the Hubbard model in the limit of large U gives rise to an additional term which is a combination of a spin-spin interaction and a hopping process. This term is usually neglected.

1.3 Two dimensional quantum antiferromagnets

As mentioned above, undoped cuprates are antiferromagnetic insulators at half-filling. The physics of the antiferromagnets are precisely, captured by the spin- $\frac{1}{2}$ antiferromagnetic Heisenberg model. This model, therefore, describes the spin degrees of freedom of the undoped cuprates. This model has been extensively studied. Although the model lacks an exact solution, a solid and strongly agreed-on picture emerges from a number of techniques. Analytical theories such as the spin wave theory, Schwinger boson mean-field theory and renormalization-group calculation as well as numerical techniques such as Quantum Monte-Carlo and exact diagonalization.

On the (bipartite), square lattice and at zero temperature, the above Heisenberg model shows long range order, Néel order. This means that the ground state of the system is ordered and the order parameter is the staggered magnetization given by

$$\vec{M} = \frac{1}{N} \sum_{\vec{r}} \vec{m}_{\vec{r}} = \frac{1}{N} \sum_{\vec{r}} (-1)^{x+y} \langle \vec{S}_{\vec{r}} \rangle, \quad (1.3.1)$$

where $\vec{m}_{\vec{r}} = (-1)^{x+y} \langle \vec{S}_{\vec{r}} \rangle$ is the local staggered spin magnetization. The Heisenberg model is rotationally invariant. This means that the Hamiltonian of the model is invariant under global rotation of all spin-vectors. The Néel state break this rotation invariance. This is a manifestation of spontaneous symmetry breaking, which is a specific feature of systems with an infinite number of degrees of freedom and which possess a continuous global symmetry. The local order parameter is smaller than the absolute value of the spin ($\frac{1}{2}$). This reduction is due to the presence of quantum fluctuations on the ground state, which are, however, not severe enough to destroy the order.

The direction of the order parameter is not specified and can be freely chosen. This freedom of rotation of the order parameter gives rise to low-energy collective modes known as the Goldstone modes. In the present case they are the wave-like spatial modulation of the local order parameter $\vec{m}_{\vec{r}}$, or spin-waves. Goldstone modes are generic features of systems exhibiting spontaneous breaking of a global continuous symmetry. The low-energy physics of the ordered state is completely dominated by these Goldstone modes.

At non-zero temperatures the long range order of the system will be eventually destroyed by thermal fluctuations. A theorem due to Mermin and Wagner[3] states that at any finite temperature in the case of 1 and 2 dimensions, the Goldstone modes destroy completely the order of the symmetry-broken state. It is therefore not possible to have spontaneous breaking of a continuous symmetry in a model with short-range interactions at non-zero temperatures in 1 and 2 dimensions. This theorem implies that the two dimensional Heisenberg model can not explain the existence of a finite Néel ordering temperature in the undoped cuprates. That it nevertheless happens is due to small magnetic couplings between the CuO_2 planes[4]. The existence of such additional interactions give rise to 3-dimensionality of the system, or they break the $SU(2)$ -invariance of the Hamiltonian. These contributions are however small and can be included in a mean field way after a more accurate treatment of the two dimensional problem[90]. The low temperature properties of the quantum Heisenberg model are well described by the Quantum Non Linear Sigma Model (QNLSM) which will be discussed in the next section.

1.4 The Quantum non Linear Sigma Model.

The Quantum Non Linear Sigma Model (QNLSM) is an effective continuum field theory describing the low-energy, long wavelength physics of the quantum Heisenberg antiferromagnets, as introduced in the above section.

Motivated by the success of the classical non linear sigma model (CNLSM) in describing the long wavelength physics of the classical Heisenberg spin lattice models, Chakravarty, Halperin and Nelson introduced in 1988 the QNLMS as a generalization of the classical version[7].

To derive the QNLMS one assumes that there is at least short-range Néel order. The order parameter \vec{n} introduced in Eq.(1.3.1) represents the local spatial average of the staggered magnetization. There are now longitudinal and transversal fluctuation of this order parameter. The longitudinal fluctuations will be integrated out and the result is an effective action for the long-wavelength transversal degrees of freedom of the order parameter. By taking the continuum limit one arrives at the QNLMS. In essence the model describes interacting spin-waves.

The standard derivation of the QNLMS employs the path-integral formulation of the problem[8]. At finite temperature the equilibrium properties of a system are determined by the partition function

$$\mathcal{Z} = \text{Tr} e^{-\beta H} \quad (1.4.1)$$

where $\beta = \frac{1}{k_B T}$, k_B is the Boltzmann constant and T is the temperature. In the path-integral one splits β in many infinitesimal intervals $\tau = \frac{\beta}{n}$ and writes the above finite-temperature partition function as an infinite product over the infinitesimal imaginary time slices τ . This will map the problem to an equivalent classical statistical mechanical in a space of one dimensional extra as compared to the original quantum problem. At non-zero temperature this extra dimension will be finite with an extent $\sim \hbar\beta$.

Using this formulation and taking the continuum limit, the partition function of the QNLMS is given by,

$$\mathcal{Z} = \int D\vec{n} \prod_i \delta(\vec{n}_i^2 - 1) e^{-S/\hbar}, \quad (1.4.2)$$

with the action

$$S = \frac{1}{2} \int_0^{\hbar\beta} d\tau \int dx dy \left[\chi_{\perp}^0 \left(\frac{\partial \vec{n}}{\partial \tau} \right)^2 + \rho_s^0 (\nabla \vec{n})^2 \right], \quad (1.4.3)$$

while periodic boundary conditions in the spatial and the imaginary time direction should be imposed. The δ -function in the integration measure is needed in order to fix the length of \vec{n}_i , which does not change due to transversal fluctuations. This constraint introduces non-linearity into the model. ρ_s^0 and χ_{\perp}^0 are the bare spin-stiffness and uniform perpendicular susceptibility. They are related to the parameters of the Heisenberg model, in the large S limit and for two dimensions, by [5]

$$\rho_s^0 = JS^2 \quad ; \quad \chi_{\perp}^0 = \frac{a^{-2}}{8J}, \quad (1.4.4)$$

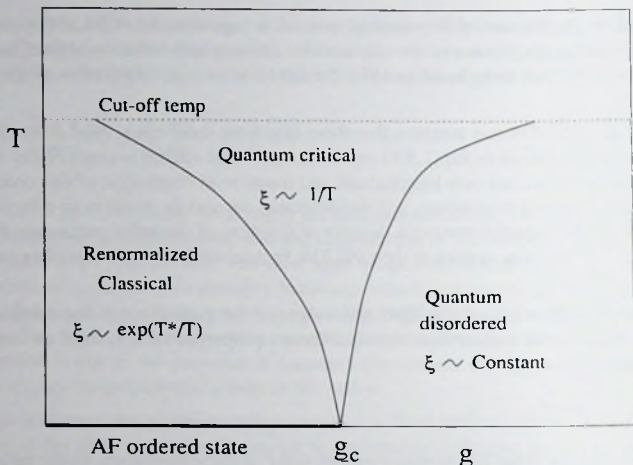


Figure 1-3. cross-over diagram of the 2D quantum non-linear sigma model

where a is the lattice spacing. These parameters are the ones defined at the lattice scale. The spin-stiffness and susceptibility measured experimentally, e.g. by neutron scattering, are related to the renormalized parameters.

The QNLMS can be written in a Lorentz invariant form. In this case the number of parameters is reduced to only one parameter: the dimensionless coupling constant[8], usually called g . It is related to the spin-stiffness and perpendicular susceptibility by

$$g_0 = \frac{1}{\sqrt{\chi_{\perp} \rho_s}} \quad (1.4.5)$$

In the large S limit the bare coupling constant g_0 is given by

$$g_0 = \frac{2\sqrt{2}}{S}. \quad (1.4.6)$$

This coupling constant controls the amount of quantum fluctuations in the system. Note the larger the spin S the smaller is g_0 and that g_0 vanishes in the classical limit $S \rightarrow \infty$.

In figure 1-3 we show the cross-over phase diagram of the 2D QNLMS as a function of the coupling constant g and temperature. There are three distinct regions with qualitatively different behavior. At zero temperature and for small g the system possesses long range order and the correlation length is infinitely large. At a finite critical value $g = g_c$ the system undergoes a quantum phase transition to a quantum disordered state characterized

by a finite correlation length and a spin gap. Upon increasing the temperature from zero, the three depicted regimes evolve naturally from the $T = 0$ states. The region above the ordered state is coined renormalized classical. Here the system does not possess long range order because of the finite temperature. However, exponentially large patches of correlated spins exist. The correlation length is therefore exponentially long and depends on the temperature as: $\xi \sim \exp(T^*/T)$. Since g is small in this region, quantum fluctuations are not too important. It is then possible to integrate out the imaginary time dependence and obtain an effective 2D classical model with renormalized parameters. This is the reason for calling this region renormalized classical.

The quantum disordered region is the region above the quantum disordered state as characterized by finite correlation length at $T = 0$. As the $T = 0$ state is gapped, the correlation length in this region is only weakly dependent on the temperature.

The most interesting region is the region evolving from the quantum critical point, g_c , where the quantum phase transition takes place at $T = 0$. Here the only relevant scale is the temperature and there is no other energy scale. The correlation length is given by $\xi \sim 1/T$. This leads to a highly universal behavior. At some high cut-off temperature the correlation length becomes of the order of the lattice constant. Above this temperature a continuum description is not valid. The physics is governed by the non-universal microscopy at the lattice constant scale and the QNLSM does not apply.

1.5 Stripes as generic feature of doped antiferromagnets.

The doped cuprates can be considered as a 2D doped quantum antiferromagnets. As said before, the $t - J$ model and the Hubbard model at large U and filling of less than half, are the ideal model for studying doped antiferromagnets. A huge amount of research was and is devoted to the understanding of the physics of these models. Recently, theoretical and numerical work suggest that both in the $t - J$ and Hubbard model there is a novel collective phase where the charges (holes) condense and collectively order in a stripe like structure and the spins occupy the region between the stripes. Across the stripe the antiferromagnetic order parameter points in opposite directions. This phase is the stripe phase seen experimentally in the High T_c cuprates and the nickelates.

To see why such a structure might occur, consider for simplicity the $t - J_z$ model, where the exchange term in the spin-spin interaction is neglected. The ground state of the model when undoped is obviously a Néel ordered antiferromagnet (it is the Ising model). Now let us dope this state with one hole. If the hole moves away from its initial position, it will create a line of oppositely ordered spins. This will cost energy which will be proportional to the distance between the initial position of the hole and its new position. This linear potential will pull the hole back and confine it near its initial position[13] (Fig. 1-4). Upon doping with another hole, the two holes will prefer to sit on nearest neighbor sites as this will minimize the number of broken bonds. In a stripe structure as in figure (1-2), the number of broken bonds is minimum, furthermore the holes can lower their kinetic energy by a

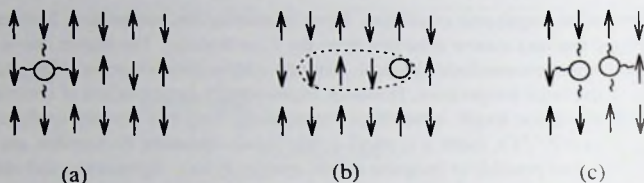


Figure 1-4. Example of a hole moving in antiferromagnetic background. A linear potential (b) is developed as the hole moves away from its initial position (a). At the hole position the superexchange energy is lost by a factor of 4 (a) while the loss is reduced as the holes comes nearest neighbor (c).

collective motion of the whole stripe or along the stripe without costing exchange energy. This suggest that both static and dynamical stripes phases are stable phases of the doped antiferromagnet. In the calculations for the Hubbard or $t - J$ models the situation is not as simple as in the above picture, however the final conclusion still survive. Prelovsek and coworkers have shown that in the full $t - J$ model the holes have a strong tendency to condense in a connected trajectories corresponding with dynamically fluctuating stripes[38]. In the Hubbard model, Zaanen and Gunnarson[9] in 1989, have shown that the static stripes phase is the semiclassical (Hartree-Fock) solution of the model. Here, the density of holes forming the stripe is more spread, that is to say, although the stripe might be centered along one line however its width is not one lattice constant. The density of holes inside the stripe is found to be one hole per stripe unit length. This conclusion has afterwards been confirmed by different groups[10].

The sophisticated density matrix renormalization group (DMRG) calculation, carried out by White and Scalapino[40], have shown that stripe are low energy stable solutions of the $t - J$ model at the superconducting dopings. Around $x = \frac{1}{8}$ the stripes are bond centered. This means they occupy two neighboring lines. The density of holes inside the stripe is not one hole per stripe unit length but could be half a hole per unit length.

Other sophisticated analytical treatments showed that the stripe might have a rich structure inside them[10]. Some other groups believe that the Hubbard model or the $t - J$ model can not account alone for the presence of the stripes and one may need to include a long range Coulomb interaction to stabilize the stripes[37]. However the Coulomb interaction as well as the electron-phonon interaction are shown to favour the formation of stripes[10].

1.6 Stripes in High T_c Cuprate superconductors

The momentum-space structure of the stripe phase and its doping dependence can be probed by the neutron scattering technique. The Néel state at half filling gives rise to magnetic Bragg peaks centered at (π, π) in the Brillion zone. In an ordered charged domain-wall array as in figure 1-2, the staggered order parameter has in addition a long wave-length

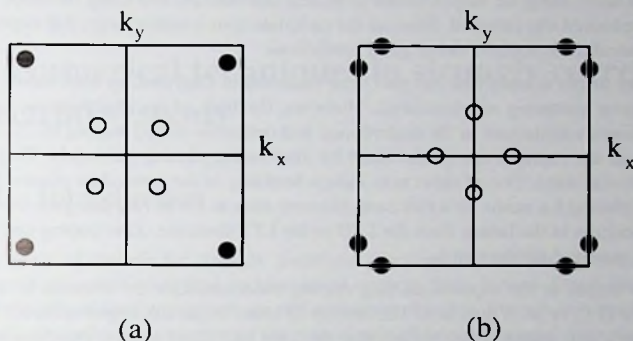


Figure 1-5. The location of the peaks corresponding to staggered spin modulation (filled circles) and charge modulation (open circles) in the Brillouin zone, for a diagonal (a) and horizontal (b) striped phase.

modulation with a period twice the domain wall separation d and the first harmonic peak is located at the incommensurate position $[(1 \pm \delta)\pi, \pi]$ or $[\pi, (1 \pm \delta)\pi]$, as indicated in figure 1-5. Moreover, because the $(1,0)$ and $(0,1)$ direction are equivalent, the incommensurate peaks will show up in both directions in the zone.

In 1994 Tranquada and coworkers published results of a neutron scattering experiment[11] performed on the nickelate $\text{La}_{2-x}\text{Sr}_x\text{NiO}_4$ compound, which is a spin-1 insulator with the same structure as that of strontium doped 214 cuprate superconducting compound, except that copper is replaced by nickel. They observed superlattice peaks corresponding to magnetic and charge peaks at incommensurate wave-vectors. The interpretation of their results corresponds with the existence of a static stripe phase, with a spin modulation period twice the period of the charge modulation. This gives the ratio 1:2 for the decommensuration periods. The hole density along the stripes is one hole per site and it is found to be site centered. The stripes are oriented diagonally along the $(1,1)$ direction, however if one makes use of a unit cell with axes rotated 45° with respect to the Ni-O bond, then in reciprocal space the magnetic peaks are split about the antiferromagnetic position $(1,0)$ along the $(1,0)$ and $(0,1)$ direction. Another feature of the nickelate stripe that is worth mentioning is the large spin magnetic moment which is found to be approximately 85% of the value found in the undoped antiferromagnetic insulator phase. This shows that the holes must be well localized within the domain walls.

These types of stripes are quite similar to the one predicted by Zaanen and Gunnarson[9] and other groups on the basis of the mean field analysis of the Hubbard model and the $t - J$ model. Although the density of holes, in these calculations, is more spread in these calculations, quite a number of features of the nickelate stripes can be understood rather well from the semiclassical calculations. These include the insulating feature of the stripes,

the density of holes along the stripes turned to be also one hole per site along the stripe and the stripes are indeed site centered. Because the nickelate spin is rather large, it is expected that semiclassical analyses give rather good predictions.

As said before stripes correlations has also been observed in Cuprates, by both elastic and inelastic neutron scattering measurements. However, the bulk of the observations reveal dynamical stripes correlations in the underdoped and optimally doped region[28, 30, 31]. Static stripes in the cuprates can be stabilized by introducing pinning potentials. This can be done in several ways. One of them is to induce buckling in the perovskite planes. This is done by replacing La atoms by a rare earth element such as Eu or Nd, that give rise to a structural transition in the lattice from the LTO to the LTT structure. Zinc doping can also act as pinning potential for the stripes.

The cuprates stripes at the superconducting doping concentrations are oriented horizontally along the (1,0) or (0,1) direction. The density of holes inside the stripes is here 1 hole per two stripe's unit length which means that they are half filled stripes. Furthermore it can be argued that the cuprate stripes are bond centered. These features can not be understood from mean field calculation, which underestimate the role of quantum fluctuations. Because of the reduced spin value of the cuprate, quantum fluctuation are more significant in this case than in the nickelates. The stripes found in the $t - J$ model using the DMRG calculation capture a number of feature of the cuprate stripes. They are bond centered and near $x = \frac{1}{8}$ doping they are indeed half filled. However, the structure inside the stripes, in this case, is more complicated and can be related to the formation of d-wave pairs. Below the superconducting doping the cuprate stripes are oriented diagonally.

1.7 Organization of the thesis

In this thesis I will address some aspects of the physics of the stripe phase. In chapter 3 and 4 I will address the physics of a single stripe. A strong coupling model for a single non-metallic stripe will be introduced and investigated rather extensively firstly and secondly we will discuss the consequence of introducing stripe metallicity. Ramification of the results with respect to the physics of the stripes in the cuprates will be discussed. In chapter 5 we will consider a spin-only model for the static stripe phase. The aim is to investigate the role of the static stripes on the magnetic properties of the cuprates. As dynamical stripes persist in the cuprates High T_c materials, in the subsequent chapter, chapter 6, I will address the problem of dynamical stripes living in a spinful background. Firstly we will review and discuss the problem of a stripe liquid/gas uncoupled to the spins, then I will introduce a model for dynamical stripes in a spinful background.

Most of the treatments for the models studied in this thesis are numerical. To give the reader insight about these treatments I will give a brief introduction to the numerical techniques used here in chapter 2.

2 Numerical techniques in strongly correlated electron systems

2.1 Introduction

The study of models for strongly correlated electrons is a difficult problem. There are no well-controlled analytical techniques to analyze them in two dimension. Mean field and variational approximations are self-consistent, but it is difficult to judge whether they actually describe the properties of the ground state of the system or of an excited state. Even in one dimension, although quite a number of analytical techniques prove to be successful in determining the solutions of 1D models and much of its properties, it is still difficult to calculate thermodynamic quantities and correlation functions. These difficulties have led numerous groups to study these models using computational and numerical techniques. As computer power is increasing, results from numerical techniques are getting better and increasingly accurate.

Many techniques are currently being used to study and investigate numerically the models for correlated electrons systems. However, the vast majority of the work done in this field can be grouped into two methods, exact diagonalization techniques and the quantum Monte-Carlo methods. All the computational work presented in this thesis is done using exact diagonalization and quantum Monte-Carlo simulation. In this chapter I will provide a brief introduction to both techniques.

2.2 Exact diagonalization techniques

Exact diagonalization techniques are typically zero-temperature methods. They are used to calculate the ground state wave function and the low-lying excitation spectrum for a finite size system with a very good accuracy. In some cases they can also be used to calculate finite temperature properties. Two methods are widely used: the Lanczos algorithm and, more recently, the density matrix renormalization group (DMRG) technique[12]. DMRG works exceptionally well for one dimensional systems. It can also be applied to higher dimensional systems, but with some difficulties and it is harder to obtain accurate results in this case. The advantage of the DMRG in one dimension is its ability to handle a rather large system, reducing finite size errors. Lanczos methods can in principle be applied to any dimension[13]. However, in practice it is used for one and two dimensions only. It works for systems of up to about 10^8 states. This restriction leads sometimes to difficulties with finite size scaling. Here we will describe the Lanczos method, which is used in the

next chapter to obtain some of the ground state properties of a model for the fluctuations of a single stripe (the quantum lattice string model)

2.2.1 Lanczos Technique

The basic idea of the Lanczos method is that one can construct a special basis where the Hamiltonian has a tridiagonal representation. This is carried out iteratively, as will be shown below. First one select an arbitrary vector $|\phi_0\rangle$ in the Hilbert space of the model being studied. If the Lanczos method is used to determine the ground-state energy and wavefunction, it is necessary that the overlap between the actual ground state $|\psi_0\rangle$ and the initial state $|\phi_0\rangle$ be nonzero. If no *a priori* information about the ground state is available, this requirement is usually easily satisfied by selecting an initial state with randomly chosen coefficients in the basis that is being used. If some other information about the ground state is known, like the subspace to which the ground state belongs, then it is convenient to initiate the iterations with a state already belonging to this subspace (and, if possible, with random coefficients within this subspace).

The special basis is found as follows. After $|\phi_0\rangle$ is selected, we can define a new vector by applying the Hamiltonian \mathcal{H} to this initial state. Subtracting the projection over $|\phi_0\rangle$, we obtain

$$|\phi_1\rangle = \mathcal{H}|\phi_0\rangle - \frac{\langle\phi_0|\mathcal{H}|\phi_0\rangle}{\langle\phi_0|\phi_0\rangle}|\phi_0\rangle, \quad (2.2.1)$$

satisfying $\langle\phi_0|\phi_1\rangle = 0$. A new state that is orthogonal to the previous two can be constructed as,

$$|\phi_2\rangle = \mathcal{H}|\phi_1\rangle - \frac{\langle\phi_1|\mathcal{H}|\phi_1\rangle}{\langle\phi_1|\phi_1\rangle}|\phi_1\rangle - \frac{\langle\phi_1|\phi_1\rangle}{\langle\phi_0|\phi_0\rangle}|\phi_0\rangle, \quad (2.2.2)$$

It is easily checked that $\langle\phi_0|\phi_2\rangle = \langle\phi_1|\phi_2\rangle = 0$. The procedure can be generalized by defining an orthogonal basis recursively as

$$|\phi_{n+1}\rangle = \mathcal{H}|\phi_n\rangle - a_n|\phi_n\rangle - b_n|\phi_{n-1}\rangle, \quad (2.2.3)$$

where $n = 0, 1, 2, \dots$, and the coefficients are given by

$$a_n = \frac{\langle\phi_n|\mathcal{H}|\phi_n\rangle}{\langle\phi_n|\phi_n\rangle} \quad b_n^2 = \frac{\langle\phi_n|\phi_n\rangle}{\langle\phi_{n-1}|\phi_{n-1}\rangle}, \quad (2.2.4)$$

supplemented by $b_0 = 0$, $|\phi_{-1}\rangle = 0$. It follows directly from 2.2.3 that the Hamiltonian matrix is represented in this basis by the following tridiagonal form

$$\mathcal{H} = \begin{bmatrix} a_0 & b_1 & 0 & 0 & \dots \\ b_1 & a_1 & b_2 & 0 & \dots \\ 0 & b_2 & a_2 & b_3 & \dots \\ 0 & 0 & b_3 & a_3 & \dots \\ \vdots & \vdots & \vdots & \vdots & \ddots \end{bmatrix} \quad (2.2.5)$$

As expected, the Hamiltonian is tridiagonal. Once in this form the matrix can be diagonalized easily using library subroutines (e.g. NAG library subroutines). However, to diagonalize \mathcal{H} completely, a number of iterations equal to the size of the Hilbert space (or the subspace under consideration) are needed. In practice, this would demand a considerable amount of CPU time. However, one of the advantages of this technique is that enough accurate information about the ground state of the problem can be obtained after a relatively small number of iterations (typically of the order of ~ 100 or less). Thus the method is suitable for the analysis of the ground state properties of the model.

To understand the rapid convergence to the ground state, it is convenient to consider a variation of this technique known as the modified Lanczos method [14, 15]. In this method, the diagonalization proceeds using " 2×2 steps"; i.e., first the Hamiltonian in the basis $|\phi_0\rangle$ and $|\phi_1\rangle$ (defined before) is diagonalized. The lowest energy state is always a better approximation to the actual ground state than $|\phi_0\rangle$. This new improved state can be used as the initial state of a next 2×2 iteration, and the procedure is repeated as many times as needed to reach convergence. It is then clear that the modified Lanczos method or in fact the original proposed Lanczos version, can be described as a systematic way to improve a given variational state that is used to represent the ground state of the system. It is therefore not surprising that the ground state properties can be obtained accurately well before the rest of the matrix eigenvalues are evaluated.

2.3 Quantum Monte-Carlo

There are two categories of quantum Monte-Carlo methods. The first one is for the finite temperature case, which is usually called path-integral Monte-Carlo. The second one is for the zero temperature case and is usually referred to as the projector quantum Monte-Carlo method. Only the first case will be reviewed here.

The average properties of a physical system can be expressed by

$$\langle Q \rangle = \frac{\sum_S Q \rho(S)}{Z} \quad (2.3.1)$$

where S is a system configuration, Q is any physical quantity e.g. energy, magnetization or spin-spin correlation and Z is the partition function, defined by $Z = \sum_S \rho(S)$, while $\rho(S)$ is the relative probability distribution or Boltzmann weight of a particular state or configuration of the system.

A Monte-Carlo simulation approximates the sum over all states of the system by a sum over a smaller set of states chosen using its Boltzmann weight as a criterium. A Monte-Carlo process that samples $\rho(S)$ is usually generated by means of the generalized Metropolis algorithm [16]. This algorithm can be formulated as follows:

Suppose a configuration S is given at some time t of the Monte Carlo process. A new configuration S' at time $t + 1$ is generated by means of a stochastic process that consists

of two steps. These steps are defined in terms of the so-called proposal and acceptance transition probabilities \mathcal{P} and \mathcal{A} . Assume that the probabilities \mathcal{P} and \mathcal{A} are given. The procedure is::

1. An intermediate configuration S'' is proposed with probability $\mathcal{P}(S''|S)$;
2. S' becomes S'' with probability $p = \mathcal{A}(S''|S)$; the proposed configuration is accepted;
3. S' becomes S'' with probability $q = 1 - \mathcal{A}(S''|S)$; the proposed configuration is rejected and the old configuration S is kept at time $t + 1$.

More explicitly, the Monte Carlo sampling is generated by means of a Markov matrix P with elements $P(S'|S)$ of the form:

$$P(S'|S) = \begin{cases} \mathcal{A}(S'|S)\mathcal{P}(S'|S) & \text{for } S' \neq S \\ 1 - \sum_{S'' \neq S} \mathcal{A}(S''|S)\mathcal{P}(S''|S) & \text{for } S' = S \end{cases}$$

The Markov matrix P is designed to satisfy detailed balance

$$P(S'|S)\rho(S) = P(S|S')\rho(S'), \quad (2.3.2)$$

so that if the process has a unique stationary distribution, this will be the $\rho(S)$ as desired. In principle one has a great freedom to choose the proposal matrix \mathcal{P} , but it is necessary to satisfy the requirement that transitions can be made between (almost) any pair of states with non-vanishing probability (density) in a finite number of steps.

The choice of the proposal matrix \mathcal{P} is limited only by the requirement that the first step of the algorithm can be executed efficiently. Once a proposal matrix \mathcal{P} is selected, an acceptance matrix is defined so that the detailed balance, Eq.(2.3.2), is satisfied,

$$\mathcal{A}(S'|S) = \min \left[1, \frac{P(S'|S)\rho(S)}{P(S|S')\rho(S')} \right]. \quad (2.3.3)$$

The Metropolis algorithm can be used to estimate the expectation values (Eq.2.3.1) as the average over Monte-Carlo "time",

$$\langle X \rangle = \frac{1}{L} \sum_{t=1}^L X(S_t). \quad (2.3.4)$$

The limitation of the Metropolis method is that it generates a time series of configurations with serial correlations. Consequently, the number of independent configurations contained in the time series S_1, \dots, S_L is not given by L , but roughly by $L_{eff} \approx L/\tau$ where τ is an appropriately defined auto-correlation time of the series. The variance of the finite- L time average featured in Eq.(2.3.4) is not given by $\text{var}(X)/L$ but approximately by $\text{var}(X)/L_{eff}$.

For classical systems the interaction are local and $\rho(S)$ is given in terms of the classical Hamiltonian of the system as $\rho(S) = e^{-\beta\mathcal{H}(S)}$, where $\beta = 1/KT$. For quantum mechanical systems one encounters many difficulties. The expectation value of a physical quantity of a quantum mechanical system is defined as

$$\langle Q \rangle = \frac{\text{Tr} Q e^{-\beta\mathcal{H}}}{Z} \quad (2.3.5)$$

with Z given by $Z = \text{Tr} e^{-\beta\mathcal{H}}$. We have therefore to diagonalize the Hamiltonian matrix, which is practically impossible for large systems. Because the quantum coherence length ranges over the whole system, even if the interaction term in the Hamiltonian is local, the effect of the term is non-local. One has to find a way to properly define $\rho(S)$ in terms of local quantities. In the following two sections I will review two methods, used in this thesis, for studying quantum systems. The central idea is to map the quantum problem to an equivalent classical one. The definition of the relative probability distribution $\rho(S)$ will then become straight forward.

2.3.1 The Suzuki-Trotter path-integral transformation

In many cases the Hamiltonian of a quantum system \mathcal{H} is composed of some partial Hamiltonians $\{\mathcal{H}_j\}$, and each \mathcal{H}_j is easily diagonalized independently. In this situation the so-called Trotter formula[17, 18] is very useful,

$$e^{\lambda(A+B)} = \lim_{n \rightarrow \infty} \left(e^{\frac{\lambda}{n}A} e^{\frac{\lambda}{n}B} \right)^n, \quad (2.3.6)$$

or more generally,

$$e^{-\beta\mathcal{H}} = e^{-\beta(\mathcal{H}_1 + \dots + \mathcal{H}_p)} = \lim_{n \rightarrow \infty} \left(e^{-\frac{\beta}{n}\mathcal{H}_1} \dots e^{-\frac{\beta}{n}\mathcal{H}_p} \right)^n. \quad (2.3.7)$$

Upon taking the trace of (2.3.7) using some orthogonal complete sets diagonalizing the partial Hamiltonians independently, the problem of calculating the partition function Z for the d -dimensional quantum system \mathcal{H} is reduced to that of calculating the partition function of the corresponding $(d+1)$ -dimensional classical system[19, 20]. This transformation is called the Suzuki-Trotter (ST)-transformation. This equivalent classical problem can be simulated with a Monte-Carlo method and this is the quantum Monte-Carlo method. Some new types of many-body interactions appear and consequently the corresponding algorithms are usually far more complicated than in the classical case.

This equivalence of a d -dimensional quantum system to a $d+1$ -dimensional classical system is known from the Feynman path-integral formulation of quantum mechanics, and the Monte-Carlo methods based on this transformation are usually called path-Integral Monte-Carlo. The extent of the extra 'time' or 'Trotter' direction represent the temperature at

which the system is simulated. At zero-temperature the system becomes truly $d + 1$ dimensional.

Many Monte-Carlo methods utilize the ST-transformation: the World-line, the Monte-Carlo power, the auxiliary-field and the loop cluster methods, to call the most popular ones. The infinite n limit is taken by simulating the system for a number of finite n 's to subsequently extrapolate to infinite n . The loop cluster method can be implemented directly in the time-continuum limit.

2.3.2 World-line algorithm

The world-line method employs directly the above path-integral transformation. The resulting classical degrees of freedom are the eigenvalues of the original quantum operators \mathcal{H}_j appearing in the Hamiltonian operator. The World-line algorithm follows the evolution of these eigenvalues in the imaginary time direction, τ . For instance in a spin problem one can choose the z component of $S_n^z(\tau)$ of spin n for a set of quantum spins and the $X - Y$ term in the partial Hamiltonians will connect these degrees of freedom along the imaginary time direction τ form the world-lines. One of the most attractive features of this approach is precisely that these world-lines trace the variables which are associated with the operators in the original quantum Hamiltonian and therefore allow a intuitive real space picture of the correlations in the system.

Consider the 1-D quantum XXZ Hamiltonian

$$\mathcal{H} = \sum_i \left[\frac{J_x}{2} (S_i^+ S_{i+1}^- + S_i^- S_{i+1}^+) + J_z S_i^z S_{i+1}^z \right] \quad (2.3.8)$$

The world-line simulation is formulated by discretizing $\beta = L \Delta \tau$ in the partition function. The Hamiltonian is decomposed such that the matrix elements of the partial Hamiltonians, which arise after the introduction of a complete set of states can be evaluated easily. The most convenient choice in this case is the "checkerboard" decomposition[21]. Here one first divides the Hamiltonian into two pieces, $\mathcal{H} = \mathcal{H}_1 + \mathcal{H}_2$ where in \mathcal{H}_1 one sums over odd sites and in \mathcal{H}_2 over even sites. Introducing a complete set of states which are diagonal in the z component of spin, the partition function takes the following form.

$$\mathcal{Z} = \sum_{s_{ij}^z} e^{h_d} \langle \{S_{i1}^z\} | e^{h_{nd}} | \{S_{i1}^z\} \rangle \langle \{S_{i2}^z\} | e^{h_{nd}} | \{S_{i3}^z\} \rangle \cdots \langle \{S_{i2L}^z\} | e^{h_{nd}} | \{S_{i1}^z\} \rangle, \quad (2.3.9)$$

where h_d and h_{nd} represent the diagonal and off-diagonal part of \mathcal{H} , respectively. Note that $2L$ time slices were introduced, where L is the Trotter height, because neither \mathcal{H}_1 nor \mathcal{H}_2 is diagonal in this basis.

The convenience of this choice is that \mathcal{H}_1 and \mathcal{H}_2 consist of independent two site pieces. Thus the matrix elements factorizes into,

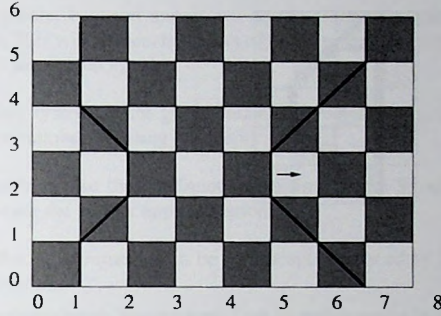


Figure 2-1. The “checkerboard” decomposition. The Hamiltonian acts on the shaded squares. We also show an example of two world-lines on it and a typical Monte-Carlo move which pulls a world-line across an unshaded square.

$$\left\langle S_{1,l}^z S_{2,l}^z \cdots S_{N,l}^z \left| e^{h_{nd}} \right| S_{1,l+1}^z S_{2,l+1}^z \cdots S_{N,l+1}^z \right\rangle = \prod_{i=odd} \left\langle S_{i,l}^z S_{i+1,l}^z \left| e^{(h_{nd})_i} \right| S_{i,l+1}^z S_{i+1,l+1}^z \right\rangle \quad (2.3.10)$$

where $(h_{nd})_i$ is the off-diagonal hamiltonian between site i and $i + 1$. Now one must only evaluate the corresponding two site expectation values. The diagonal part of the Hamiltonian can be written as a product of terms representing the two sites between adjacent time slices and then included with the above off-diagonal term. Hence, the partition function can be written in the following useful form:

$$\mathcal{Z} = \sum_{\{S_i\}} \prod_l \prod_{i=odd}^L \prod_{j=even}^N \left\langle S_{i,2l}^z S_{i+1,2l}^z \left| e^{(h_d + h_{nd})_i} \right| S_{i,2l+1}^z S_{i+1,2l+1}^z \right\rangle \cdot \left\langle S_{j,2l+1}^z S_{j+1,2l+1}^z \left| e^{(h_d + h_{nd})_j} \right| S_{j,2l+2}^z S_{j+1,2l+2}^z \right\rangle \quad (2.3.11)$$

In fig. 2-1 we picture the structure of the checkerboard break-up by drawing the $(1 + 1)$ -dimensional array of spins and shading the squares corresponding to the bonds across which a piece of that the Hamiltonian acts. Because the total z -component of the spin is conserved, only configurations satisfying $S_{1,l}^z + S_{2,l}^z = S_{1,l+1}^z + S_{2,l+1}^z$ in a shaded square are allowed. These conservation laws can best be visualized as follows: draw lines connecting the sites of the up spins. Since the number of up spins is conserved from time slice to time slice, the result is a set of continuous “world-lines”. The world-lines can cross only the shaded squares of the checkerboard, since it is only on these squares the Hamiltonian acts.

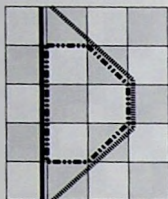


Figure 2-2. Example of a loop update on the “checkerboard” decomposition. The thick solid line denotes a single worldline, the dot-dashed line shows a possible loop. By flipping the spins on all sites along the loop the original worldline will be deformed into the dashed one. Note that this update is nonlocal.

The product of the matrix elements for each “classical” spin configuration or world-line configuration defines the relative probability distribution or the weight $\rho(S)$ for the configuration.

The only allowed local Monte-Carlo moves which preserve all local conservation laws resulting in a non-zero weight are those which “pull” a world-line across an unshaded square of the checkerboard lattice assuming that the original configuration was allowed. Four spin variables are changed in such an update, and the values of the matrix elements on four of the plaquettes are modified. This means that the decision making process is local. An acceptance-rejection step using the Metropolis algorithm can be carried out. Here the move is accepted with probability $p = \min(1, R)$, where R is the ratio of the product of new and old values of the matrix elements on the four modified plaquettes. This method satisfies the detailed balance, and will generate spin configurations with Boltzmann weight equal to the product of all the matrix elements.

2.3.3 The Loop cluster Algorithm

The world-line method suffers from many problems. When the simulations move towards a critical point, the autocorrelation time τ become extremely large rendering the simulations inefficient. Another limitation is that it can only be used in the canonical ensemble, which means that one can not simulate system with varying magnetization or occupation number. For a number of models these problems were solved by using cluster algorithms. The cluster algorithm for quantum spin systems is the loop cluster algorithm[96]. The algorithm constructs closed loops of spins and flips them simultaneously. This algorithm possesses a number of features making it extremely powerful for studying quantum spin systems. These feature are:

- The autocorrelations between successive Monte-Carlo configurations are significantly reduced. This will reduce, by orders of magnitude, the number of Monte-Carlo sweeps needed for a given system.
- One can simulate systems in the grand-canonical ensemble (e.g. varying magnetization, occupation number, winding numbers).
- It is also possible to take the continuous time limit in the Suzuki-Trotter formula. This will eliminate the Trotter approximation.
- The errors in the measurements can be significantly reduced by using the so called Improved Estimators.

The algorithm constructs loops. Once a loop is constructed, a new configuration is proposed by flipping all the spins on the loop. The power of the loop algorithm is that this new configuration is accepted with probability 1. Here I show how loops are constructed for the case of the Heisenberg chain and show how this construction obeys the detailed balance. Having the above "checkerboard" decomposition in mind, a loop is constructed by first selecting at random a point (x, t) in the $1+1$ dimensional lattice. The extra dimension is along the Trotter axis, which we will refer to as the Euclidean time. The spin $s(x, t)$ belongs to two plaquettes of interaction, see fig 2-1, one at Euclidean times before t and one at Euclidean times after t . When $s(x, t)$ is up, one has to consider the plaquette interaction at the later time, and for a down $s(x, t)$ the plaquette interaction at earlier times is considered.

The spin configuration on the plaquette considered is characterized by the spin orientation at the four corners $A = [s(x, t), s(x + \delta x, t), s(x, t + \delta t), s(x + \delta x, t + \delta t)]$. The next point on the loop will be one of these four corners depending on the spin configuration. For configurations $A_1 = [1, 1, 1, 1]$ or $[-1, -1, -1, -1]$ the next point is the nearest neighbor of (x, t) on the plaquette along the Euclidean time direction. For configurations $A_2 = [1, -1, -1, 1]$ or $[-1, 1, 1, -1]$ the next point along the loop is again the nearest neighbor of (x, t) on the plaquette but now along the space direction. For configuration $A_3 = [1, -1, 1, -1]$ or $[-1, 1, -1, 1]$ the next point on the loop is with probability $p = 2/(exp(\tau J) + 1)$ the nearest neighbor of (x, t) along the time direction, and with probability $1 - p$ the nearest neighbor of (x, t) along the space direction. Once the next point on the loop is found the process is repeated until the loop closes. As said before, the new configuration is found by flipping all the spins on the loop simultaneously.

The algorithm obeys the detailed balance, in this case it is,

$$p(A_i)\rho(A_i/A_j) = p(A_j)\rho(A_j/A_i) \quad (2.3.12)$$

where $p(A_1) = 1$, $p(A_2) = \frac{1}{2}(exp(\tau J) - 1)$, $p(A_3) = \frac{1}{2}(exp(\tau J) + 1)$ and as before $\rho(A_i/A_j)$ is the transition probability to go from a plaquette configuration A_i to A_j . This can easily be checked.

One of the principle advantages of the loop cluster algorithm is that it allow for the use of so called improved estimators for observables[97]. This technique drastically reduces the statistical errors of measurements.

In this technique, the thermal average of an observable is calculated from the generated loops considering each loop as an independed system with a certain weight. For example for an observable \mathcal{O} the improved estimator for its thermal average is given by

$$\langle \mathcal{O} \rangle = \left\langle \frac{\mathcal{O}_c}{|C|} \right\rangle \quad (2.3.13)$$

where \mathcal{O}_c is the value of the observable \mathcal{O} in the loop C and $|C|$ is the size of, or number of points in, loop c .

Unfortunately this technique does not work for all observables. For example the internal energy can not be calculated in this way and one has to calculate it in the usual way. However the spin-spin correlations, uniform and staggered susceptibilities can all be calculated with the improved estimator method. The improved estimator formulae for the uniform and staggered susceptibilities in the 1 dimensional Heisenberg model are:

$$\begin{aligned} \chi_u^{imp} &= \frac{\beta}{2N} \left\langle \frac{M_c^2}{|C|} \right\rangle \\ \chi_s^{imp} &= \frac{\beta}{2N} \left\langle \frac{M_{c,stag}^2}{|C|} \right\rangle \end{aligned} \quad (2.3.14)$$

where $M_c = \sum_{i \in C} S_i^z$, $M_{c,stag} = \sum_{i \in C} (-1)^i S_i^z$ and N is the Trotter dimension.

3 The single stripe problem

3.1 Introduction

Because stripes are linelike objects, the charge sector of the electronic state of the high T_c cuprates might be looked at as a *quantum string liquid*[32, 34, 35]. Little is known in general about such problems, and theoretical analysis is needed. In order to address the problem of many interacting strings, it is first necessary to find out the physics of a single string/stripe in isolation. A string is an extended object, carrying a non-trivial collective dynamics — in contrast to particle-like problems, the elementary constituent of the string liquid poses already a serious problem. The physics of quantum strings is a rich subject. This is most easily discussed in terms of path-integrals. In $d+1$ dimensional Euclidean space time, a particle corresponds to a world line, and so the quantum string corresponds to a “worldsheet”. The statistical physics of membranes is a rich subject, which is still under active investigation[36].

The debate on the microscopic origin of the stripe instability is far from closed[9, 10, 37, 38, 39, 35, 40]. Nevertheless, in this work we will attempt to isolate some characteristics which might be common to all present proposals for the microscopy, to arrive at some general considerations regarding the quantum meandering dynamics. From those we will abstract a minimal model for the string dynamics. The phase diagram of this model can be mapped out completely, and turns out to be remarkably rich.

These characteristic features are: (i) It is assumed that the charge carriers are confined to domain walls. This is the major limitation of the present work and it is hoped that at least some general characteristics of this strong coupling regime survive in the likely less strongly coupled regime where nature appears to be. (ii) In addition, we assume that domain walls are not broken up, as sketched in Fig. 3-1*b*, as this would lead to strong spin frustration. (iii) Most importantly, we assume a dominant role of lattice commensuration on the scale of the lattice constant. Configuration space is built from strings which consist of “holes” which live on the sites of an underlying lattice. An example of such a string configuration is sketched in Fig. 3-1*c*. This automatically implies that the microscopic dynamics is that of *kinks* along the string (Figs. 1 *c,d*), and this leads to major simplifications with regard to the long wavelength behavior of the string as a whole. Note that there is ample evidence for the importance of lattice commensuration: the scaling of the incommensurability with hole density x for $x < 1/8$ [28], the special stability at $x = 1/8$ [26], the LTT pinning mechanism[25]. (iv) It is assumed that the strings do not carry other low lying internal degrees of freedom, apart from the shape fluctuations. Physically this means that localized strings would be electronic insulators. The data of Yamada *et al.*[27] indicate that this might well be the case at dopings $x \leq 1/8$ (the linear dependence of the incommensurability on x indicates an on-domain wall charge commensuration), but it is definitely

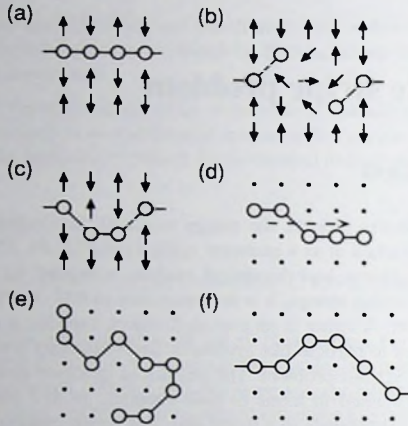


Figure 3-1. (a) A charged domain wall separating spin domains of opposite AFM order parameter. (b) Breaking up domain walls causes spin frustration, while (c) "kinks" do not. (d) Kinks can gain kinetic energy by moving along the domain wall. (e) A typical rough wall. (f) An example of a directed string.

violated at larger dopings where the strings should be metallic[40, 41, 42, 43].

Given these requirements, one would like to consider a quantum sine-Gordon model[45] for the string dynamics,

$$H = \frac{1}{2} \int dl \left[\Pi(l)^2 + c^2 \left(\frac{\delta z(l)}{\delta l} \right)^2 + g \sin \left(\frac{2\pi z(l)}{a} \right) \right]. \quad (3.1.1)$$

Here $z(l)$ is the transversal displacement at point l on the string, and $\Pi(l)$ its conjugate momentum defined through the commutation relation $[\Pi(l), z(l')] = i\delta(l - l')$, and c is the transversal sound velocity. The first two terms in Eq. (3.1.1) describe a free string, while the last term is responsible for the lattice commensuration effects: every time the string is displaced by a lattice constant, the potential energy is at a minimum. This model is well understood[45]. When the strength of the nonlinear interaction exceeds a critical value ($g > g_c$), the interaction term is relevant and the string localizes. The excitation spectrum develops a gap and it is characterized by well-defined kink and anti-kink excitations. When $g < g_c$ the sine term is irrelevant, and although the dynamics is at least initially kink-like on microscopic scales, the string behaves as a free string at long wavelength. The latter is the most elementary of all quantum strings. It follows immediately that the relative transversal displacement of two points separated by an arclength l along the string diverges

as $\langle (z(l) - z(0))^2 \rangle \sim \ln l$ [32]. The string as a whole is therefore delocalized, and this is the simplest example of a "critical" string.

A central result of this work is that Eq. (3.1.1) is, at least in principle, not fully representative for the present lattice problem. More precisely: starting from a more complete microscopic kink dynamics model (section II) a richer infrared fixed point structure is found. The phase diagram incorporates phases associated with the quantum sine-Gordon model fixed point, but also includes additional phases which are intimately connected with the effects of the lattice and of the nearest neighbor interactions between the holes. In section 3.3, we derive the path integral representation of our model. It turns out that the worldsheet of this string in Euclidean space time corresponds with two coupled restricted solid-on-solid (RSOS) surfaces [46], each of which describes the motion of the string in either the x or y direction on the two dimensional lattice.

The bare model is invariant under rotations of the string in space. As discussed in section 3.4, we find indications for a generic zero-temperature spontaneous symmetry breaking: for physical choices of parameters, the invariance under symmetry operations of the lattice is broken. Even when the string is critical (delocalized in space), it acquires a sense of *direction*. On average, the trajectories corresponding with the string configurations move always forward in one direction while the string might delocalize in the other direction, see Fig. 3-1f. This involves an order-out-of-disorder phenomenon which is relatively easy to understand intuitively. Quantum mechanics effectively enhances the fluctuation dimension by stretching out the string into a world sheet in the time direction, and the enhancement of the effective dimension increase the effect of fluctuations. Thermal fluctuations destroy this directedness, but they do so more effectively when the string is less quantum mechanical.

This directedness simplifies the remaining problem considerably. It will be shown that the directed string problem is equivalent to a well known problem in surface statistical physics: its worldsheet is equivalent to a single RSOS surface. At the same time, this model is easily shown to be equivalent to a generalized XXZ quantum spin chain problem. The particular model studied is actually equivalent to the $S = 1$ spin chain, which has been studied in great detail. The RSOS surface problem and the quantum spin chain problem are therefore also related to each other.

A large part of this chapter (sections 3.5- 3.8) is devoted to a study of this directed string model. Some powerful statistical physics notions apply directly to the present model, and these allow to arrive at a complete description of the phase diagram of the quantum string. This phase diagram is surprisingly rich: there are in total ten distinct phases. In the context of the quantum spin chain/RSOS surfaces, already six of those were previously identified. However, viewing this problem from the perspective of the quantum string, it becomes natural to consider a larger number of potentially relevant operators and the other four phases become obvious.

Compared to strings described by Eq. (3.1.1), a much richer behavior was found but this is limited to the regime where lattice commensuration dominates over the kinetic energy so that the string as a whole is localized — we use "localized" here in the sense that the transversal string fluctuations of two widely separated points remain finite, $\langle (z(\ell) -$

$z(0)^2 \rightarrow \text{const.}$ as $\ell \rightarrow \infty$. Besides the different directions the purely classical strings can take in the lattice, also a number of localized strings were found, which have a highly non-trivial internal structures: the "disordered flat" strings, characterized by a proliferation of kinks, but where the kink flavors condense so that the string as a whole remains localized. On the other hand, the quantum-delocalized (critical) strings are all of the free field variety and as we will argue in the final section, this might be a very general consequence of the presence of a lattice cut-off.

3.2 Model: The meandering lattice string

Whatever one thinks about the microscopy of the stripes, in the end any theory will end up considering the charged domain walls as a collection of particles bound to form a connected trajectory, or such a model will be an important ingredient of it. Moreover, these trajectories will communicate with the crystal lattice, because the electrons from which the strings are built do so as well. This fact alone puts some strong constraints on the collective dynamics of the charged domain walls.

Firstly consider the string configuration space. On the lattice this will appear as a collection of particles living on lattice sites, while every particle is connected to two other particles via links connecting pairs of sites. The precise microscopic identity of these particles is unimportant: they might be single holes (filled charged domain walls[9, 10] as in the nickelates[48]), an electron-hole pair (the charge density waves of Nayak and Wilczek[35], or Zaanen and Oles[39]), or a piece of metallic-[41] or even superconducting[49] domain wall. All what matters is that these entities have a preferred position with regard to the underlying lattice (site ordered[9], or bond ordered[40]). Quite generally, curvature will cost potential energy and a classical string will therefore be straight, oriented along one of the high symmetry directions of the lattice. Without loss of generality, it can be assumed that the lattice is a square lattice while the string lies along the (1,0) ('x') direction. Denoting as N_y the number of lattice sites in the y direction and assuming periodic boundary conditions, this straight string can be positioned in N_y ways on the lattice. Obviously, such a string will delocalize by *local* quantum moves: the particles tunnel from site to site[38, 50]. Moving the whole string one position in the y direction involves an infinity of local moves in the thermodynamic limit, and the different classical strings occupy dynamically disconnected regions of Hilbert space.

This is analogous to what is found in one dimensional systems with a discrete order parameter[51]. In the case of, e.g., polyacetylene the order parameter is of the Z_2 kind: the bond order wave can be either $\cdots - A - B - A - B - \cdots$ or $\cdots - B - A - B - A - \cdots$ (A single bond, B double bond), while a single translation over the lattice constant transforms the first state of the staggered order parameter into the second kind of state. This is a discrete operation, because the lattice forces the bond-order to localize on the center of the bonds. Such an order parameter structure implies the existence of topological defects, which are Ising domain walls: $\cdots - A - B - A - B - B - A - B - A - \cdots$ ("kink") and

$\cdots - B - A - B - A - A - B - A - B - \cdots$ ("antikink"). When they occur in isolated form, these are also genuine building blocks for the quantum dynamics, because although their energy is finite, it involves an infinity of local moves to get rid of them (topological stability). In the particular problem of polyacetylene, these kinks only proliferate under doping (charged solitons). Although topological quantum numbers are no longer strictly obeyed when the density of topological defects is finite, it has been shown in a number of cases that they nevertheless remain genuine ultraviolet quantities as long as they do not overlap too strongly [52, 53].

If one considers a (locally) directed piece of string, the string is analogous, except that the symmetry is now Z_{N_y} : on the torus, a half-infinity of the string is localized at y position n_y , and the other half can be displaced to $n_y + 1, n_y + 2, \dots, n_y - 1$. Hence, in total there are $N_y - 1$ distinct kink excitations with the topological invariants corresponding with the net displacement of the half-string in the y direction. Because the kink operators can occur in many flavors, this problem is therefore in principle richer than that of one dimensional solids.

Clearly, kinks with different flavors have to be dynamically inequivalent. Since there is apparently a reason for the particles to form connected trajectories, it should be more favorable to create a kink corresponding with a small displacement than one corresponding with a large jump. In this thesis we will focus on the simplest possibility: only kinks occur, corresponding with a displacement of *one* lattice constant in the y -direction. This restriction is physically motivated by the fact that the string is thought to separate two antiferromagnetically ordered states; so, if the displacement of successive holes would be larger than one lattice constant, the antiferromagnetic ordering would be strongly suppressed — after all, this is the very reason that holes tend to line up in stripes. In addition, only the "neutral" string will be considered here. It will be assumed that the string is characterized by a gap in its charge and spin excitation spectrum, so that the strings with kinks contain the same number of particles as the classical reference configurations. The model we will consider might apply literally to the charge commensurate stripes of the nickelate [48]. In the cuprates, it might be better to consider the stripes as one dimensional metals or superconductors, characterized by massless internal excitations. In these cases, it remains to be demonstrated that eventually the transversal string fluctuations decouple from the internal excitations for the present model to be of relevance. An attempt to justify this will be discussed in the next chapter.

Given the above consideration, we propose the following strong hole (particle)-binding model for quantum domain walls (stripes), the *quantum lattice strings*. These are connected strings of holes on the two-dimensional (2D) square lattice. The string configurations are completely specified by the positions of the particles (holes) $\mathbf{r}_l = (x_l, y_l)$ on the 2D square lattice. Two successive particles l and $l + 1$ should either be nearest neighbours or next nearest neighbours. Therefore they can only be apart by distances of either 1 or $\sqrt{2}$ lattice constants, i.e. $|\mathbf{r}_{l+1} - \mathbf{r}_l| = 1$ or $\sqrt{2}$. We will call these connection between successive particles *links*. Two classes of links, those of length 1 (flat links) and those of length $\sqrt{2}$ (diagonal links) exist. Taking the order of the particles into account there are 8 distinct

links. We assume that the number of particles in the string is fixed. Therefore the arc length along the string can only change by increasing the density of diagonal links relative to the density of flat links. The Hilbert space is spanned by all real-space configurations satisfying the above string constraint. The string delocalizes by nearest neighbour hops of individual particles under the condition that the initial and final configurations are in the set of allowed string configuration.

Strictly speaking, such a string problem lives in 2+1 dimensions. However, in the thermodynamic limit it reduces to a 1+1D problem as long as no other objects are present. Consider an arbitrary string configuration λ connecting N_λ sites. Single out an arbitrary point on this trajectory $\vec{x}_v = (x_0, y_0) \in \{\lambda\}$ (Which we refer to as the guider particle). The remainder of this trajectory is now completely specified by the set of $N_\lambda - 1$ vectors $\begin{pmatrix} \xi_l \\ \nu_l \end{pmatrix}$, the links, with $l = 1, N_\lambda - 1$, representing directed links. Both ξ_l and ν_l can take the values 1, 0, -1, but they can not be both 0: $\begin{pmatrix} \xi_l \\ \nu_l \end{pmatrix} \neq \begin{pmatrix} 0 \\ 0 \end{pmatrix}$. Hence, the configuration space is build up by first choosing the particular guider particle \vec{x}_v and attaching all possible string configurations $\{ \begin{pmatrix} \xi_l \\ \nu_l \end{pmatrix} \}_\mu$ to this guider particle, followed by a move of the guider particle according to the hopping prescription. This will lead to an orthogonal space of string configurations. The Hilbert space is thus spanned by the basis,

$$\Phi_{v,\mu} = \left| \vec{x}_v; \left\{ \begin{pmatrix} \xi_l \\ \nu_l \end{pmatrix} \right\}_\mu \right\rangle, \quad (3.2.1)$$

and the wave functionals of the strings are

$$\Psi_\Lambda = \sum_{v,\mu} \alpha_{v,\mu}(\Lambda) \Phi_{v,\mu} \quad (3.2.2)$$

Such that

$$\mathcal{H}\Psi_\Lambda = E_\Lambda \Psi_\Lambda \quad (3.2.3)$$

Where \mathcal{H} is the string Hamiltonian. In the thermodynamic limit, the motion of the guider particle \vec{x}_v becomes unimportant and the dynamics of the link vectors $\{ \begin{pmatrix} \xi_l \\ \nu_l \end{pmatrix} \}_\mu$ corresponds to a 1 dimensional problem.

In Euclidean space time, the string will trace out a surface (world sheet). One way to approach this problem is by identifying the classical surface problem which corresponds to the quantum string via the transfer matrix or the Suzuki-Trotter mapping. This will be done in the next section.

We turn to a site representation of the string configuration space. We define variables η_i^x and η_i^y , integer numbers denoting the 'height' above the x and y -axis, respectively, of the

string's particle at site l ,

$$\begin{aligned}\eta_l^x &= x_0 + \sum_{l'} \xi_{l'} \\ \eta_l^y &= y_0 + \sum_{l'} v_{l'}\end{aligned}\quad (3.2.4)$$

in terms of the link vectors and the guider particle. String configurations can be projected out from the total space of points $\vec{\eta}_l = (\eta_l^x, \eta_l^y)$ using projection operators

$$|\vec{\eta}(\text{strings})\rangle = \prod_l \mathcal{P}(\vec{\eta}_{l+1} - \vec{\eta}_l) |\vec{\eta}\rangle, \quad (3.2.5)$$

where $\hat{\eta}_l^\alpha |\vec{\eta}\rangle = \eta_l^\alpha |\vec{\eta}\rangle$ and

$$\mathcal{P}(\vec{\eta}_l) = \delta(|\vec{\eta}_l| - 1) + \delta(|\vec{\eta}_l| - \sqrt{2}). \quad (3.2.6)$$

Eq. 3.2.5 ensures that neighbouring particles are not farther apart than 1 or $\sqrt{2}$ lattice constant.

The Hamiltonian \mathcal{H} consists of a classical part and a quantum hopping part. In writing the classical Hamiltonian we will assume short range interactions. We write the interactions as a sum of nearest and next nearest neighbour local discretized string-tensions, where the energies will depend on the distances between successive particles and the curvature, or the angle in the string, at a certain particle. In terms of links, assuming that the interactions between links are short range we can consider the classical Hamiltonian to be a successive sum of a single, two, etc, link interactions. Thus,

$$\mathcal{H}_{Cl} = \mathcal{H}_{Cl}^1 + \mathcal{H}_{Cl}^2 + \dots, \quad (3.2.7)$$

where \mathcal{H}_{Cl}^1 is a single link interaction given by,

$$\mathcal{H}_{Cl}^1 = \sum_l \mathcal{K} \delta(|\hat{\eta}_{l+1}^x - \hat{\eta}_l^x| - 1) \delta(|\hat{\eta}_{l+1}^y - \hat{\eta}_l^y| - 1) \quad (3.2.8)$$

\mathcal{K} discriminates between diagonal and flat links. It has a clear physical interpretation in terms of a commensuration energy. If \mathcal{K} is large and positive, the string will tend to orient along $(1,0), (0,1)$ directions, while diagonal $(1, \pm 1)$ directions are stabilized by $\mathcal{K} \ll 0$.

The two-link interactions can be written in the following compact form,

$$\mathcal{H}_{Cl}^2 = \sum_l \sum_{i,j=0}^2 \mathcal{L}_{ij} \delta(|\eta_{l+2}^x - \eta_l^x| - i) \delta(|\eta_{l+2}^y - \eta_l^y| - j), \quad (3.2.9)$$

with $\mathcal{L}_{ij} = \mathcal{L}_{ji}$.

These two-link interactions correspond to discretized curvature energy. \mathcal{L}_{00} stabilize configurations where the string returns to its origin after two links. In the present context we will require that strings do not cross i.e. two particles can not occupy the same site. Therefore such configurations will be projected out. Negative \mathcal{L}_{10} stabilizes steep and sharp ($\pi/4$) corners. These represent strings with an extreme curvature and are therefore unphysical. We will exclude such strings ($\mathcal{L}_{10} \rightarrow \infty$). The remainder of these interactions stabilize string configurations which makes sense as charged domain wall configurations. \mathcal{L}_{11} measures the energy of a $\pi/2$ 'corner'. In a mean-field calculation by Vartiö and Rice[50], it was concluded that the state of a diagonal domain wall with an additional hole is more stable than the diagonal one. Such a stable configuration can lead to configurations where $\pi/2$ 'corners' are presents. It looks natural to include such configurations. \mathcal{L}_{20} and \mathcal{L}_{22} discriminate between configurations which have a net orientation along the horizontal/vertical or diagonal, respectively, on a scale of two links. \mathcal{L}_{20} can be set to zero if a straight, horizontal/vertical string is taken as the energy reference. Finally \mathcal{L}_{21} is needed to discriminate between isolated kink configurations (a diagonal link with a neighbouring horizontal/vertical links or vice versa) and the double kink configuration.

In addition one can include interactions involving a larger number of links. However, it seems safe to neglect those in the light of the rather localized nature of the underlying microscopic problem. On the other hand, self avoidance is a serious problem. Physically, one would not like the strings to self-intersect forming a closed loops. At the crossing points the direction of the string is ill defined. We will therefore add to the classical Hamiltonian the crossing term,

$$\mathcal{M} \sum_{l \neq m} \delta(\eta_l^x - \eta_m^x) \delta(\eta_l^y - \eta_m^y) \quad (3.2.10)$$

and then take the physically relevant limit $\mathcal{M} \rightarrow \infty$, so that particles do not occupy the same site (\mathcal{L}_{00} is now irrelevant). Therefore the model is parameterized by \mathcal{K} , \mathcal{L}_{11} , \mathcal{L}_{21} and \mathcal{L}_{22} . The various local configurations and interaction energies are shown in Fig. 3-2.

Quantizing the string amounts to allowing the particles to hop to nearest neighbour positions in either the x or y direction, with the constraint that these hops should occur within the string configuration space. This is accomplished by associating with the integer "height" variables η_l^α of particle l operators $\hat{\eta}_l^\alpha$ ($\alpha = x, y$) and then introducing the conjugate momenta $\hat{\pi}_l^\alpha$,

$$[\hat{\eta}_l^\alpha, \hat{\pi}_m^\beta] = i \delta_{l,m} \delta_{\alpha,\beta}. \quad (3.2.11)$$

The operator $e^{in\hat{\pi}_l^\alpha}$ acts as a ladder operator in the space of height states, i.e. it will cause particle l to hop a distance n in the α -direction. Therefore, the quantum term of the Hamiltonian in its simplest nearest neighbour form is,

$$\mathcal{P}(\vec{\eta}_l) = \delta(|\vec{\eta}_l| - 1) + \delta(|\vec{\eta}_l| - \sqrt{2}).$$

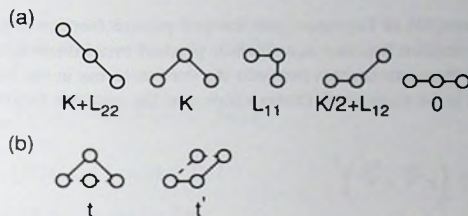


Figure 3-2. (a) Energies (of the central hole) and (b) tunneling amplitude of various local-bond configurations. The tunneling process is between the dashed configuration and the one drawn in full.

$$\mathcal{H}^{Qu} = \tau \sum_l \mathcal{P}_{Str}^x(l) \mathcal{P}_{Str}^y(l) \left(e^{i\hat{\pi}_l^x} + e^{-i\hat{\pi}_l^x} + e^{i\hat{\pi}_l^y} + e^{-i\hat{\pi}_l^y} \right). \quad (3.2.12)$$

where $\mathcal{P}_{Str}^\alpha(l)$ is a projection operator which, in terms of $\hat{\eta}_l^\alpha$ is given by,

$$\mathcal{P}_{Str}^\alpha(l) \equiv \mathcal{P}(\hat{\eta}_{l-1}^\alpha - \hat{\eta}_l^\alpha) \mathcal{P}(\hat{\eta}_l^\alpha - \hat{\eta}_{l+1}^\alpha) \quad (3.2.13)$$

\mathcal{H}^{Qu} is therefore the kinetic energy operator of the string. The holes in the string can hop one lattice unit upward, downwards, to the left or to the right with a hopping amplitude τ , while the projection operators \mathcal{P} impose that these movements are only allowed as long as the resultant configuration is in the string configuration space.

Equations (3.2.8, 3.2.9, 3.2.10 and 3.2.12) define a general quantum model for the charged domain walls, the quantum lattice string model.

3.3 Relation to RSOS-like surface models

The problem introduced in the previous section can be reformulated as the classical problem of a two dimensional surface (worldsheet) embedded in 2+1 dimensional space, using the Suzuki-Trotter mapping. The model can be seen as two coupled RSOS (restricted solid-on-solid) surfaces. The solid-on-solid models[46] are classical models for surface roughening. They describe stacks of atoms of integer height in two dimensions, with an interaction between adjacent stacks depending on the height differences. With this construction overhangs are excluded. In the restricted SOS models these height differences are limited to be smaller or equal to some integer n . In the present case, the two RSOS models parametrize the motions of the world sheet in the spatial x - and y directions, respectively, while the (strong) couplings between the two takes care of the integrity of the world sheet as a whole.

In the Suzuki-Trotter[54] or Feynman path integral picture (section 2.3.1) one writes the finite temperature partition function as an infinite product over infinitesimal imaginary time slices. In this limit the commutators between the various terms in the Hamiltonian vanish like $1/n^2$, where n is the number of Trotter slices, and the partition function can be written as,

$$Z = \lim_{n \rightarrow \infty} \text{Tr} \left(e^{\frac{\mathcal{H}_{CI}}{n}} e^{\frac{\mathcal{H}_Q}{n}} \right)^n. \quad (3.3.1)$$

To show the relation with RSOS models, we will cast the transfer matrices T in the form of a two-dimensional classical effective Hamiltonian. This implies writing the matrix elements of the T -matrix between configurations $\{\mathbf{r}_l\}$ in terms of an effective classical energy depending on the worldsheet positions $\{\mathbf{r}_{l,k}\}$, where k is the imaginary time index running from 1 to n with periodic boundary conditions. Schematically,

$$\lim_{n \rightarrow \infty} \langle \{\mathbf{r}_l\}_k | e^{\frac{1}{n} \mathcal{H}} | \{\mathbf{r}_l\}_{k+1} \rangle \rightarrow e^{\mathcal{H}_{eff}(\{\mathbf{r}_l\}_k, \{\mathbf{r}_l\}_{k+1})}. \quad (3.3.2)$$

Since \mathcal{H}_{CI} is diagonal in the real-space string basis, it is already in the required form,

$$\lim_{n \rightarrow \infty} \langle \{\mathbf{r}_l\}_k | e^{\frac{1}{n} \mathcal{H}_{CI}} \rightarrow e^{\frac{1}{n} \mathcal{H}_{CI}(\{\mathbf{r}_l\}_k)} \langle \{\mathbf{r}_l\}_k|. \quad (3.3.3)$$

For \mathcal{H}_Q a few more steps are needed,

$$\begin{aligned} & \langle \{\mathbf{r}_l\}_k | e^{\frac{1}{n} \mathcal{H}_Q} | \{\mathbf{r}_l\}_{k+1} \rangle \\ &= \langle \{\mathbf{r}_l\}_k | \sum_{m=0}^{\infty} \frac{1}{m!} \left(\frac{\mathcal{H}_Q}{n} \right)^m | \{\mathbf{r}_l\}_{k+1} \rangle \\ &= \langle \{\mathbf{r}_l\}_k | 1 + \frac{\mathcal{H}_Q}{n} | \{\mathbf{r}_l\}_{k+1} \rangle + \mathcal{O}\left(\frac{1}{n^2}\right) \\ &= \prod_l \prod_{\alpha=x,y} (\delta(\alpha_{l,k+1} - \alpha_{l,k}) \\ &\quad + \frac{\mathcal{T}}{n} \delta(|\alpha_{l,k+1} - \alpha_{l,k}| - 1)) \\ &= e^{\sum_l \ln\left(\frac{\mathcal{T}}{n}\right) [\delta(|x_{l,k+1} - x_{l,k}| - 1) + \delta(|y_{l,k+1} - y_{l,k}| - 1)]}. \end{aligned} \quad (3.3.4)$$

The expression in the last line is of course only valid for states in which the α_l 's in successive time slices differ by at most one unit. Combining these two energy contributions we arrive at the following classical problem,

$$\begin{aligned} Z &= \lim_{n \rightarrow \infty} \text{Tr} e^{\mathcal{H}_{eff}} \\ \mathcal{H}_{eff} &= \sum_{l,k} \left[\frac{\mathcal{K}}{n} \delta(|x_{l+1,k} - x_{l,k}| - 1) \delta(|y_{l+1,k} - y_{l,k}| - 1) \right] \end{aligned}$$

$$\begin{aligned}
& + \sum_{i,j=0}^2 \frac{\mathcal{C}_{ij}}{n} \delta(|x_{l+1,k} - x_{l-1,k}| - i) \delta(|y_{l+1,k} - y_{l-1,k}| - j) \\
& + \frac{M}{n} \sum_m \delta(x_{l,k} - x_{m,k}) \delta(y_{l,k} - y_{m,k}) \\
& + \ln\left(\frac{\mathcal{T}}{n}\right) [\delta(|x_{l,k+1} - x_{l,k}| - 1) \\
& \quad + \delta(|y_{l,k+1} - y_{l,k}| - 1)].
\end{aligned} \tag{3.3.5}$$

This classical world sheet is constrained to $|x_{l,k+1} - x_{l,k}| \leq 1$ and $|y_{l,k+1} - y_{l,k}| \leq 1$, and the interactions are anisotropic. The above classical model can be viewed as two coupled two-dimensional RSOS surfaces, $x_{l,k}$ and $y_{l,k}$. The x coordinate of hole l at the time slice k is now identified as the height of an RSOS column positioned at (l, k) in the square lattice. In a similar way the y coordinates define a second RSOS surface, coupled strongly to the first by the above classical interactions. Since the steps Δx can at most be equal to 1, the RSOS sheets are restricted to height differences 0, ± 1 between neighboring columns. The classical model as defined above is not unique. While the above mapping allows us to exploit the connection to other models most efficiently, for the numerical Monte-Carlo calculations a different decomposition is used, which allows for a more efficient approach to the time continuum limit. This is further discussed in the appendix.

3.4 Spontaneous orientation of the quantum lattice string.

It is actually not easy to find any similarity of the statistical physics problem of the previous section with any existing model. RSOS problems are well understood, but it should be realized that in the present model the two RSOS problems are strongly coupled, defining a novel dynamical problem. When we studied this problem with quantum Monte-Carlo, we discovered a generic zero temperature symmetry breaking: although the string can be quantum delocalized, it picks spontaneously a *direction* in space. This symmetry breaking happens always in the part of parameter space which is of physical relevance. At first sight, one might expect that the quantum fluctuations (kinetic energy) would tend to disorder the string, i.e., to decrease the tendency for the string to be directed. That the opposite effect happens, can be seen as follows. A first intuition can be obtained by considering the analogy with surface statistical mechanics. As showed in the preceding section, the quantum string problem can be formulated as a classical problem of a two dimensional surface (world sheet) in 2+1 dimension, where the third direction is the imaginary time direction. The larger the kinetic term, or the smaller the temperature, the further the world-sheet stretches out in the time direction. At zero temperature, the worldsheet becomes infinite in this direction as well. The statistical physics of a string is then equivalent to that of a fluctuating sheet in three dimensions. Now, it is well known from studies of classical interfaces[55] that while a one-dimensional classical interface in two dimensions does not stay directed due to the strong fluctuations, for a two-dimensional sheet the entropic

fluctuations are so small that interfaces can stay macroscopically flat in the presence of a lattice[56, 57] — for this reason, the roughening transition in a three-dimensional Ising model is properly described by (i.e., is in the same universality class as) a Solid-on-Solid model in which overhangs are neglected[56, 57]. In other words, even if microscopic configurations with overhangs are allowed, a classical interface on a lattice in three dimensions can stay macroscopically flat or "directed", in agreement with the findings from our specific model which we will present here. In the present context, we will show that the directedness is caused by an order-out-of-disorder mechanism: in order to maximize the fluctuations transversal to the local string directions, overhangs should be avoided on the worldsheet. It remains to be seen if this mechanism is of a more general application.

The string model introduced in section 3.2 is invariant under rotation of the string in space. As will be discussed below, we find that for physical choices of the parameters the invariance under symmetry operations of the lattice is broken. The string acquires a sense of *direction* in space. This occurs even when the string is critical (delocalized in space). The string's trajectories, on average, are such that they move forward in one direction while the string might delocalize in the other direction.

Let us now discuss the numerical results. It is clear that the directedness property is a *global* quantity. For a string living in 2D lattice with open boundary conditions, directedness means that if it starts at, say, the left boundary it has to end at the right boundary and will never end at the top or the bottom boundaries of the lattice. Although in the above model one can introduce a local order parameter to measure the directedness of a string, a more general quantitative measure for this global property can be constructed. This measure is not easily evaluated analytically but it can easily be calculated numerically; most importantly it illustrates clearly and effectively the directedness phenomenon. Every string configuration s defines a curve in the 2D space $[x(t), y(t)]$, where t could for instance be the discrete label of the successive particles along the string. When this curve can be parametrized by a *single-valued* function $x(y)$ or $y(x)$, we call the string configuration directed. The quantum string vacuum is a linear superposition of many string configurations. When all configurations in the vacuum correspond to single valued functions $x(y)$ or $y(x)$, the string vacuum is directed. At zero temperature, the ground state wave function of the string is

$$|\Psi_0\rangle = \sum_{\{x_l, y_l\}} \alpha_0(\{x_l, y_l\}) |\{x_l, y_l\}\rangle, \quad (3.4.1)$$

where every state in the string configuration space ($|\{x_l, y_l\}\rangle$) corresponds to a trajectory $[x(t), y(t)]$. Consider first the case of a continuous string. For every configuration, the total string arclength is given by

$$L(\{x_l, y_l\})_{tot} = \int ds = \int \sqrt{dx^2 + dy^2}. \quad (3.4.2)$$

Consider now an indicator function $g_y(x)$ which equals 1 when the string is single valued when projected onto the x -axis, and zero otherwise, and analogously a function $g_x(y)$

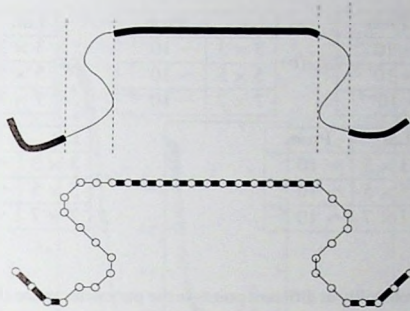


Figure 3-3. Illustration of the way we measure the directedness of a string in the continuum case (a) and on the lattice (b). The heavy solid parts of the string indicate the parts where the projection of the string onto the x axis is single-valued, and for which the indicator function $g_y(x)$ equals 1.

which equals 1 when the curve is single-valued when projected onto the y -axis, and zero otherwise (see Fig. 3-3). The total directed lengths in the x and y directions are defined as

$$\begin{aligned} L(\{x_l, y_l\})_{dir,x} &= \int dx g_y(x) \sqrt{1 + \left(\frac{dy}{dx}\right)^2}, \\ L(\{x_l, y_l\})_{dir,y} &= \int dy g_x(y) \sqrt{1 + \left(\frac{dx}{dy}\right)^2}. \end{aligned} \quad (3.4.3)$$

The measure of directedness is then defined as the larger of $N_{dir}^x(0)$ and $N_{dir}^y(0)$, where

$$N_{dir}^\eta(0) = \sum_{\{x_l, y_l\}} |\alpha_0(\{x_l, y_l\})|^2 \frac{L(\{x_l, y_l\})_{dir,\eta}}{L(\{x_l, y_l\})_{tot}}, \quad (3.4.4)$$

and $\eta = x, y$. On the lattice, one measures the directedness in analogy with the above definition, except that we just count the number of directed bonds, irrespective of whether they are oriented diagonally or horizontally. The finite temperature measure of the directedness density is simply given by thermally averaging the above definition.

$$N_{dir}^\eta(T) = \sum_n e^{-\beta(E_n - E_0)} N_{dir}^\eta(n), \quad (3.4.5)$$

where $N_{dir}^\eta(n)$ is the directedness density of an excited string with energy E_n .

To study the directedness property we performed exact diagonalization and quantum Monte-Carlo studies. Although the quantum Monte-Carlo study is the more extensive one

(a)	Lat.	Prob.	(b)	Lat.	Prob.	(c)	Lat.	Prob.
	3×3	$\sim 10^{-1}$		3×3	$\sim 10^{-1}$		3×3	$\sim 10^{-2}$
	5×5	$\sim 10^{-5}$		5×5	$\sim 10^{-3}$		5×5	$\sim 10^{-5}$
	7×7	$\sim 10^{-11}$		7×7	$\sim 10^{-9}$		7×7	$\sim 10^{-10}$

(d)	Lat.	Prob.	(e)	Lat.	Prob.
	3×3	$\sim 10^{-2}$		3×3	$\sim 10^{-1}$
	5×5	$\sim 10^{-4}$		5×5	$\sim 10^{-4}$
	7×7	$\sim 10^{-6}$		7×7	$\sim 10^{-7}$

Table 3-1. Tunnelling probability at different points in the parameter space (K , \mathcal{L}_{12} , \mathcal{L}_{22}) (a) (0,0,0), (b) (0, -0.25, -1.0), (c) (6.0, -3.0, -2.0), (d) (7.0, -4.0, -6.0), (e) (3.0, -3.25, -3.0).

we start by discussing the exact diagonalization results, as it will give a clear indication for the symmetry breaking directly at zero temperature. Here we consider an $N \times N$ lattice. We think of a string living in such a finite lattice as part of an infinite one and therefore the ends of the string should live on the boundaries of the cluster. To fix the length of the string inside the cluster, we take as a criterion that the energy per particle be minimum. We plot the energy per particle versus the number of particles in the string. The minimum defines the optimal length of a string in the cluster. Upon setting the parameter \mathcal{L}_{11} to zero and investigating different points in the parameter space, we found that the optimal length one should consider is the linear dimension of the lattice. Therefore in an $N \times N$ lattice we will consider a string of length N . Such a string can be directed along the x (horizontal) or y (vertical) direction. If the directedness assumption is fulfilled, the Hilbert space will effectively split into two subspaces: strings directed along the x direction and those along the y . If nondirected strings are present there should be a non-zero tunnelling probability between the two sectors. By measuring the probability to tunnel from the x - to the y -sectors as a function of the linear dimension of the system, it should be possible to see the tendency towards spontaneous directedness symmetry breaking in the thermodynamic limit. Table 3-1 gives this tunnelling probability for different points in the parameter space. For all cases we set $\mathcal{L}_{11} = 0$. The choice of these points was motivated by the directed string problem[34]. The data are shown for lattices up to 7×7 . For a 9×9 lattice the tunnelling probability turns out to be less than the accuracy of our numerical technique.

These results clearly indicate that in the thermodynamic limit there is no tunnelling between the two sectors and the string should be directed either along the x or the y direction.

3.5 Directedness at low but finite temperature

We subsequently used quantum Monte-Carlo to calculate the directedness density as a function of temperature. Eq. (3.4.5) can be straightforwardly calculated using quantum

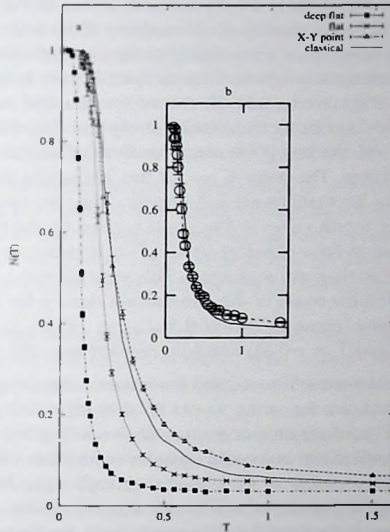


Figure 3-4. A Monte-Carlo result for the directedness density $N_{dir}(T)$ at 4 points. (a) The XY point (Triangles) where all curvature energy are zero. Two points in the flat phase, with $K = 1.8$ (crosses) and $K = 4.0$ (filled squares) the rest of the curvature energies are zero. (b) Inset: A point in the middle of the gaussian phase with parameters $K = 0.5$, $L_{21} = -0.25$, $L_{22} = -1.0$, $L_{11} = 0$ (open circles). The full line in both figures is the result for a classical string where only flat bonds and $\frac{\pi}{2}$ corners are present with $L_{11} = 1$.

Monte-Carlo. A Monte-Carlo snapshot defines a stack of coupled string configurations along the imaginary time direction (the Trotter direction). We calculate N_{dir}^x for every Trotter slice by calculating the fraction of the string length in this configuration which is single valued in the x -direction. This is given by the number of bonds which step forward in the x -direction divided by the total number of bonds in the string. We then average this quantity over the string world sheet (Trotter direction) and then over the Monte-Carlo measurements. The same is done for $N_{dir}^y(n)$. The larger of $N_{dir}^x(n)$ and $N_{dir}^y(n)$ is then the density of directedness at the given temperature.

In Fig. 3-4 we show results of typical Monte-Carlo calculations for the density of directedness as a function of temperature $N_{dir}(T)$. We have considered four points in parameter space; as will be discussed later, these points are representative for phases with interest-

ing quantum fluctuations, and serve to clarify our conclusion. In Fig. 3-4(a) the triangles (dashed line) are the result for the density of directedness at the point where all the classical curvature energies are zero, i.e., corresponding to the pure quantum string. The crosses (dotted line) and the filled squares (dashed-dotted line) are the results for points where $\mathcal{K} = 1.8$ and $\mathcal{K} = 4.0$, respectively, and the rest of the classical curvature energies are zero. In terms of the phase diagram for the directed string problem of Fig. 3-8 in section VI and Table 3-4 in section VII, the first point corresponds to a Gaussian string and the other two correspond to flat strings. The point $\mathcal{K} = 1.8$ lies just inside the flat string phase II where significant quantum fluctuations are still present, while the point $\mathcal{K} = 4.0$ lies deep inside the flat phase. The fourth curve in Fig. 3-4(a), given by the full line, is the result of a Monte-Carlo calculation for a classical string ($T = 0$) where only flat segments and $\pi/2$ corners are allowed (no diagonal segments). This same classical result is shown again in Fig. 3-4(b) together with the result of the directedness density for a point in the middle of the Gaussian (XY) phase, phase IV, [$\mathcal{K} = 0.5$, $\mathcal{L}_{21} = -0.25$, $\mathcal{L}_{22} = -1.0$, $\mathcal{L}_{11} = 0$ corresponding to $D = 0$ and $J = -0.5$], which correspond to a critical string.

Consider first the classical limit ($T = 0$, and for instance the energy of the $\pi/2$ corner $\mathcal{L}_{11} = 1$). At zero temperature the string would be straight, running along (say) a (1,0) direction. A local 'corner' configuration of the type shown in Fig. 3-2a would be an excitation with energy \mathcal{L}_{11} (alternatively, one could consider two kinks). Clearly, a single corner suffices to destroy the directedness of the classical ground state. At any finite temperature, the probability of the occurrence of at least one corner is finite: $P = N \exp(-\beta \mathcal{L}_{11})$. Hence, directedness order cannot exist at finite temperatures, for the same reasons that long range order is destroyed at any non-zero temperature in one dimension. In the simulations the string is of finite length, and the infinite temperature limit of $N_{dir}(T)$ is therefore not zero but rather a small but nonzero value[74] (~ 0.03 for a domain wall of length 50). $N_{dir}(T)$ is already close to this value for all temperatures of order \mathcal{L}_{11} and larger. For an infinitely long domain wall $N_{dir}(T)$ drops very fast to zero with increasing temperature. At the other limit, for low T where $T \ll \mathcal{L}_{11}$, $N_{dir}(T)$ grows very rapidly to 1. Again because the string is of finite length, it becomes directed already at a finite temperature: for all temperatures such that $L \exp(-\beta \mathcal{L}_{11}) < 1$ the string configurations in our simulations are typically completely directed. An infinitely long classical string becomes directed only at $T = 0$, of course, since at any nonzero temperature always some corners will occur in a sufficiently long string.

For the quantum string, all the curves look strikingly similar to the classical one. When the temperature is very much higher than the kinetic term, $T \gg T_c$, all curves merge together and the classical limit is reached. At low T , where $T \ll T_c$, $N_{dir}(T)$ again grows very fast to 1, as in the classical case; it reaches this value at a finite temperature for the finite length string. This is even true for the purely quantum string at the XY point, where all classical microscopic curvature energies are zero (see the dashed line in Fig. 3-4(a)). We can understand this in terms of an effective corner or bend energy $\tilde{\mathcal{L}}$ that is produced by the quantum fluctuations. As in the classical case the probability for the occurrence of a bend is proportional to $\sim \exp(-\beta \tilde{\mathcal{L}})$. At zero temperature no bend is present and the string becomes directed. A finite length string effectively becomes directed already at a temper-

ature such that $L \exp(-\beta \tilde{\mathcal{L}}) < 1$. At intermediate temperatures, where the temperature is of the order of the kinetic term, things are more difficult and it is far from obvious what is going on. Especially in this region, all the various classical curvature energies may play a role, and the interplay of these on the directedness is unclear. Nevertheless, as is clear from the data of Fig. 3-4(a), this region connects the high and low temperature limits smoothly. Moreover, by comparing the results for the three quantum strings in this figure it is also clear that $N_{dir}(T)$ is higher when the string is more quantum mechanical.

I end this part by giving a brief qualitative description of observations concerning spontaneous directedness at low but finite temperatures in regions of the phase diagram where the directed string has other type of ordering than that already discussed above. All the results apply to $\mathcal{L}_{11} = 0$, and we refer to Table 3-4 in section 3.8 for a quick introduction to the various phases of the directed string problem and for the numbering (I-X) of the various phases.

— The entire zero temperature phase diagram of the directed string is reproduced.

— Phase I is very stable with respect to bends. With “stable” we mean that *finite* strings do not change their appearance when increasing the temperature from zero to a moderately small temperature, of the order of $0.1 \mathcal{T}$.

— Deep in the horizontal phase II (large positive \mathcal{K}) quantum fluctuations are strongly suppressed, and at the same time the string becomes susceptible to $\pi/2$ corners. On the other hand, when we approach from phase II the boundaries with phases IV and V, the fluctuations increase and the string stiffens, Fig. 3-4. This is in agreement with the picture sketched before that quantum fluctuations orient the string.

— Deep inside phase III the string changes constantly between horizontal zigzags and vertical zigzags. A $\pi/2$ turn costs no extra energy. Again close to phase V quantum fluctuations have the effect of removing bends.

— The Haldane phase V and the rough phase IV are very robust, and a considerable fraction of $\pi/2$ bends occurs only at relatively high temperatures of the order of $0.2 \mathcal{T}$.

— In the slanted phase VII high temperatures are needed before down diagonal links come in. On the other hand horizontal links are easily replaced by vertical ones. This only increases the energy very slightly, but the entropy gain is considerable. A typical low temperature string is shown in Fig. 3-10 in section 3.8. To zeroth order the horizontal and vertical links can be thought of as spinless fermions moving coherently along the string. In the dilute limit these links have only a weak interaction. The order of the links is conserved, and at zero temperature the ground state has only horizontal links. However our simulations indicate that for a small range of negative L_{11} values a diagonal string with alternating horizontal and vertical links is favoured. It is again the kinetic energy of the horizontal and vertical links that keeps the string oriented in the (1,1) direction.

The conclusion we draw from the above extensive Monte-Carlo studies of the behavior in several parts of the phases space, is that *apart from some extreme classical limits, the general lattice string model at zero temperatures is a directed string*. The phase diagram of the general string model introduced in section II will essentially be the same (apart from special limits) as the corresponding phase diagram of the simplified directed string model. In the coming sections of this chapter we will therefore focus on the phases and phase

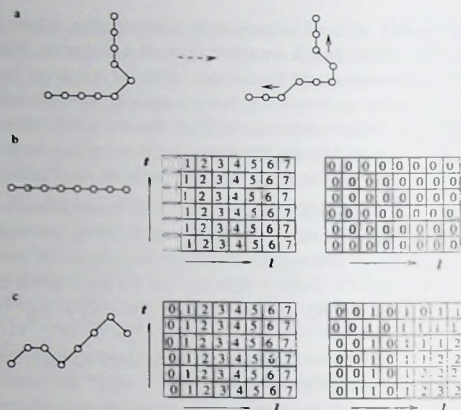


Figure 3-5. (a) An undirected string with two kinks propagating along different directions. Note that the bend blocks the propagation of kinks. (b) a (1,0) string and the corresponding two (coupled) RSOS surfaces along the x and the y directions respectively. The numbers correspond to x (y) position of hole l at imaginary time t . (c) a disordered *directed* string and the corresponding ordered and disordered RSOS surfaces

transitions of the directed string.

Although we have not found yet a formally rigorous description of the directedness symmetry breaking, we can offer a qualitative explanation at least on the level of our specific model. As we showed in the previous section, the string problem can be mapped on the problem of two strongly coupled classical RSOS surface problems. The symmetry breakings of a *single* RSOS surface will be discussed in great detail later, but for the present discussion it suffices to know that such a single surface can be fully ordered, as well as (partly) disordered. Because of the strong coupling, it would a priori appear questionable to discuss the dynamics of the full model of Section II in terms of the dynamics of the two separate RSOS subproblems. However, in the context of directedness it is quite convenient to do so. When both the x and y RSOS problems would be fully disordered, it is easy to see that the string vacuum would be undirected. This is illustrated in Fig. 3-5a: two kinks moving the string from a (1,0) to a (0,1) direction in the lattice correspond with one kink which can move freely in the horizontal part of the string, and one kink which can move freely in the vertical part of the string. On the other hand, when both RSOS problems are ordered, the string is also ordered. For instance, the (1,0) string can be thought of as a combination of an RSOS surface which always steps upwards in the x direction, and one which is horizontal in the y direction (Fig. 3-5b).

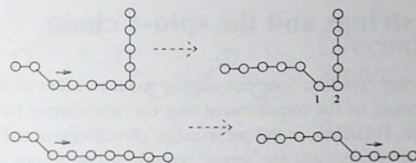


Figure 3-6. Illustration of the fact that a bend blocks the propagation of links along the string. Note holes 1 and 2 cannot move.

A third possibility is that one of the RSOS subproblems is ordered, while the other is disordered. Dismissing crumpled phases (like condensates of the L_{11} type corners), the only possibility remaining is that one of the RSOS problems steps up always, while the other is disordered, as illustrated in Fig. 3-5c. This results in a disordered *directed* string vacuum: the string steps always forward in, say, the x direction while it freely fluctuates in the y direction. Hence, the local order parameter underlying the directedness corresponds with the diagonal flat order (Phase I of fig. 3-8) of at least one of the two RSOS surfaces describing the string.

What is the source of the condensation energy? As we already stated, violation of directedness implies that $\pi/2$ bends occur on the string, equivalent to overhangs on the worldsheet. As can be easily seen, these bends block the propagation of links along the chain. Close to the bend itself the particles in the chain cannot move as freely as in the rest of the chain. This effect is shown in Fig. 3-6. Therefore, the presence of these bends increase the kinetic energy associated with the kink propagation, and it makes no difference whether the bend consists of a single $\pi/2$ corner or two $\pi/4$ corners. This kinetic energy cost disappears when one of the two RSOS surfaces straightens and this drives the directedness condensation. It might be called a quantum order-out-of-disorder mechanism and it is suspected that a theory of the Hartree mean field type can be formulated catching the phenomenon on a more quantitative level (with the kinks playing the role of electrons and the second surface offering the potentials). To emphasize the order-out-of-disorder aspect, it is easy to see that in the classical case, $T = 0$, in many regions of parameter space the problem becomes that of a self-avoiding walk on a lattice in the limit $T \rightarrow 0$ which does not exhibit the directedness order.

Lastly, it is obvious that the directedness order is rather fragile. *It cannot exist at any finite temperature.* When temperature is finite, the width of the worldsheet in the imaginary time direction becomes finite as well, and the long wavelength fluctuations of the string becomes a 1D statistical problem, which cannot be directed.

3.6 Directed strings and the spin-1 chain

Quite generally, the string problem does not simply reduce to that of the internal dynamics of the worldsheet, because of the requirement that the worldsheet has to be embedded in $D+1$ dimensional space. However, in the presence of directedness order and in the absence of particle number fluctuations[42] the string boundary conditions are trivially fulfilled and the string problem is equivalent to that of a single "world sheet" in $1+1$ dimensions. Assume the string to be directed along the x direction. Since the string steps always forward in this direction, the number of particles in the string has to be equal to the number of lattice sites in the x -direction, and every directed string configuration will connect the boundaries in this direction. The string is still free to move along the y direction. Instead of labeling the positions in the 2D plane the string is completely specified by the list of links, for which there are only 3 possibilities (in the $(1, 1)$, $(1, 0)$, or $(1, -1)$ direction), and the position of a single "guider point". As a guider point we can take the position r of any one of the particles, which, together with the relative coordinates given by the links, fixes the position of the entire string. Since the guider represents just a single degree of freedom, and since the thermodynamic behavior of a chain is determined by the link interactions, the guider coordinates will be irrelevant for the behavior of the chain. Apart from this guider degree of freedom the directed string problem reduces to a one-dimensional quantum problem with three flavors.

From Eq. (3.3.5) one directly deduces the Hamiltonian of the string directed along x ,

$$\mathcal{H}_{eff} = \sum_{l,k} \left[\frac{\mathcal{K}}{n} \delta(|y_{l+1,k} - y_{l,k}| - 1) + \frac{\mathcal{L}_{12}}{n} \delta(|y_{l+1,k} - y_{l-1,k}| - 1) + \frac{\mathcal{L}_{22}}{n} \delta(|y_{l+1,k} - y_{l-1,k}| - 2) + \ln\left(\frac{\mathcal{T}}{n}\right) \delta(|y_{l,k} - y_{l,k+1}| - 1) \right]. \quad (3.6.1)$$

It is clear that the directedness simplifies the model considerable. The directed version can not self-intersect, and the excluded volume constraint is satisfied automatically. Furthermore the \mathcal{L}_{11} -type of configurations are not allowed, thus the directed model is specified by three parameters and the temperature ($\mathcal{T} = 1$). Because of the preceding considerations, Eq. (3.6.1) corresponds with a $1+1$ D problem, which is actually equivalent to a general quantum spin-1 chain.

We identify the spin with the string *height difference* $y_{l+1} - y_l$, which can be either 0, 1 or -1 , see Fig. 3-7. These link dynamical variables specifying the string can be directly identified with the $m_s = 0, \pm 1$ variables of the spins living on the sites of the spin chain. Defining the latter using hard core bosons b_m^\dagger , the spin operators for the $S = 1$ case become $S^- = b_1^\dagger b_1 - b_{-1}^\dagger b_{-1}$, $S^+ = \sqrt{2}(b_1^\dagger b_0 + b_0^\dagger b_{-1})$ and by comparing the action of the spin- and string operators on their respective Hilbert spaces one arrives at operator identities[47]. A quantum hop from y to $y + 1$ increases the height difference on the left of l by one, and decreases it by one on the right, as is easily seen by inspecting the two hopping terms in

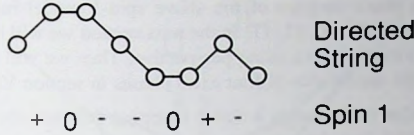


Figure 3-7. The relation between spin-1 and directed strings, $S_l^z = y_{l+1} - y_l$.

Fig. 3-2. Therefore [47],

$$\begin{aligned}
 S_l^z &= y_{l+1} - y_l, \\
 S_{l-1}^\pm S_l^\mp &= 2P_{Str}(y_l - y_{l-1})P_{Str}(y_{l+1} - y_l)e^{\pm i\pi l}.
 \end{aligned} \tag{3.6.2}$$

The following identities, for $S = 1$,

$$\begin{aligned}
 \delta(|y_{l+1} - y_l| - 1) &= (S_l^z)^2, \\
 \delta(|y_{l+1} - y_{l-1}| - 1) &= (S_l^z)^2 + (S_{l-1}^z)^2 - 2(S_l^z S_{l-1}^z)^2, \\
 \delta(|y_{l+1} - y_{l-1}| - 2) &= \frac{1}{2}S_l^z S_{l-1}^z [1 + S_l^z S_{l+1}^z],
 \end{aligned} \tag{3.6.3}$$

are easily checked. The directed string problem can now be reformulated in spin language as,

$$\begin{aligned}
 \mathcal{H}_{spin} = \sum_l & \left[(\mathcal{K} + 2\mathcal{L}_{12})(S_l^z)^2 + \frac{\mathcal{L}_{22}}{2}S_l^z S_{l-1}^z \right. \\
 & + \left(\frac{\mathcal{L}_{22}}{2} - 2\mathcal{L}_{12} \right) (S_l^z S_{l-1}^z)^2 \\
 & \left. + \frac{\mathcal{T}}{2}(S_l^+ S_{l-1}^- + S_l^- S_{l-1}^+) \right].
 \end{aligned} \tag{3.6.4}$$

Following the spin-1 literature we define the following parameters,

$$\begin{aligned}
 D &= \mathcal{K} + 2\mathcal{L}_{12}, \\
 J &= \mathcal{L}_{12}/2, \\
 E &= \mathcal{L}_{22}/2 - 2\mathcal{L}_{12}.
 \end{aligned} \tag{3.6.5}$$

The E term is new. It is a quartic Ising term, leading to extra phases and phase transitions. For the special choice $E = 0$ ($\mathcal{T} = 1$), the above Hamiltonian reduces to the familiar XXZ model with on-site anisotropy,

$$\mathcal{H}_{XXZ} = \sum_l \left[D(S_l^z)^2 + JS_l^z S_{l-1}^z + \frac{1}{2}(S_l^+ S_{l-1}^- + S_l^- S_{l-1}^+) \right]. \tag{3.6.6}$$

The zero temperature phase diagram of the above spin-1 model has been discussed in detail in the literature. [58, 59, 60, 61, 47] In the next section we will briefly review the six phases found for this model, from a string perspective. Then we will show that a nonzero E parameter leads to the appearance of four extra phases in section VII.

Den Nijs and Rommelse [47] discuss a direct mapping between the spin chain and the RSOS surface. We stress that this mapping in fact involves two steps: First the RSOS model is mapped on a string problem, using the T matrix. Then the spins are identified as shown above. Thus the quantum string is a *natural intermediate* of the two other models. Den Nijs and Rommelse make use of the freedom in the choice of the T matrix to define a mapping which is slightly different from ours, since they introduce a transfer matrix along a diagonal, while we introduce one along the x -direction. As a result, in their case there are only interactions between next nearest neighbors along the $(1, 1)$ direction, while our choice allows for interactions between next nearest neighbors along the x -direction. Therefore, our RSOS model differs slightly from theirs.

The RSOS representation is more transparent than the quantum model. The spin-1 phases and the nature of the phase transitions all have a natural interpretation in space-time. For instance the Haldane phase, or AKLT wavefunction, with its mysterious hidden string order parameter is identified as a "disordered flat" RSOS surface [47] with a simple local order parameter. The height representation, dual to the spins, gives a similar local order parameter for the quantum string.

3.7 The phases ($E=0$)

In this section we will simplify the general string Hamiltonian by leaving out the quartic Ising term ($E = 0$ in Eqs. (3.6.4) and (3.6.5)). The string problem is now equal to the spin-1 XXZ model. The zero-temperature phase diagram of the string problem is surprisingly rich, and even for the case $E = 0$ there are 6 phases and a large variety of phase transitions. These phases can be classified in three groups: classical strings localized in space, quantum rough strings of the free variety, and partly delocalized phases of which the disordered flat phase is a remarkable example. In this section we will briefly review the six phases as discussed in the literature on the spin-1 XXZ problem (3.6.6). The problem will be addressed from the quantum string perspective. For more details we refer to Ref. [47]. In the next section it will be shown that with a finite $E > 0$ four additional phases are stabilized.

The phase diagram of the quantum string is shown in Fig. 3-8, as a function of D and J . The XXZ model parameters, defined in Eq. (3.6.5), have been used such that the phase diagram can be compared directly with the spin-1 literature [58, 59, 60, 61] and in particular with Fig. 13 of Ref. [47]. The various order parameters that have been introduced in this reference to distinguish the six phases in this phase diagram will be introduced below. The relation between the more general ($E \neq 0$) string and spin phases will be clarified in the next section.

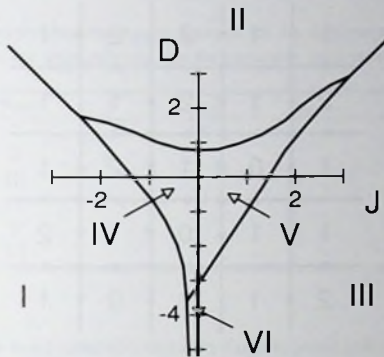


Figure 3-8. The phases and phase transitions of the directed quantum string as a function of the on-site anisotropy D and the Ising interaction J of the corresponding spin-1 XXZ model. The parameter E is set to zero.

There is first of all a horizontal and a diagonal string phase. In the diagonal phase I no quantum fluctuations are allowed, since a diagonal string does not couple to other states by \mathcal{H}_Q (this is illustrated in Fig. 3-13 of the appendix, to which we refer for further details). This phase is stabilized by a large and negative \mathcal{L}_{22} , so that since $E = 0$ also $J = \mathcal{L}_{12}/2 = \mathcal{L}_{22}/8$ is large and negative. A suitable variable introduced to define order parameters, following Ref. [47], is the Ising spin variable $\sigma_l = (-1)^{y_l}$, which identifies whether a given height is in an even or odd layer. This underlying spin model can have "ferromagnetic" or antiferromagnetic" order, and so we introduce the corresponding order parameters[62]

$$\begin{aligned} \rho &= \langle \sigma_l \rangle, & \rho_{stag} &= \langle (-1)^l \sigma_l \rangle, \\ \rho_{str} &= \langle \sigma_l (y_{l+1} - y_l) \rangle. \end{aligned} \quad (3.7.1)$$

Here the brackets denote the ground state expectation value as well as an average over string segments l . In (3.7.1), we have also included the order parameter ρ_{str} discussed below. In the horizontal phase II one particular height is favoured, thus the order parameter ρ is nonzero here. This phase is stabilized by a large positive \mathcal{K} , which suppresses diagonal links. However \mathcal{H}_Q causes virtual transitions from two horizontal links into two diagonal ones, see Fig. 3-2. On the 2D worldsheet these fluctuations show up as local terraces that do not overlap and thus do not destroy the long-range order. In both phases the elementary excitations are gapped.

Upon lowering \mathcal{K} the terraces grow and at some point they will form a percolated network

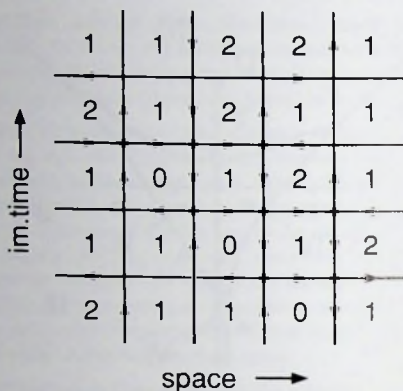


Figure 3-9. Vertices (thick dots) on the space, imaginary time string worldsheet. The numbers correspond to the heights $y_{l,t}$. Arrows are drawn when the heights of neighbors differ. When four arrows occur at a crossing point this is called a vertex.

— the string has become disordered in both space and imaginary time. Via the well-known Kosterlitz-Thouless roughening transition[56] phase IV is entered for $J < 0$. This phase belongs to the well known XY universality class, characterized by algebraic correlation functions and gapless meandering excitations. The roughness, however, is extremely “soft” and the height difference diverges only logarithmically, $\langle (y_l - y_m)^2 \rangle \sim \ln |l - m|$. The transition from the Gaussian phase, which is rough and on average oriented horizontally, to the “frozen” diagonal phase is a “quasi first-order” KDP transition[47].

For large negative K diagonal links are favored over horizontal ones. There is a transition to a second rough phase (phase VI). It is distinguished from the first by the order parameter ρ_{stag} , which is zero in phase IV. In this phase horizontal links are virtual and occur in pairs. As we will discuss later in section 3.8, for large negative K the model can therefore be reduced to an effective spin 1/2 problem.

For negative K and positive J ($=\mathcal{L}_{22}/2$) the string becomes a (physically unlikely) zigzag with alternating up and down diagonal pieces. Excitations to pairs of horizontal links are gapped. Again $\rho_{stag} = \langle (-1)^{-l} \sigma_l \rangle$ serves as an order parameter. Upon increasing K the islands formed by pairs of horizontal links start to overlap and there is an Ising transition into the Haldane or disordered flat (DOF) phase.

The point $J = 1, D = 0$ belongs to the gapped DOF phase, in agreement with Haldane's educated guess[63, 64] that integer spin chains are gapped at the Heisenberg antiferromagnetic point. In this “disordered horizontal” string phase the prototype wavefunction, equal

Table 3-2. Order parameters that distinguish between the six different phases in the phase diagram for $E = 0$. A + entry in the table indicates that the particular order parameter is nonzero.

Phase	ρ	ρ_{stag}	ρ_{sir}	ρ_{slope}
I		+		+
II	+			
III		+	+	
IV				
V			+	
VI		+		

to the AKLT valence bond state[65], has every up diagonal link followed by a down link, with a random number of horizontal links in between. The height y_l takes just two values, say 0 and 1. The local order parameter is, ρ_{sir} , defined in (3.7.1). This order parameter measures the correlation between the next step direction and whether one is in a layer of even or odd height. When $\rho_{sir} = 1$, the string just steps up and down between two layers, but the steps can occur at arbitrary positions. Note that the height is a global quantity in spin language, i.e., it is the accumulated sum over spins, $y_l = \sum_{m=0}^l S_m^z$. Because of this the above order parameter becomes non-local when rewritten in terms of the "string" of spins. Therefore, it is often called the string order parameter. This name will also be used, but it should be stressed that the "string of spins" to which this name refers should not be confused with the general strings which are the basis of the model, and that the other order parameters are nonlocal as well in terms of the original spins S .

This phase diagram can be rationalized by writing the RSOS problem as the product of a 6-vertex model and the 2D Ising model of s spins on the 6-vertex lattice, as discussed in detail by Den Nijs and Rommelse [47]. The horizontal, diagonal, zigzag but also the second rough phase VI all correspond to Ising order: $\rho = \langle \sigma_l \rangle$ is nonzero in the horizontal phase II, while $\rho_{stag} = \langle (-1)^l \sigma_l \rangle$ is nonzero in the diagonal phase I, the zigzag phase III and the rough phase VI. The six-vertex part is defined on the crossing points of steps on the surface — see Fig. 3-9. This is a (sometimes highly) diluted set of points. The Ising degree of freedom disorders on the transition between the phases III and V, and between IV and VI, while the six-vertex part remains unchanged. Therefore these transitions are Ising like. Transitions $I \rightarrow IV$, $I \rightarrow VI$, $IV \rightarrow V$ and $III \rightarrow VI$ are related to the six-vertex part becoming critical, and these KDP and KT transitions are known from the quantum spin-1/2 chain. The transition II to IV is related to the famous surface-roughening transition, of the Kosterlitz-Thouless type.[56, 57] The subtle transition between phase II and V, is coined "preroughening transition" by den Nijs. It separates two gapped phases. At the transition the gap closes and the system is Gaussian, with varying exponents along the transition line.[58, 59, 60, 61]

Almost all the phases can be distinguished by the above order parameters ρ , ρ_{stag} and ρ_{sir} ,

1

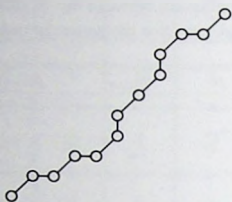


Figure 3-10. A typical low temperature string in the slanted parameter region VII.

except that these do not discriminate between the diagonal phase I and the rough phase VI. These two phases can be identified by also introducing an order parameter which detects the presence of an average slope, $\rho_{slope} = \langle y_{l+1} - y_l \rangle$. In Table 3-2 we list the various phases for $E = 0$ and the order parameters.

As we shall see in the next section, in the general case $E \neq 0$ it is more convenient to introduce slightly different spin variables to identify all the ten different phases that occur then. The choice of Ref. [47] discussed here is somewhat more convenient for understanding the universality classes of the various phase transitions.

3.8 The full phase diagram

As mentioned above the quartic Ising term with prefactor E generalizes the XXZ Hamiltonian and leads to extra phases. Below it will motivate that four extra phases are to be expected, and show that they are stabilized by a positive E parameter. The most disordered phase is still the Gaussian phase.

Using a similar decomposition as above, one can determine how many different phases to expect for a general spin-1 chain with z -axis anisotropy and nearest-neighbor interactions[66]. Think of the spin 1 as consisting of two spins $\frac{1}{2}$, see Table 3-3. The first is $\sigma^z = \downarrow$ when the spin 1 has $S^z = 0$ and $\sigma^z = \uparrow$ when $S^z = \pm 1$, similar to the Ising degree of freedom defined above. This spin thus indicates the presence or absence of a step. The

Table 3-3. Spin 1 S seen as a combination of two spins $1/2$, σ and s .

S	1	0	-1
σ	\uparrow	\downarrow	\uparrow
s	\uparrow	-	\downarrow

second spin $\frac{1}{2}$ s , is defined as $s^z = S^z/2$ when $S^z = \pm 1$ and is absent when $S^z = 0$. This is related to the diluted vertex network discussed by den Nijs and Rommelse, in that if there is a step, the z -component of s indicates whether this step is up or down. The spins s can have ferromagnetic (F) or antiferromagnetic (AF) order, or they can be disordered (D). For σ the two ferromagnetic cases correspond to different physical situations, and we have to distinguish ferromagnetic \downarrow (F2), a horizontal string, from ferromagnetic \uparrow (F1). When σ has F2 order, s becomes irrelevant (or better — there are disconnected finite terraces of s spins with short-range correlations). Therefore one expects 10 phases, depending on the order of the two spin species: 1 F2 phase, 3 F1 phases, 3 σ -disordered phases, and 3 σ -antiferromagnetically ordered phases. These are listed in Table 3-4. An example of a phase diagram in a case in which all ten phases are present is shown in Fig. 3-12, which corresponds to the case $E = 5$. The detailed of how this phase diagram was obtained will be discussed below.

There are four new phases, VII to X, compared to the phase diagram discussed in the previous section. All four are stabilized by a positive E parameter in Eq. (3.6.4). Three phases, VIII to X, result from an antiferromagnetic order of the σ spin. This corresponds to alternating horizontal and diagonal string links (see Table 3-4). The diagonal links can be either all up (FM, phase VIII), alternatingly up and down (AFM, phase X) or disordered (phase IX). In phase VII the σ spin is disordered, while the s spin is in the FM phase. This is a diagonal wall diluted with horizontal links. These links coherently move up and down along the wall, lowering the kinetic energy. The wall can take any average angle between $-\pi/4$ and $\pi/4$, and this angle is fixed by the value of the parameters. This has been called the "slanted" phase [22]. In terms of the decomposition into an Ising spin model and a six-vertex model of den Nijs and Rommelse it is easy to see that the horizontal links change the orientation of the Ising spin and act like a Bloch wall. The Ising spin is therefore disordered. The six-vertex term is irrelevant for the existence of the slanted phase — in the case of a single horizontal link, i.e., on the boundary between the slanted and diagonal string phase, there are no vertices.

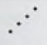

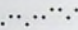
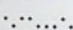
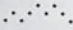
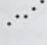
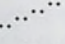
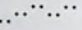

As shown in Ref. [22], a large part of the phase boundaries can be estimated exactly, almost exactly, or to a fair approximation. Here it will be shown how this is done and later I will summarize the numerical analysis results used to fill the details of the phase diagram.

Firstly, focus on the classical phases. The diagonal, horizontal and zigzag phases have the following energies in the classical approximation in which there are no fluctuations, as is easily verified,

$$\begin{aligned} E_I &= L(K + \mathcal{L}_{22}) = L(D + J + E), \\ E_{II} &\approx 0, \\ E_{III} &\approx LK = L(D - J + E). \end{aligned} \quad (3.8.1)$$

where L is the length of the chain. The first-order transitions will therefore occur close to the lines $K = -\mathcal{L}_{22}$ ($D = -J - E$) between phases I and II, $\mathcal{L}_{22} = 0$ ($J = 0$) between phases I and III, and $K = 0$ ($D = J - E$) between phases II and III. These transitions become exact in the classical or large-spin limit.

Table 3-4. A schematic representation of the different phases. Also shown is the long-range order of the two spins $1/2$, s and σ as defined in the text. F = ferromagnetic, F1 = up-spin ferromagnetic, F2 = down-spin ferromagnetic, AF = antiferromagnetic, D = disordered

Phase	σ	s	String	Spin 1
I	F1	F		+++++++
II	F2	-	0 0 0 0 0 0 0
III	F1	AF		+ - + - + - + -
IV	D	D		+0- +0+0-+
V	D	AF		-+0-0 0+ -
VI	F1	D		+ - + - + - + -
VII	D	F		0+0+ +0+0 0
VIII	AF	F		0+0+0+0+0
IX	AF	D		0+0+0-0+0
X	AF	AF		0+0-0+0-0

The transition between phase I and VII, the diagonal and slanted phase, can be found exactly. The transition is of the Pokrovsky-Talapov, or conventional 1D metal-insulator type (see, for instance, Ref. [46]). The horizontal link can be seen as a hard-core particle or a spinless fermion, with the parameters determining an effective chemical potential. For a critical chemical potential equal to the bottom of the band of the hard-core particle the band will start to fill up. The transition occurs when the diagonal string becomes unstable with respect to a diagonal string with one horizontal link added. This single link delocalizes along the string with a momentum k and a kinetic energy $2T \cos(k)$. The minimal energy is $(L-1)K + (L-2)\mathcal{L}_{22} + 2\mathcal{L}_{12} - 2T$, and the transition occurs when $K = 2(\mathcal{L}_{12} - \mathcal{L}_{22} - T)$ or, with $T = 1$, when

$$\text{I to VII transition: } D = -2(J + E + 1). \quad (3.8.2)$$

The transition between phase III and V will occur when horizontal link pairs unbind in the zigzag background. A rough estimate, neglecting fluctuations, is obtained by comparing the energy of a single horizontal link with that of a perfect zigzag. In the same way as above one estimate the phase boundary to be close to $D = 2(J - E - 1)$. Similarly the transition from phase II to V or IV is determined by the energy of a single diagonal step in a horizontal wall, which becomes favourable when $D = 2$. This last estimate turns out to be very crude, in that it largely underestimates the stability of the flat phase.

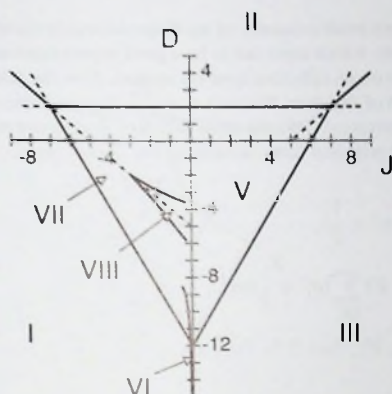


Figure 3-11. The various phase transitions (as given in Ref. [22]), obtained from semiclassical estimates, exact arguments and perturbative mappings to spin 1/2.

For large negative K the horizontal links are strongly suppressed, and the string can be mapped perturbatively on a spin 1/2 chain. Identify $S^z = 1$ (diagonal upward) with $s^z = \uparrow$ and $S^z = -1$ (diagonal downward) with $s^z = \downarrow$. Via a virtual $(0,0)$ spin pair (two horizontal links) the spins can still fluctuate, $(1,-1) \rightarrow (0,0) \rightarrow (-1,1)$. One finds, using second-order perturbation theory in T/K ,

$$\begin{aligned} \mathcal{H}_{eff}(D \rightarrow -\infty) &= (4J + j_{\pm}) \sum_I s_I^z s_{I+1}^z \\ &\quad + j_{\pm} \frac{1}{2} \sum_I (s_I^+ s_{I+1}^- + s_I^- s_{I+1}^+) , \\ j_{\pm} &= \frac{2T^2}{|2D + 3E|} . \end{aligned} \quad (3.8.3)$$

Here an irrelevant constant term has been subtracted. This has the form of the well studied spin 1/2 Heisenberg chain with Ising anisotropy. Transitions occur when $(4J + j_{\pm}) = \pm j_{\pm}$, or when $J = 0$ (III to VI) and $J = -1/|2D + 3E|$ (I to VI) (setting $T = 1$).

The above estimates seem to suggest that the line $J = 0$ is special. The results of the numerical analysis[22] showed that it describes the transition between III and VI accurately, but also the transition between IV and V. This agrees with the arguments given by den Nijs and Rommelse[47] that the Kosterlitz-Thouless transition between IV and V should occur precisely at the $J = 0$ line.

The slanted phase consists predominantly of up diagonal and horizontal links. Neglecting down diagonals altogether, which turns out to be a good approximation, one can again map the string or spin-1 chain on an effective spin 1/2 system. Now the relevant degree of freedom is the σ Ising degree of freedom. Because $\sigma = \uparrow$ (a diagonal link) is not symmetrically equivalent to $\sigma = \downarrow$ (a horizontal link) the spins will feel an effective magnetic field, which regulates the density of horizontal links. Rewriting Eq. (3.6.4) gives.

$$\begin{aligned} \mathcal{H}_{eff} = & D \sum_i (\sigma_i^z + \frac{1}{2}) \\ & + (J + E) \sum_i (\sigma_i^z + \frac{1}{2})(\sigma_{i+1}^z + \frac{1}{2}) \\ & + T \sum_i (\sigma_i^+ \sigma_{i+1}^- + \sigma_i^- \sigma_{i+1}^+) . \end{aligned} \quad (3.8.4)$$

and, after rescaling and putting $T = 1$,

$$\begin{aligned} \mathcal{H}_{eff} = & h \sum_i \sigma_i^z + \Delta \sum_i \sigma_i^z \sigma_{i+1}^z \\ & + \frac{1}{2} \sum_i (\sigma_i^+ \sigma_{i+1}^- + \sigma_i^- \sigma_{i+1}^+) . \end{aligned} \quad (3.8.5)$$

with the field $h = (D + J + E)/2$ and Ising coupling $\Delta = (J + E)/2$. On the line $h = 0$ the number of up diagonal links equals the number of horizontal links. The average tilt angle is thus 22.5° in this approximation. The phase diagram of the spin 1/2 chain in the h - Δ plane was discussed by Johnson and McCoy[67]. For $h = 0$ there are three phases. The ferromagnet corresponds to phase I, the antiferromagnet with phase VIII, and the gapless disordered phase translates to the slanted string phase VII. Increasing the field h in the AFM phase will cause a transition to the gapless phase with a finite magnetization. In the approximation that down diagonals are neglected, it follows from the results of Johnson and McCoy[67] that the point $\Delta = 1, h = 0$ or $J = 2 - E$ is the point with the most negative value of J where phase VIII is stable. For $E = 0$ (as well as for small values of E) this occurs in the positive J side of the phase diagram, meaning that phase VIII to X will in fact not be stable: for positive values of J , down steps in the original model proliferate. To have a phase diagram with all 10 phases present, in Ref. [22] E was set to be equal to 5.

In Fig. 3-11 the various phase-boundary estimates given above are summarized. The topology of the main part of the phase diagram has now become clear. In the centre of the figure for $E = 5$ the Johnson-McCoy phase diagram is inserted. The estimates suggest that at least phase VII and VIII are stabilized by taking $E = 5$. The dotted line through phase VIII is the line where the effective field h is zero, and the number of diagonal links is (nearly) equal to the number of horizontal ones.

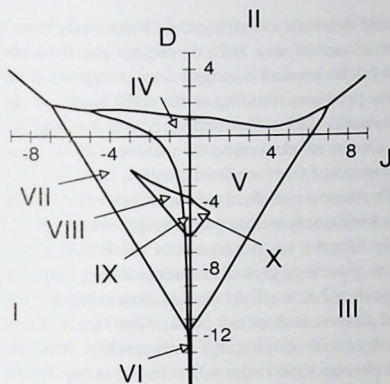


Figure 3-12. The phases and phase transitions of the quantum string for $E = 5$ as a function of t . On the axis are the on-site anisotropy D and the Ising interaction J .

3.9 Discussion and conclusions

Motivated by stripes, a lattice string model for quantum domain walls was introduced and its full phase diagram was mapped out. A generic zero temperature symmetry breaking was shown to occur: the string acquires a direction in all cases. The main reason is that bends in the string prohibit the quantum transport, or, vice versa, the quantum motion of kinks straightens out the string (the "garden hose" effect of Nayak and Wilczek[35]). We arrive at the counter-intuitive conclusion that for increasing kink quantum disorder the orientational preference of the string grows. The directed string problem which remains appears to be related to a well understood surface statistical physics (RSOS) model and simultaneously to a $S = 1$ XXZ quantum spin chain with single site anisotropy. Motivated by the string interpretation, we found a number of phases described by this class of models which were previously not identified.

Physically, the phases fall in three main categories: classical (flat worldsheet), Gaussian (rough worldsheet) and 'disordered flat' phases. The phases are further distinguished by the direction they take in the embedding space. Besides the flat strings in the horizontal and diagonal directions, we find that the disordered flat phases show here a rich behavior. Apart from the known phase with horizontal direction, which is associated with the incompressible phase of the spin model, a new category of disordered flat phases which take, depending on parameters, arbitrary directions in space (the "slanted" phases) was identified.

Although this does not apply to the localized strings, we suspect that a strong universality

principle might apply to the delocalized strings: *At least away from the phase boundaries to the localized phases, the underlying lattice renders the delocalized strings to be described by free field theory.* The reason is simple: *regardless of the terms that one adds to the lattice scale action, the problem remains of the XXZ kind and the massless phases fall into the 1+1D $O(2)$ universality class.* For instance, one can add other kink-kink interactions, etcetera, and these can be all described by products of S^z operators. Although these operators determine the nature of the localized phases, they turn into irrelevant operators in the massless phases. The kinetic sector is more subtle. For instance, one would like to release the constraint that kinks only occur with 'height flavor' ± 1 . This means in surface language that one partially lifts the restrictedness of the RSOS model, or in spin language that one *increases the total spin*: e.g., $S = 2$ means in string language that kinks occur describing height differences of ± 2 as well. Although increasing the magnitude of spin has an influence on the localized phases, it does not change the fact that the massless phase away from the phase boundaries is still obeying XY universality. A point of caution is that the 'holes' in principle could change their order when larger excursions are allowed. However, these 'exchange loops' are strictly local and therefore irrelevant for the long wavelength behavior as long as the string is internally an insulator. These could represent more of a problem for strings which are internally superconductors or metals.

It should also be stressed that it follows from the arguments of den Nijs and Rommelse[47] that the occurrence of a gapped Haldane type phase for strings is not a peculiar feature of the spin 1 representation, but a general consequence of the existence of further neighbor interactions between the holes in strings.

Do these findings bear any relevance to the stripes in cuprates? At least they do bring up some interesting questions:

(a) Is the stripe solidification in for instance the LTT cuprates[25] in first instance driven by a single string effect or by a collective transition of the string liquid? In the end it has to be the latter, since a single string cannot undergo phase transitions at finite temperatures. However, it can be well imagined that the effect of the LTT-pinning potential is to stabilize (1,0) directed stripes over (1,1) stripes. In the language of this paper, this amounts to an increase of the parameter K which could move the stripe from the Gaussian phase into the horizontal flat phase. At zero temperature, this would turn individual stripes in straight rods which are obviously much easier to order than meandering strings. At finite temperatures, this could increase the single string persistence length substantially, so that stripe-stripe interactions become more effective in stabilizing a stripe solid at finite temperatures[71]. Further work is needed to establish if these single stripe transitions are of relevance.

(b) Do the 'disordered flat' string phases exist? The simplest disordered flat phase is the horizontal one (phase V) corresponding with the Haldane phase of the $S = 1$ spin chain. In string language, this is nothing else than a localized string along the (1,0) direction in the lattice which is however not site-centered (as phase II) but, on average, *bond centered*. Bond centered stripes show up in the numerical study of the t - J model by White and Scalapino[40], which shows that the ground state of this model at finite dopings is a stripe phase. A main difference with the mean-field stripes is that these t - J stripes are bond centered. In first instance, one could be tempted to think that this has a truly microscopic

reason: charges in t - J prefer to live on links. However, it could also be due to a *collective string effect* — it could be “our” phase V. This can be easily established by measuring the appropriate (string) correlators. Is it the case that on equal times the charges live on sites while the kinks take care of delocalizing the stripes over two lattice rows, or is it so that on all times the charges are living on the links? This is obviously an important question in the light of recent works relating the bond centering via Hubbard-ladder physics to superconductivity[43]. We also notice that there are experimental indications for bond-centering in the nickelates[72] where disordered flatness could possibly also play a role.

(c) If well developed stripes exist in the superconductors and/or metals, these have to occur in the form of a quantum disordered stripe phase, or a ‘quantum string liquid’. What is learnt in this regard from the present study of a single string? A prerequisite for the existence of a quantum string liquid is that a single string is delocalized. If our conjecture that a single critical string is described by free field theory turns out to be correct, this amounts to a considerable simplification. In Euclidean space time, the single free string worldsheet is like a Gaussian membrane and a system of strings becomes a system of interacting Gaussian membranes, embedded in $2+1$ dimensions. Because the single string is directed, these membranes will be directed along both the imaginary time direction and the $x-y$ plane. A limiting case of such a problem is studied exploiting its connection with a hard core bose problem. This problem will be reviewed in chapter 6.

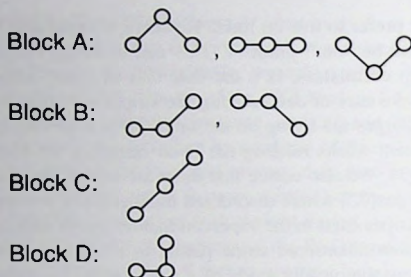


Figure 3-13. The four subblocks of the local t -matrix. The other equivalent, symmetry related blocks are obtained by $\pi/2$ rotations and reflections in the x or y axis.

3.10 APPENDIX

In this appendix the specifics of the numerical calculations will be discussed. This includes (a) a transfer matrix formalism which is quite efficient numerically and (b) some specifics regarding the updates.

3.10.1 Transfer matrix formalism

The transfer matrix is constructed as follows. The partition function is

$$\begin{aligned} \mathcal{Z} &= \text{Tr} e^{\mathcal{H}_C + \mathcal{H}_Q} \\ &= \lim_{n \rightarrow \infty} \text{Tr} (I T_A I T_B)^n. \end{aligned} \quad (3.10.1)$$

In the above formula I is the identity operator, in our case a complete set of string configurations. We have chosen to split the T -matrix into a contribution from even and odd sites, or A and B sublattice (checkerboard decomposition),

$$T_A = \exp \left[\frac{1}{n} \sum_{l=1}^{L/2} (\mathcal{H}_{C,l,2l} + \mathcal{H}_{Q,2l}) \right], \quad (3.10.2)$$

and a similar expression for the odd sites. $\mathcal{H}(2l)$ is the Hamiltonian of the even string element $2l$, equal to Eq. (3.2.7) or (3.2.12) without the sum over string links. L is the

number of links in the chain. Because of the sublattice decomposition, T_A is a simple product of local T -matrices and Z becomes,

$$Z = \lim_{n \rightarrow \infty} \sum_{\{\mathbf{r}_{l,k}, \mathbf{r}'_{l,k}\}} \prod_{k=1}^n \prod_{l=1}^{L/2} \langle \{\mathbf{r}_l\}_k | t_A^{2l,k} | \{\mathbf{r}_l'\}_k \rangle \langle \{\mathbf{r}_l'\}_k | t_B^{2l+1,k} | \{\mathbf{r}_l\}_{k+1} \rangle. \quad (3.10.3)$$

Each timeslice is split in two sublattices, \mathbf{r} and \mathbf{r}' . The notation $\{\mathbf{r}_l\}_k$ denotes the set of positions \mathbf{r}_l at the given time slice with index k . Note that the t matrices are independent of l and k , and these indices only label the position of the t matrix in the 2D world sheet. The local t matrices, t_A and t_B , depend only on three positions. For instance,

$$\langle \{\mathbf{r}_l\}_k | t_A^{2l,k} | \{\mathbf{r}_l'\}_k \rangle = \langle \mathbf{r}_{2l-1,k} \mathbf{r}_{2l,k} \mathbf{r}_{2l+1,k} | t_A^{2l,k} | \mathbf{r}'_{2l-1,k} \mathbf{r}'_{2l,k} \mathbf{r}'_{2l+1,k} \rangle \quad (3.10.4)$$

with the restriction $\mathbf{r}_{2l-1,k} = \mathbf{r}'_{2l-1,k}$ and $\mathbf{r}_{2l+1,k} = \mathbf{r}'_{2l+1,k}$. Since each link has 8 different orientations, the local t matrix connects in general $8 \times 8 = 64$ possibilities. However most of the t matrix elements are zero, and it decomposes into subblocks, of which the biggest one is 3×3 . The states which are connected via the local t matrix, or the Hamiltonian, are listed in Fig. 3-13. The local t -matrix at position l and Trotter slice k is defined as,

$$\langle \mathbf{r}_{l-1,k}, \mathbf{r}_{l,k}, \mathbf{r}_{l+1,k} | \exp \frac{1}{n} \mathcal{H}_l | \mathbf{r}'_{l-1,k}, \mathbf{r}'_{l,k}, \mathbf{r}'_{l+1,k} \rangle. \quad (3.10.5)$$

The matrix elements depend on the positions of three members of the string, $l-1$, l and $l+1$. The positions of $l-1$ and $l+1$ are required to be identical $\mathbf{r}_{l-1,k} = \mathbf{r}'_{l-1,k}$ in the two Trotter sublattices involved, due to the checkerboard decomposition, but the position of member l can be different, leading to off-diagonal matrix elements. The matrix elements of the t -matrix are easily found by first diagonalizing \mathcal{H}_l and expanding the basis vectors in terms of the eigenvectors.

Block A: This block contains three configurations, see Fig. 3-13. We use the same order for the states as in the figure. Note that only half of the energy \mathcal{K} of the diagonal link between $l-1$ and l and the link between l and $l+1$ should be contributed to l . The Hamiltonian,

$$\mathcal{H} = \begin{pmatrix} \mathcal{K} & \mathcal{T} & 0 \\ \mathcal{T} & 0 & \mathcal{T} \\ 0 & \mathcal{T} & \mathcal{K} \end{pmatrix}, \quad (3.10.6)$$

is easily diagonalized. The eigenvalues are \mathcal{K} , E_+ and E_- . The t -matrix is,

$$t = \begin{pmatrix} t_{11} & t_{12} & t_{13} \\ t_{12} & t_{22} & t_{12} \\ t_{13} & t_{12} & t_{11} \end{pmatrix},$$

$$t_{11} = \frac{1}{2} e^{\mathcal{K}/n} + N_+^2 e^{E_+/n} + N_-^2 e^{E_-/n},$$

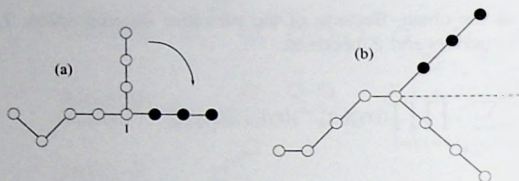


Figure 3-14. Two additional Monte Carlo operations used for the simulations of the general string. The 90 degree rotation (a) around position 1 in this example turns a non-directed string into a directed one. The mirror operation (b) is important to quench defects in diagonal strings (mirror plane indicated by the dashed line).

$$\begin{aligned}
 t_{12} &= N_+^2 \alpha_+ e^{E_+/n} + N_-^2 \alpha_- e^{E_-/n}, \\
 t_{13} &= -\frac{1}{2} e^{\mathcal{K}/n} + N_+^2 e^{E_+/n} + N_-^2 e^{E_-/n}, \\
 t_{22} &= N_+^2 \alpha_+^2 e^{E_+/n} + N_-^2 e^{E_-/n}, \\
 E_{\pm} &= \frac{2 \pm \sqrt{\mathcal{K}^2 + 8\mathcal{T}^2}}{2}, \\
 \alpha_{\pm} &= \frac{E_{\pm} - \mathcal{K}}{\mathcal{T}}, \quad N_{\pm} = \frac{1}{\sqrt{2 + \alpha_{\pm}^2}}.
 \end{aligned} \tag{3.10.7}$$

Here n is the number of Trotter slices and \mathcal{K} , \mathcal{L}_{12} , \mathcal{L}_{22} , \mathcal{L}_{11} and \mathcal{T} are the string model parameters.

Block B contains two configurations, each with one horizontal and one diagonal link. Repeating the above procedure one finds,

$$\begin{aligned}
 t &= \begin{pmatrix} e^D \cosh(\mathcal{T}/n) & e^D \sinh(\mathcal{T}/n) \\ e^D \sinh(\mathcal{T}/n) & e^D \cosh(\mathcal{T}/n) \end{pmatrix}, \\
 D &= \frac{\mathcal{K}}{2n} + \frac{\mathcal{L}_{12}}{n}
 \end{aligned} \tag{3.10.8}$$

Block C contains a single configuration of two diagonal links, and the energy and t -matrix therefore contain \mathcal{L}_{22} ,

$$t = \exp\left(\frac{\mathcal{K}}{n} + \frac{\mathcal{L}_{22}}{n}\right), \tag{3.10.9}$$

Block D consists of a square corner between one horizontal and one vertical link, and \mathcal{L}_{11} is involved,

$$t = \exp\left(\frac{\mathcal{L}_{11}}{n}\right), \tag{3.10.10}$$

3.10.2 Global Monte-Carlo moves

For the Monte-Carlo program to produce sensible results it is crucial to have operations that add and remove bends easily. We added global mirror and $\pi/2$ rotation operations illustrated in Fig. 3-14. In the latter case half of the string is rotated around any of the sites $l \in 2..L-1$. This means that for instance the position of all holes $m > l$ are replaced by $(x_m, y_m) \rightarrow (x_l, y_l) + (y_m - y_l, -(x_m - x_l))$. Such operations turn out to be very efficient — completely wrapped high temperature strings unwrap in just a couple of Monte Carlo steps at low temperature.

4 Metallic stripes: Separation of spin, charge and string fluctuations

In this chapter we will consider the problem of a one-dimensional metal living on a delocalized trajectory in two-dimensional space: the metallic lattice string. A model is constructed with maximal coupling between longitudinal and transversal charge motion. The model nevertheless renormalizes into a minimal generalization of the Luttinger liquid: besides the spin and charge modes an independent set of string modes has to be added to the long-wavelength theory, with a dynamics governed by the quantum sine-Gordon model.

4.1 Introduction

A series of experimental evidences appeared recently indicating that the superconducting state in the cuprates is closely related to, and is in a tight competition with, the stripe phase. In this stripe phase the active charge degrees of freedom live on the antiphase domain walls in the antiferromagnetic background, the stripes. This occurs over most of the doping range [29, 27, 24]. There are also evidences that the stripes are internally charge compressible and it can then be argued that the stripes might be internally like one-dimensional (1D) metals. Several theoretical works have appeared taking this "self organized" one dimensionality as a starting point, [75]. However, compared to conventional one dimensional metals, stripes are at the least qualitatively different from electrons in one dimensions as one has to account for the possibility that *the trajectory on which the metal lives is itself delocalized in the two space dimension*, obviously so because static stripe order is absent in either the superconducting or the normal state. Actually inelastic neutron measurements yield compelling evidence for strong dynamical stripe correlations in the superconductors [27]. This implies the presence of additional collective excitations to the one dimensional 'electronic' excitations: the 'string fluctuations', driving the quantum meandering motion of the stripes as a whole. The question arises as to what can be said about the general nature of a quantum string which is internally a metal. According to the Luttinger liquid theory, the generic theory of one dimensional metallicity, all what matters at long wave-length are the collective charge and spin oscillations (holons and spinons) which are governed by quantum sine-Gordon field theories [76]. As was discussed in the preceding chapter, the presence of the crystal lattice leads to considerable simplifications in the 'string' theory describing the motion of the stripe as a whole in space, and it can be demonstrated that quantum delocalized lattice strings exist which are governed by a free string fixed point: the long wave-length dynamics of the string can be parametrized in terms of its transversal sound excitations, described by a quantum sine-Gordon theory as well.

Here we will demonstrate that a fixed point theory exists which is a minimal generalization of the Luttinger liquid theory: a metallic string can be like a Luttinger liquid, except that, next to the decoupled spin and longitudinal charge modes governing the internal metallicity of the stripe, a set of independent string modes, governing the transversal motion of the stripe, should be added for the theory to be complete. This involves the extrapolation of the principle of charge spin separation to the separation of spin, charge and string modes. As in the spin and charge sectors, this transversal dynamics is described by a sine-Gordon field theory. In a conventional one dimensional metal, an external electron, or hole, decays into the charge and spin modes of the Luttinger liquid. The same is true here, except that part of the electron is carried away as well by the transversal modes of the string.

In the absence of a microscopic theory of metallic stripes it is impossible to proceed rigorously. Instead we will lean heavily on the principle of adiabatic continuation, which has proven itself in the one dimensional context. We will construct a model which incorporates next to the general requirements imposed by symmetry the fact that the charge carriers are confined to a connected trajectory. Deliberately we construct the model in such a way that both the coupling to the underlying lattice, and the lattice scale coupling between the transversal string dynamics and the internal charge dynamics is maximal. This model can be looked at as being representative for the strong coupling limit of this problem and at least as long as the system renormalizes towards weak coupling, its long wavelength behavior should be representative for a less strongly coupled microscopic physics.

4.2 Construction

Our construction rests on the assumption that a reference string state exists which is at the same time localized in space and internally charge-incompressible due to a charge density wave (CDW) instability. The CDW solitons emerging under doping make the string position fluctuate and the resulting charged kink gas maps on a spin-full fermion problem with a Luttinger liquid long wavelength regime.

Although the microscopics of the stripe instability is not yet understood in detail, some general characteristics can be directly inferred from experiments. For cuprates, it appears that a state exists where (a) the electronic system on the stripe has solidified becoming insulating, and (b) the stripe as a whole is localized. We refer to the state at $x = 1/8$; the stripes are localized along the (1,0) or the (0,1) directions in the cuprate planes, and one hole stabilizes a length twice the domain wall unit length. This later on-wall charge commensurability is not an accident, Yamada et al found that the incommensurability ε of the dynamical stripe fluctuations scales linearly with x for all $x \leq 1/8$ [27] or the average stripe separation d decreases like $1/x$ in this doping regime. This shows that at least on average this charge commensurability holds in a large doping regime and this is possible only when the electron system on the stripes is charge incompressible. At the same time, the static stripe phase shows a special stability at $x = 1/8$; which reflects a tendency towards localization of the stripe. For modelling purposes we assume the electronic system

on the stripe is dominated by short range repulsive interactions, implying that the charge order on the stripe to be of the site centered $4k_F$ CDW type as suggested by Nayak and Wilczek[78] (Fig. 4-1a). This is mainly for modeling purposes. Bond centered stripes with internal superconducting, and $2k_F$ charge ordering tendencies are more complicated, but not necessarily qualitatively different in the present context.

In addition, we assume that the charge-commensurate string is localized in space. As we discussed extensively in the last chapter, in contrast to continuum strings such classical strings are allowed on general grounds because they live on a lattice. Microscopically, the string fluctuation is driven by hole motions on a minimum scale of the lattice constant and the resulting kinks carry therefore a non-zero energy which has to be overcome by their kinetic energy before their proliferation causes a quantum melting of the string. Finally, it is assumed that the 2D spin system in which the string moves remains in the Néel state. As will be discussed later, the on-wall dynamics is not directly influenced by this vacuum, but this could be different in a non-classical spin background[37]. This choice of Néel background is motivated by the experimental observation that the spin-spin correlation length is large compared to the length scales of relevance to the string dynamics. Notice that the spins inside the half-filled walls are not necessarily ordered. However, on general grounds the correlations between these spins are expected to be antiferromagnetic and the Néel ordering in Fig. 4-1a is only introduced for counting purposes. Finally, it is assumed that the spin system separates at the very beginning and can be ignored all along. Since the stripe sweeps through a spin-full background, the neglect of spin is certainly not justifiable, and further work is needed on this fascinating problem.

What can happen when the half-filled wall is doped? In the 1d crystal, all what can happen is that the charge density increases and because of the charge commensuration there is a restoring force (half the energy gap). The stripe can, however, respond in a different way: because its shape is not fixed from the onset, but instead a dynamical quantity of its own, it can relax the cost of enhancing the density by letting the charge escape in the direction transversal to the stripe, which amounts to a shape fluctuation. Alternatively, the charge commensuration can be looked at as a rule that every hole adds a fixed length to the string. The additional length coming with the doped hole can be stored by deforming the string, at the expense of a curvature energy.

If the string does not delocalize, the remaining problem of a doped $4k_F$ charge density wave is well understood[79, 80], generically, charge and spin separate. A representative model, in the sense of adiabatic continuity, is the extended Hubbard model with both U (on-site repulsion) and V (nearest-neighbor repulsion) large compared to the bandwidth. At low doping, lattice commensuration dominates and the relevant lattice scale physics is that of half-charged *solitons*. Using simple kinematics, Kivelson and Schrieffer[81] pointed out that the injected hole splits apart into propagating soliton- and anti-soliton excitations, both carrying half the charge of the hole (fig. 1b). Since the solitons are subjected to a hard-core condition, while the soliton flavor does not carry physical consequence, the soliton

dynamics is described in terms of a *spinless* fermion problem:

$$H_{CDW} = \sum_{ij} t'(ij) c_i^\dagger c_j + \sum_{ij} V'(ij) n_i n_j. \quad (4.2.1)$$

Where c^\dagger creates a soliton and $n = c^\dagger c$. Solitons are subject to short range hoppings (t') and (repulsive) interactions (V'). It is well established that, using bosonization techniques, this problem is dual to a bosonic quantum sine-Gordon theory with action,

$$H_{p,ren} = \frac{v_\rho}{2} \int dx \left[K_\rho \Pi_\rho^2 + \frac{1}{K_\rho} (\partial_x \phi_\rho)^2 + g \sin(\alpha \phi_\rho) \right], \quad (4.2.2)$$

where x is along the stripe, v_ρ and K_ρ correspond with the charge velocity and charge stiffness, respectively. In terms of the field ϕ_c , the charge density is $\rho_0(x) = (1/\pi) \partial_x \phi_c(x)$. At quarter filling the sine term (originating in the Umklapp scattering) is relevant and a charge gap develops. Away from quarter filling, this theory is in the weak coupling regime (the sine interaction is an irrelevant operator) and the long wavelength dynamics is governed by free field theory (Luttinger liquid), completely specified by the renormalized stiffness and velocity. Alternatively, at finite but small dopings the system might be considered as a *low density gas of solitons and antisolitons (domain walls in the CDW), each carrying half the hole charge*. These parameters have to be calculated numerically, and their behavior is well documented for the extended Hubbard model [79, 80].

The most elementary physical interpretation of the quantum sine-Gordon model, Eq. (4.2.2), actually corresponds with a free string moving on a lattice: the field ϕ is the transversal displacement ($z(l)$) at point l of the string, while the cosine term describes the lattice washboard on which the string moves ($\alpha \phi_c \rightarrow 2\pi z(l)/a$). The weak- and strong coupling limits are easily understood as a freely meandering string and one which is fully localized due to the lattice potential, respectively. As was discussed in detail in the preceding chapter [77], this notion is of relevance in the context of fluctuating insulating stripes. In analogy with the charge density wave problem, the relevant lattice scale dynamics is that of transversal solitons or 'kinks'. Consider the vicinity of the string delocalization transition. Because the lattice potential dominates, the microscopic configurations tend to be those of Fig. 4-1d, where the string is localized on a particular lattice row n , and the exceptions are where the string jumps to neighboring rows $n \pm 1$. The origin of the collective motions of the string lies in the microscopic dynamics of these kink-excitations. The tightly localized kinks of Fig. 4-1 are assumed to be a legitimate starting point to discuss string fluctuations, in the sense that they are connected by adiabatic continuation to more realistic string microscopies.

The existence of a localized stripe with internal $4k_F$ density wave allows for a simple unification of the microscopic string- and internal charge dynamics. Obviously, the fixed 1D electron trajectory assumed in the Luttinger liquid is no longer a given for electronic stripes. For a fixed trajectory, it costs an energy equal to the jump in the thermodynamic potential $\delta\mu$ to dope the charge density wave with an additional carrier. On the stripe,

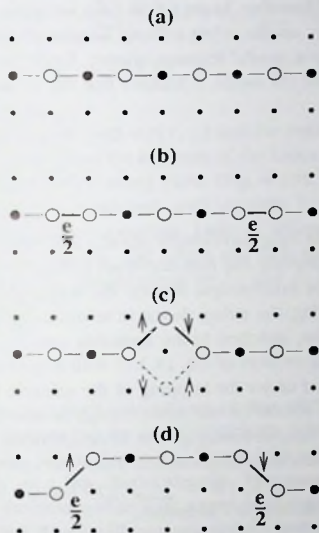


Figure 4-1. Soliton dynamics in a strongly coupled doped $4k_F$ stripe. (a) The reference state: localized stripe with $4k_F$ charge density wave. (b) If the stripe is rigid, the doped hole separates in a left- and right moving soliton, both carrying half the electron charge. (c) When the curvature energy becomes less than the charge compressibility energy, the hole can escape 'sideways'. (d) As a result, the solitons now carry a transversal (step up/down) flavor, which is like a spin degree of freedom. Holes tunneling through the stripe lead to fluctuations in the transversal flavor, see (c).

this ('longitudinal') energy cost can be reduced by letting the charge escape 'sideways', causing a transversal displacement, at the expense of paying a curvature energy. Hence, when this curvature energy becomes less than the energy cost associated with compressing the charge, the doped holes will 'carry a string fluctuation'. In terms of the strong coupling kinks/solitons, the microscopic mechanism of transversal relaxation is obvious: *the doped hole corresponds with a double kink in the string which is at the same time a soliton-antisoliton pair in the on-string charge density wave* – see Fig. 4-1. Starting from the CDW/localized string reference state, the kinks and the solitons are the same objects. This scenario corresponds with the strongest possible microscopic coupling between the on-string metallicity and the string fluctuation. Due to the string fluctuation, the CDW solitons acquire a *transversal flavour*: the soliton/antisoliton can move the string either in an 'upward' (\uparrow) or 'downward' (\downarrow) direction (Fig. 4-1c,d). This transversal freedom is like a

$s = 1/2$ iso-spin degree of freedom. In the CDW case, solitons can be described in terms of spinless fermions. However, on the string solitons acquire an additional two-valued flavour and the dynamics relates to a *spinful* fermion system. Since the string dynamics is like the spin dynamics in a standard 1D metal, it follows that the separation of charge- and string dynamics is generic.

4.3 The Model

The qualitative nature of the long wavelength physics can be inferred from the strong coupling cartoon of Fig. 4-1, leaving the non-universal parameters of the theory to be determined from a more realistic microscopic theory. We seek a generalization of the spinless fermion model, incorporating the string flavor in terms of isospin labels \uparrow for 'upward' and \downarrow for 'downward' kinks, attached to the fermions (see Fig. 4-1c,d). As a first guess, one could take the spin-full version of Eq. (4.2.1) with a hard-core ($U \rightarrow \infty$) condition: the string flavor is conserved under the hopping of the solitons. However, this neglects the specifics of the transversal sector: (i) curvature energy is associated with the order of the iso-spins. Obviously a $\uparrow\downarrow$ isospin configuration of neighboring solitons involves a different curvature energy than parallel configurations. These curvature energies can be absorbed in isospin-only Ising terms $\sim S_i^z S_j^z$ ($\bar{S}_i = \sum_{\alpha\beta} c_{i\alpha}^\dagger (\bar{\sigma})_{\alpha\beta} c_{i\beta}$). (ii) The overall transversal string displacement u after arclength r becomes,

$$u(r) - u(0) = a_0 \int_0^r dx \sigma^z(x), \quad (4.3.1)$$

where a_0 is the lattice constant and $\bar{\sigma}(x) = \sum_m \bar{S}_m \delta(x - x_m)$ (x_m is the position of the m -th kink). As long as this quantity is conserved the string remains localized. For $U \rightarrow \infty$ there is no kinetic exchange, and Ising isospin terms do not cause fluctuations in $u(l)$ either. In order to make the string displacement fluctuate, the isospins should be exchanged and this is possible if and only if two kinks recombine into a hole, because the hole can tunnel through the string, see Fig. 4-1c. The simplicity of the argument is deceptive: *this is an explicit realization of the idea of topological confinement*[82]. Because of their topological nature, the kinks are strictly limited to the 1D string trajectory. In order to sweep the string through 2D space, the kinks have to pair up in holes, because the latter can propagate in 2D.

In isospin language, the hole tunneling corresponds with spin-flip (XY) terms $\sim S_i^+ S_j^- + h.c.$. Notice that the energy barrier involves the *difference* in curvature energy and the charge-compression energy. This might well be a small number, and the hole-tunneling rate can in principle be large. Assuming everything to be short ranged, we arrive at the following model,

$$H_0^{str} = -t \sum_{n\sigma} (c_{n+1,\sigma}^\dagger c_{n\sigma} + c_{n\sigma}^\dagger c_{n+1,\sigma})$$

$$\begin{aligned}
& +V \sum_n n_n n_{n+1} + U \sum_n n_{n\uparrow} n_{n\downarrow} + J_{//} \sum_{\langle nml \rangle} S_n^z S_m^z \\
& + \frac{J_{\perp}}{2} \sum_{\langle nml \rangle} (S_n^+ S_m^- + S_n^- S_m^+) .
\end{aligned} \quad (4.3.2)$$

where c_σ^\dagger create a soliton/antisoliton with $\sigma \in \{\uparrow, \downarrow\}$ and the notation is standard otherwise ($n = n_\uparrow + n_\downarrow$). The first term describes the hopping of the kinks with hopping amplitude t . This hopping, obviously, conserves the string flavor (Fig. 4-1d). The second term describes the 'string neutral' soliton-soliton repulsions with strength V . The third term has to be added to strictly enforce the hard core condition: kinks of different flavor cannot pass each other and U should be taken to infinity. The fourth and fifth terms describe the curvature energy and the hole tunneling rate, parametrized by $J_{//}$ and J_{\perp} respectively.

4.4 Discussion

Although we are not aware of explicit calculations on this particular model, the structure of the long wavelength dynamics can be deduced directly from the work by Luther and Emery[83] (see also ref. [4]). When $J_{//} = J_{\perp}$, Eq. (4.3.2) is like the extended Hubbard model with finite U , at a low carrier density. The general case $J_{//} \neq J_{\perp}$ corresponds with an interacting electron system with a spin-orbit coupling causing uniaxial spin anisotropy. Charge and string flavor will separate always and the charge dynamics is described by the QSG model, Eq. (4.2.2). Away from the quarter-filled point, Umklapp scattering becomes irrelevant and the charge dynamics at long wavelength is described by free fields characterized by the fully renormalized charge-velocity and -stiffness, \bar{v}_ρ and \bar{K}_ρ which will behave similarly as to the ones of the extended Hubbard model in the strongly coupled regime.

A crucial observation is that the gross behavior in the string sector is determined by the 'isospin-only' problem. The isospin dependencies of the interactions are explicit in Eq. (4.3.2), and the isospin-only problem is nothing else but a XXZ problem with $S = 1/2$, which has been solved a long time ago[84]. If $-1 < J_{//}/J_{\perp} < 1$, the Ising interaction is irrelevant and the system falls in the XY universality class, as described by free-field theory – the free string is recovered. When $|J_{//}| > |J_{\perp}|$ the Ising anisotropy takes over and the string modes acquire a mass – metallicity is a necessary but insufficient condition for the string delocalization. Physically, strings in this regime are of the 'disordered flat' variety (see section 3.8)[77]. Although kinks proliferate and delocalize, their internal string flavor (isospin) is ordered, as a compromise between kinetic energy and lattice commensuration energy. The 'ferromagnetic' case ($J_{//} < |J_{\perp}|$) corresponds with a 'slanted' phase (see section 3.8)[77]: the string is still localized, but it takes some direction in space determined by the density of kinks. For $J_{//} > |J_{\perp}|$ the string is on average bond centered: this phase is related to the hidden order present in Haldane spin chains[77].

The most interesting phase is the delocalized string, and we will now show that the asymptotic structure of Luttinger liquid theory implies a rather weak influence of the string-

metallicity on the string fluctuation. A quantity of physical interest is the mean square transversal displacement of the string[32], using Eq. (4.3.1),

$$\langle (u(r) - u(0))^2 \rangle = a_0^2 \int_0^r dx dx' \langle \sigma^z(x) \sigma^z(x') \rangle. \quad (4.4.1)$$

The spin-spin correlation function of a one dimensional metal has the asymptote behavior.

$$\langle \sigma^z(x) \sigma^z(0) \rangle = \frac{C_1}{x^2} + \frac{C_2 \cos(2k_F x)}{|x|^\eta}, \quad (4.4.2)$$

where $\eta = K_\sigma + K_\rho$ and K_σ, K_ρ are the spin and charge-stiffness respectively. Although $\eta \geq 1$, η can be less than 2; in this case the staggered component of the spin-spin correlator could become important for the string correlator, Eq. (4.4.1). However, it is easy to see that in the additional integrations in Eq. (4.4.1) the staggered component behaves as if it falls off by one power more than η ($\int dx \cos(2k_F x)/x^\eta \rightarrow \int dx 1/x^{\eta+1}$). Since $\eta \geq 1$ it follows that the large r asymptote of Eq. (4.4.1) is governed by the uniform component $\sim C_1$ in Eq.(4.4.2). Using that $\int_0^r dx dx' f(x - x') = \int_{-r}^r (2r - |x|) f(x)$ and the fact that $\int_{-\infty}^{\infty} dx \langle \sigma^z(x) \sigma^z(0) \rangle = 0$ it follows that the metallic string behaves asymptotically as a free string[32],

$$\langle (u(r) - u(0))^2 \rangle = -2a_0^2 C_1 \ln(r/r_c) + const. \quad (4.4.3)$$

with a constant coming from short wavelength physics and where r_c is a microscopic cut-off.

Although not often discussed, the amplitude C_1 of the uniform component of the spin-spin correlation is also in the metal entirely determined by the spin sector, which implies in the present context that the strength of the string fluctuation is determined primarily by the transversal sector. This can be easily understood from the insight by Schulz[85] that the charge sector of the Luttinger liquids is nothing else than a 1D harmonic ('floating') Wigner crystal of (in our case) solitons. To every soliton a spin is attached and Schulz shows that by factorizing $\langle \sigma^z(z) \sigma^z(0) \rangle$ in a spin- and a charge correlator and by treating the charge sector on the Gaussian level, it follows that the exponent η in the staggered component of Eq. (4.4.2) is the sum of the charge- and spin stiffnesses K_σ and K_ρ because the spin system 'rides' on the harmonically fluctuating charge solid. Following the same alley, it is straightforward to show that this charge fluctuation is invisible in the uniform correlations responsible for the string delocalization.

We are now in the position to completely quantify Eq. (4.4.3). Using Haldane's expressions for the Luttinger liquid correlation functions[86] and realizing that the cut-off r_c corresponds with the lattice constant a of the soliton Wigner crystal, we get

$$\langle (u(r) - u(0))^2 \rangle = \frac{a_0^2 K_\sigma}{2\pi^2} \ln(r/a) + const. \quad (4.4.4)$$

Let us now assume that the above model applies literally to cuprates. Assuming that finite range string-string interactions are unimportant, a measure for the importance of the single string quantum fluctuations is the quantum collision length ξ_c , obtained by demanding that the r.m.s. displacement of a string becomes of order of the mean string-string separation d ($\simeq 4a_0$) [32]: $\langle (u(\xi_c) - u(0))^2 \rangle = d^2$. Using that the soliton lattice constant $a = a_0/(8x - 1)$ in terms of the doping density x , together with the expression for the spin stiffness [84] $K_\sigma^{-1} = 1/2 + (1/\pi) \arcsin(J_{//}/J_\perp)$, we obtain

$$\xi_c = \frac{a_0}{8x - 1} e^{(d/a_0)^2 [\pi^2 + 2\pi \arcsin(J_{//}/J_\perp)]} \quad (4.4.5)$$

The doping density only enters in the prefactor via the trivial soliton-lattice constant rescaling, while ξ_c depends exponentially on the stripe separation and the transversal scales. Hence, the metallicity induced long-wavelength string fluctuations can only play a decisive role in the quantum melting of the stripe phase if the factor in the exponent becomes of order unity. Because of the various numerical factors, this only happens if the string sector is very close to the 'ferromagnetic' point $J_{//}/J_\perp \rightarrow -1$. It appears as very unlikely that such a fine tuning occurs in cuprates so we conclude that on-string metallicity is *not* an important factor for the quantum melting of the stripe phase.

4.5 Conclusion

The problem of a lattice string which has been internally a metal is addressed. Starting from a specific microscopic assumption inspired by cuprate stripes, it has been shown that the long wavelength dynamics of a metallic string is a straightforward generalization of the Luttinger liquid where the usual theory has to be extended with a sector of transversal sound modes corresponding to the string transversal mode fluctuations. Although intended as a demonstration of the existence of a fixed-point (with probably a finite basin of attraction), a literal interpretation of the microscopic model shows that the string fluctuation is quite insensitive to the internal metallicity of the stripe. As applied to cuprates, this observation offers a rational for the surprising *insensitivity* of the static stripe phases in e.g. LTT materials against stripe doping.

5 Quantum magnetism of the static stripe phase

5.1 QNLMS description of the static stripe phase

In the previous chapters we have presented a detailed study of a model for the fluctuation of a single stripe. The stripe phase is complicated by the fact that stripes live in a spinfull background. For the single stripe model (the quantum lattice string) the spin background was neglected. In this chapter we will present a study of a model for static stripes in the antiferromagnetic background. This will be a model for the charged-ordered stripe phase. Our goal is to investigate the anomalous spin dynamics of the charged-ordered stripe phase in the cuprates. The spin ordering temperature of such a stripe phase appears to be strongly suppressed compared to half-filling, the undoped case. The Néel temperature T_N for the charged ordered stripe phase can be as low as 3K while T_N for the undoped material is around 300K. For quite some time, before the discovery of the stripe phase, it was believed that this anomalous spin dynamics of the high T_c superconducting cuprates originates in the proximity to a quantum critical point [87, 88] and it was even conjectured that the relevant field theory would be the $O(3)$ quantum nonlinear sigma model (QNLMS), describing the collective dynamics of a quantum anti-ferromagnet[7]. Actually the available experimental data suggest that this anomalous spin dynamics is characterized by a close proximity to the QNLMS zero-temperature transition. As this is a theory for a spin-only dynamics at long wave length, it was asserted that at low energies spin-charge separation should be complete. This final conclusion is very much questionable and has never been supported experimentally. However the discovery of the stripe phase[25] and of a strong dynamical stripe correlations in the cuprates superconductors opens a new perspective on these matters. Below the stripe-charge ordering temperature, charge fluctuations have to become inconsequential and the remaining spin dynamics should fall automatically in QNLMS universality class. The main purpose of the study presented in this chapter is to put forward a strategy by which the spin-only aspects of the magnetic dynamics in the cuprate high T_c superconductors can be disentangled, exploiting the charge ordering associated with the stripe order.

The enhancement of the quantum-spin fluctuations as compared to the half-filled antiferromagnet can have a variety of microscopic sources. Here we will focus on the possibility that these are due entirely to the charge-ordering induced spatial anisotropy in the spin system. Although the influence of spatial anisotropy is well understood on the field-theoretic level[89, 90], the charge can be bond-ordered or site ordered[9] and this links the spin physics of the stripe phase to that of coupled spin ladders[91, 92, 93]. At optimal superconducting doping concentrations, bond- and site order translate into coupled two-leg and three-leg spin ladders, respectively. An in-depth quantitative analysis of both problems will be presented, showing that spatial spin-anisotropy has to be largely irrelevant for site-

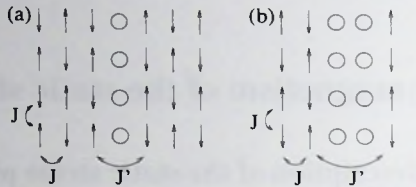


Figure 5-1. Schematic distinction between site ordered (a) and bond ordered (b) stripes.

ordered stripes, while it might well be the primary source of quantum spin fluctuations in the bond-ordered case. Specifically, it will be shown that it might well be that much of the increase of the quantum-spin fluctuations can be attributed to the transversal (spin-only) sector alone *if* the stripes turn out to be bond ordered. Conversely, if the stripes are site ordered, microscopic charge fluctuations are bound to play a crucial role in the spin sector as well. A strategy will be presented to disentangle these matters by experiment.

Let us first comment on the available information regarding the stripe phase spin system. The spin ordering temperature appears to be strongly suppressed as compared to half-filling[25]. A first cause can be a decrease of the microscopic exchange interactions. However, the more interesting possibility is that some microscopic disordering influence has moved the antiferromagnet closer to the zero-temperature order-disorder transition (quantum critical point). The few data available at present seem to favor the second possibility. We specifically refer to the ESR work by Kataev *et al.*[94] on $\text{La}_{1.99-x-y}\text{Eu}_y\text{Gd}_{0.01}\text{Sr}_x\text{CuO}_4$ exploiting the Gd local moments to probe the spin system in the CuO planes. Quite remarkably, little change is seen in the spin-lattice relaxation rate ($1/T_1$) at the charge ordering temperature, $T_{co} \simeq 70\text{K}$. Above T_{co} the $1/T_1$ is quite similar to that in $\text{La}_{2-x}\text{Sr}_x\text{CuO}_4$ where it is known from e.g. neutron scattering that the magnetic correlation length ξ is already quite large at the temperatures of interest: since the width of the incommensurate peaks is smaller than their separation, the correlation length is larger than the stripe spacing[95]. It follows that at $T \simeq T_{co}$ a continuum description of the spin dynamics should be sensible. Below T_{co} $1/T_1$ starts to increase exponentially upon lowering temperature, signalling the diverging correlation length associated with the renormalized classical regime. Taken together, this fits quite well the expectations for a quantum antiferromagnet which is rather close to its quantum critical point, with a crossover temperature from the renormalized classical- to the quantum critical regime $T^* \simeq T_{co}$.

5.2 The coupled spin ladders model

The increase of the coupling constant g_0 , controlling the long wavelength fluctuations of the quantum non linear sigma model, originates in some microscopic phenomenon. A limiting case is the one in which charge can be regarded as completely static even on the scale

of the lattice constant, such that its effect is to cause a spatially anisotropic distribution of exchange interactions. The relevant model is that of a regular stripe structure as depicted in Fig 5-2. This simple picture is considered by various groups[89, 90]. The physics of such a model is similar to that of the Hubbard model at half-filling. At low-energy, the relevant degrees of freedom of the system are the transversal fluctuations of the antiferromagnetic order parameter in the spin system. The interaction between neighboring spin domains is generated by the virtual excitations across the stripes, spins hops back and forth across the stripes generating an effective antiferromagnetic interaction between spins on different sides of the stripe. The unique antiphase-domain spin structure of the stripe phase seen in the experiment is then recovered, Fig. 5-2. The spin-spin interaction J' across the stripe will obviously be smaller than the interaction in the spin domain J . This weakness of the exchange interaction across the stripes will have a disordering influence on the stripe spin system. To see this, consider the following two limiting cases. At $J' = J$, the spin system is equivalent to an isotropic two-dimensional Heisenberg system, which possesses long range order at $T = 0$. On the other hand, for $J' = 0$ the system is effectively one dimensional and according to the Mermin-Wagner theorem long range order can not develop even at $T = 0$. The system can be switched between the two physically different cases by tuning the parameter $\alpha = J'/J$.

As indicated in Fig. 5-1, there are two options[9]: the stripes can be *bond* or *site* ordered. It is expected that the spin dynamics associated with the hole-rich regions is characterized by a short time scale and the magnetic ordering phenomena are therefore associated with the magnetic domains. The spin-only model of relevance becomes either a spin $S = 1/2$ Heisenberg model describing three-leg ladders (site ordered) or two-leg ladders (bond ordered) with uniform exchange interactions (J), mutually coupled by a weaker exchange interaction coupling (αJ , $\alpha < 1$). This model is explicitly,

$$\mathcal{H} = J \sum_{\vec{i}} \vec{S}_{\vec{i}} \vec{S}_{\vec{i}+\vec{\delta}_y} + J \sum_{i_x \neq pn_1, i_y} \vec{S}_{\vec{i}} \vec{S}_{\vec{i}+\vec{\delta}_x} + \alpha J \sum_{i_x=pn_1, i_y} \vec{S}_{\vec{i}} \vec{S}_{\vec{i}+\vec{\delta}_x}, \quad (5.2.1)$$

where $\vec{i} = (i_x, i_y)$ runs over a square lattice, $\vec{\delta}_x = (1, 0)$, $\vec{\delta}_y = (0, 1)$. n_1 measures the

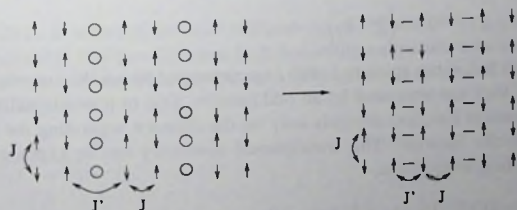


Figure 5-2. Schematic representation of the static stripe model. Stripes live on bonds between the spins.

width of the ladder and p counts the ladders.

Since the interest is in non-universal quantities as related to the non-trivial lattice cut-off, the model Eq.(5.2.1) is studied numerically. We used a highly efficient loop cluster algorithm Quantum Monte-Carlo method[96]. Cluster algorithm has the ability to completely eliminate the critical slowing down problem. Moreover, as discussed earlier a significant advantage of the loop algorithm is that it allows for the implementation of a technique known as the improved estimators technique[97]. The use of the improved estimator reduces the time for collecting statistically independent measurements by a few orders of magnitudes. It is quite efficient in calculating all quantities that can be reduced to the calculation of spin-spin correlations. A rather detailed description of the loop cluster algorithm and the idea of improved estimators is provided in section 2.3 in chapter 2.

Although the loop algorithm can be implemented directly in continuum time, we used the discrete version of the algorithm[99]. In terms of accuracy there is actually no advantage in using the time continuum version, but one gains time since no extrapolation is required. We, however, carefully checked that the systematic errors were not exceeding the statistical errors, which turned out to be quite small relative to the required accuracy. The advantage of using the discrete version, in our case, will become clear later, (chapter 6) where we will generalize the present model to one where the stripes are not static but rather dynamical. A generalization of the discrete loop algorithm to include dynamical stripes will there be considered.

To keep track of the various finite temperature cross-overs we focussed on the temperature dependence of the staggered correlation length in both the directions parallel- (ξ_y) and perpendicular (ξ_x) to the stripes. To ensure complete thermalization, we typically insisted on $3 \cdot 10^4$ loop updates for equilibration and for measurements we generated up to $(2 - 3) \cdot 10^5$ loops updates. To get rid of finite size effects, the spatial extend of the system in the x and y directions is always kept at $L_{x,y} \geq 6 \cdot \xi_{x,y}$ [98]. Although this rule has proved to be quite good, we have also checked that increasing the system size does not lead to a noticeable improvement in the accuracy.

To determine the correlation length, one has first to compute the staggered spin-spin correlation function, defined as

$$C(i, j) = (-1)^{\text{sign}(i, j)} \left\langle \vec{S}_i \cdot \vec{S}_j \right\rangle, \quad (5.2.2)$$

where $\text{sign}(i, j)$ is 1 if the spins at i and j are separated by an even number of exchange bonds and -1 if they are separated by an odd number. Due to translational invariance, the staggered correlation function depends only on the distance separating the two spins and not on their specific location. This translational symmetry can be exploited to write the correlation function in the form,

$$C(\vec{r}) = (-1)^{r_x + r_y} \left\langle \vec{S}_{i+r} \cdot \vec{S}_i \right\rangle, \quad (5.2.3)$$

At large distances, $r/\xi \gg 1$, $C(r)$ decays exponentially,

$$C(r) = r^{-\lambda} e^{-r/\xi}. \quad (5.2.4)$$

with $\lambda = 1/2$, which is equivalent to the two dimensional Ornstein-Zernike (OZ) form. For a finite lattice with periodic boundary condition one should in fact use the OZ expression defined on a 2 dimensional torus,

$$C(r) = A(r^{-1/2}e^{-r/\xi} + (L-r)^{-1/2}e^{-(L-r)/\xi}). \quad (5.2.5)$$

To extract the correlation length from the measured staggered spin-spin correlation, we fitted the measurements to the above OZ form, separately for the x - ($\vec{r} = (r, 0)$, $L = L_x$) and y ($\vec{r} = (0, r)$, $L = L_y$) directions. To ensure asymptoticity, we have omitted the first few points.

We checked our results against the known results for both isolated ladders by Greven *et al.*[100] ($\alpha = 0$, $n_l = 1, 2, 3$) and the low temperature results for the isotropic ($\alpha = 1$) limit[97, 99].

Since $O(3)$ universality is bound to apply at scales much larger than any lattice related cross-over scale, universal forms for the temperature dependence of the correlation length can be used to further characterize the long wavelength dynamics. The absolute lattice cut-off is reached at a temperature (T_{max}) where the correlation length parallel to the stripes (ξ_y) becomes of order of the lattice constant. However, the problem is characterized by a second cut-off: when the correlation length is less than the lattice constant in the direction perpendicular to the stripes (a_x), the dynamics is that of N_x independently fluctuating spin ladders. We define T_0 as the temperature where $\xi_x \simeq a_x$ being the cross-over temperature below which the system approaches 2+1D $O(3)$ universality. In this latter regime, further cross-overs are present. When the effective coupling constant (g_0) is less than the critical coupling constant (g_c) a cross-over occurs from a 'high' temperature quantum critical-(QC) to a low temperature renormalized classical (RC) regime. In the QC regime $\xi \sim 1/T$ while the cross-over temperature T^* to the RC regime can be deduced from the exponential increase of the correlation length at low T , using[7, 98, 101],

$$\xi(T) \propto \frac{e^{T^*/T}}{2T^* + T}. \quad (5.2.6)$$

where $T^* = 2\pi\rho_s$ in terms of the spin stiffness $\rho_s(\alpha)$. When $g_0 > g_c$, the ground state is quantum disordered (QD) as signalled by ξ becoming temperature independent, and the crossover temperature T' between the QC- and QD regimes is estimated from the approximate relation[100],

$$T' = \frac{c_y}{\xi_y(T \rightarrow 0)}, \quad (5.2.7)$$

where c_y is spin wave velocity in the strong direction.

We determined the various cross-over lines as function of α for the cases $n_l = 1, 2$ and 3 (anisotropic Heisenberg, coupled two- and three leg ladders, respectively). To determine T_0 , we used for α close to 1 the same criterium as for the T_{max} determination in the isotropic

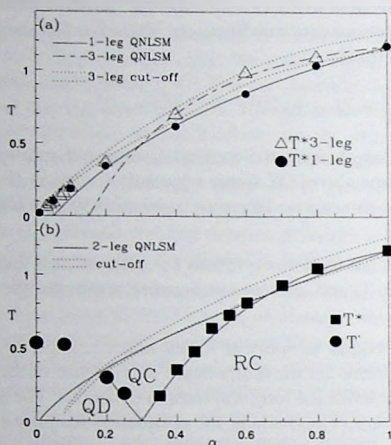


Figure 5-3. Crossover temperatures as a function of anisotropy α for the coupled three-leg (a) and two-leg (b) spin-ladder models. The lines and points refer to the analytical- and numerical results, respectively, for the various scales. Notice that the 1-leg 'cut-off' (1D-2D cross-over) follows closely the results for T^* .

problem ($\xi_x(T^0) = 0.7 - 0.8$). This becomes inconsistent for small α where one better incorporates the width of the ladder ($\xi_x(T_0) = n_l \times (0.7 - 0.8)$) and we used a linear interpolation to connect smoothly both limits. We checked that below the T_0 , determined in this way, both ξ_x and ξ_y exhibited the same dependence on temperature after an overall change of scale, demonstrating that the collective dynamics is indeed in a 2+1D regime. We have also checked that, along the stripe direction the one dimensional OZ form ($\lambda = 1$) fits better to our data than the two dimensional one above T_0 .

In Fig. 5-3 we summarize our results in the form of a cross-over diagram as function of α and temperature, both for the 1- and 3-leg (Fig.5-3a) and the 2-leg (Fig.5-3b) cases. Consistent with analytic predictions[92], the behavior is radically different for the half-integer spin 1- and 3 leg cases on the one hand, and the 'integer spin' 2-leg case on the other hand. Let us first discuss the former. Here the ground state remains in the renormalized classical regime for any finite α . The reason is obvious. In isolated ladders ($\alpha = 0$) with an uneven number of legs the ground state is a Luttinger liquid exhibiting algebraic long range order, meaning that the spin-spin correlation function behave algebraically, (see Eqs. 5.2.8 and 6.3.2 in section 6.3). Now for such a system any finite ladder-to-ladder cou-

pling/interaction will suffice to transform this algebraic behavior to/and stabilize true long range order at $T = 0$ [92, 93] in $(2+1)$ dimension. A simple argument to understand this is as follows: The quasi long range order implies that an infinitely large number of spins, in each ladder, behave collectively. Coupling such a long patches of collective spins is like coupling an infinitely large spins. Obviously any finite coupling of infinitely large spins will lock them together.

This in turn implies that T^* should be finite, so that the classical nature of the ground state becomes visible. Interestingly, our calculations indicate that T^* and T^0 basically coincide for any α for odd leg ladders. This means that at the moment the system discovers that it is $2+1$ dimensional, the classical behavior sets in.

Our finding that T^0 increases linearly with α for small α (Fig.5-3a) confirms the scaling theory by Affleck and Halperin for this problem[93]. The behavior of the spin-spin correlator for an isolated chain,

$$\langle S(x)S(0) \rangle \sim (1/x) \exp(-x/\xi_1), \quad (5.2.8)$$

with $\xi_1 \sim 1/T$, signals the approach to the Gaussian fixed point: within the thermal length ξ_1 the system exhibits algebraic long range order. For finite α the crossover temperature T^0 , from the $1+1$ D behavior to the $2+1$ D behavior, can be found using the standard mean-field consideration: at T^0 temperature becomes of order of the exchange interaction, per unit length, between two patches of correlated spins on neighboring chains. The size of these patch is of the order of the correlation length ξ_1 . Therefore we have,

$$k_B T^0 \simeq \alpha \Phi_1^2 / \xi_1 (T^0) \quad (5.2.9)$$

where Φ_1 is the staggered magnetization of the a patch of spins of length ξ_1 and is given by

$$\Phi_1 = \xi_1 \langle T^0 \rangle \phi. \quad (5.2.10)$$

ϕ being the Néel order parameter or the microscopic staggered magnetization. Taking ϕ to be independent of α would yield the erroneous result that $T^0 \sim \sqrt{\alpha}$. The subtlety is that when α is sufficiently small, the quantum dynamics within the correlation volume ξ_1 is already in the $2+1$ D regime[90]. Using the $T = 0$ result in the $2+1$ D derived by Affleck and Halperin that $\phi \sim \sqrt{\alpha}$ [93], we recover $T^0 \sim \alpha$, $\alpha \ll 1$.

The other feature worthwhile mentioning is that T^0 and T^* are identical for the 1- and 3-leg cases for small α 's. This is in line with the observations by Frishmut *et al.*[102] that these spin ladders renormalize in identical Luttinger liquids when the ladder exchange interactions are isotropic.

In the two-leg ladders case (Fig.5-3b) the quantum order-disorder transition occurs at a finite value of α , $\alpha_c = 0.30(2)$. This is in line with the qualitative expectations (see also

[103, 104]). Since the isolated two leg ladders are incompressible spin systems, the ladder-to ladder interaction has to overcome the single ladder energy gap before the two dimensional lock-in can occur. This critical α is rather large, and in addition, the $1+1$ D \rightarrow $2+1$ D crossover temperature T^0 shows the upward curvature ($T^0 \sim \sqrt{\alpha}$) previously predicted from a scaling analysis of the anisotropic QNLS model (AQNLS)[90]. As a ramification, T^0 and T^* (as well as T') separate and a *large, genuinely 2+1 D quantum critical regime opens up* around α_c . This is in marked contrast with the isotropic Heisenberg model where the renormalized classical regime sets in essentially at the lattice cut-off[106, 107].

5.3 Comparison with renormalization group analysis

The gross α dependences of the various cross-over temperatures can be understood by considering the anisotropic quantum nonlinear sigma model (AQNLMS) model relevant for the coupled spin-ladders problem. This is obtained by taking the naive continuum limit for the ladder problem. An average staggered field $\bar{\phi}$ is introduced for a block of $2 \times n_l$ sites. Integrating out the quadratic fluctuations[108], the effective action for $\bar{\phi}$ becomes the AQNLS model with anisotropic spin wave velocities,

$$c_x^2 = \alpha c_0^2 \begin{cases} \frac{(3+\alpha)}{2(1+\alpha)} & \text{for } n_l = 2 \\ \frac{9(7+3\alpha)}{2(1+2\alpha)(13+2\alpha)} & \text{for } n_l = 3 \end{cases} \quad (5.3.1)$$

$$c_y^2 = c_0^2 \begin{cases} \frac{(3+\alpha)}{4} & \text{for } n_l = 2 \\ \frac{3(7+3\alpha)}{2(13+2\alpha)} & \text{for } n_l = 3 \end{cases}, \quad (5.3.2)$$

where c_0 is the spin wave velocity in the isotropic limit. The coupling constant g_0 is α independent and the same as for the isotropic model.

Van Duin and Zaanen carried out a complete scaling analysis for the spatially anisotropic quantum non-linear sigma model, Ref.[90]. According to their analysis the renormalized spin-stiffness becomes in terms of the velocities $c_{x,y}$,

$$\rho_s(\alpha) = \rho_s \frac{c_x(1 - \frac{g_0}{g_c(\alpha)})}{c_y(1 - \frac{g_0}{g_c(1)})} \quad (5.3.3)$$

where

$$g_c(\alpha) = 4\pi \sqrt{c_0/c_y} \left(1 + \frac{2}{\pi} (c_y \operatorname{arsinh}[c_x/c_y]/c_x + \ln[c_y(1 + \sqrt{1 + c_x^2/c_y^2})/c_x/(1 + \sqrt{2})^2]) \right) \quad (5.3.4)$$

and ρ_s is the spin stiffness for $\alpha = 1$. Moreover, they found the following dependence of the crossover temperatures scales, T^* , T^0 and T' , on the α . $T^* = 2\pi\rho_s(\alpha)$, $T^0 =$

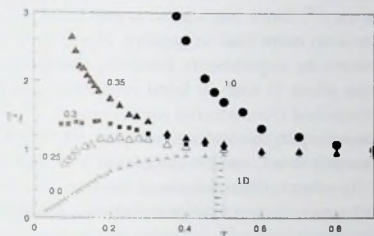


Figure 5-4. $\xi_y T$ versus temperature for the 2-leg system, when the α 's are close to critical point. Results for $\alpha = 0.0$ (isolated ladders) and 1.0 (isotropic limit) are added for comparison. The vertical bar indicates the 1D-2D cross-over temperature.

$2\pi\rho_s c_x(g_0/(4\pi c_0) + (1 - g_0/g_c)/c_y)$ and $T' = \text{const.}|\rho_s(\alpha)|$. It turns out that for the bare coupling constant g^0 as determined for the isotropic case ($g^0 = 9.1$), the order-disorder transition occurs at a somewhat small value of $\alpha = 0.08$, which is not surprising given the approximations involved (one-loop level). However, by adjusting g_0 to shift α_c to its numerical value ($g_0 = 11.0$), we find a very close agreement between the numerical- and analytical results for the various cross-over temperatures (Fig.5-3b). As can be seen from (Fig.5-3a), the above analysis also works quite well for the three-leg ladders for $\alpha \geq 0.4$. Remarkably, it seems that T^* switches rather suddenly from the AQNLS behavior at large α to the linear behavior expected for the Luttinger liquid regime, as if the topological terms start to dominate rather suddenly.

5.4 Conclusions

Besides its intrinsic interest, the above does have potentially important ramifications for the understanding of the quantum-magnetism in cuprates: bond ordering of stripes would imply that already at rather moderate values of the anisotropy α , spin-ladder physics alone would enhance the quantum spin fluctuations substantially. This can be further illustrated by comparing the temperature dependence of $T\xi_y(T)$ for the isotropic spin system $\alpha = 1$ with that of the coupled two-leg ladders in the vicinity of the critical α (Fig.5.3). This quantity can be directly compared with the spin-spin relaxation rate $1/T_{2G}$ and, with some

caution, also to $1/T$ [106, 109] (a dynamical critical exponent $z = 1$ is only strictly obeyed in the QC regime). As compared to the isotropic case, the exponential increase of $T\xi$ (signalling the renormalized classical regime) is shifted to a low temperature, while over most of the temperature range $T\xi(T)$ is constant, as is found in cuprates. It is noted that the 'quantum-critical signature' $\xi \sim 1/T$ extends in the temperature range above the dimensional crossover temperature T^0 . Since this regime is non-universal this should be regarded as a quasi-criticality. This is no more than suggestive. However, it points at a simple strategy to clear up these matters by experiments involving the static stripe phase. It should be established if the stripe phase is site- or bond ordered which can be done by NMR. Next, the α should be determined from neutron measurements of the spin-wave velocities, Eq.(5.3.2). Using these as an input, the temperature dependence of the correlation-length, as well as the NMR relaxation rates, can be calculated to a high precision starting from a microscopic spin-only dynamics. Comparison of these quantities to experiment should yield insights in the microscopic origin of the peculiar spin dynamics in doped cuprates.

6 Dynamical stripes in an antiferromagnetic spin background

6.1 Introduction

In chapter 3 we concluded that a single stripe is directed and moreover, depending on the curvature energy, it can either be classical, disordered flat or Gaussian. The most interesting of these are the Gaussian strings, as they are delocalized and could be possible ingredients for a string liquid. In chapter 5, a model of static stripes in a spin background is considered. These are either bond-centered or site-centered. The spin dynamics was studied and it was shown that for bond-centered stripes much of the spin fluctuations will originate in the spin sector. An interesting quantum phase transition takes place at a finite charge induced anisotropy. For site-centered stripes the charge should play the central role for the quantum spin fluctuations to be present. An interesting question is what happens when the charge stripes themselves become delocalized quantum mechanically. In this final chapter we will introduce, and study numerically, a model of a system of interacting, quantum fluctuating, anti-phase stripes living in a quantum antiferromagnetic spin background. The stripe system will correspond with a quantum string liquid and because the fluctuating stripes are anti-phase boundaries for the spin system, they will fluctuate the spin system as well.

In the first section we will review a work on a pure quantum strings system. In the second section we show that a topological spin-charge hidden order exists for such a stripe system. We then introduce the model, discuss what phases and order one might expect. And finally the numerical results will be presented and discussed extensively in the light of the first two sections.

6.2 The Quantum string gas

Before considering the problem of fluctuating strings in a spinfull background we review in this section the work by Zaanen [110] on a gas of elastic quantum strings living in 2+1 dimensions.

Motivated by the cuprate stripes, which are viewed as preformed line-like textures (chapter 3), Zaanen considered a gas of quantum strings with a finite tension, embedded in a 2+1 dimensional space-time. The main question addressed is whether it is possible to quantum melt a system of completely intact, infinitely long stripes. Even in this limit the stripes themselves can still execute quantum meandering motions and a consensus has been growing that a single stripe is like a quantum string with finite line-tension [34, 77, 78, 111, 112]. The ideal string gas is defined as the low density limit where the width of the strings

can be neglected, while the strings only interact via the requirement that they cannot intersect[113], i.e. via a hard-core condition. This is obviously the limit where quantum kinetic energy is most important. It is shown that in 2+1 dimensions even in this limit this string system turns into a solid at zero temperature. This solidification is driven by the quantum-mechanical analogue of the entropic interactions known from statistical mechanics. In a system with steric interactions between its constituents, entropy is paid at collisions in the classical system and kinetic energy in the quantum system. This causes an effective repulsion and these 'quantum entropic' interactions dominate to such an extent in the string gas that they cause it to solidify always.

As discussed in chapter 3, in the path integral representation, the quantum string gas becomes equivalent to the statistical physics problem of a stack of elastic membranes ('world-sheets') which do not interact except for the requirement that the membranes do not intersect. A seminal contribution in the study of entropic interactions in classical systems composed of extended entities is the analysis by Helfrich[115] of a system of extrinsic curvature membranes in 3D, interacting only via an excluded volume constraint. In the quantum context, this method will be illustrated here by reviewing the analysis of the hard-core Bose gas in 1+1D, which is closely related to Helfrich's extrinsic curvature membranes in 3D. The string gas will turn out to be a straightforward, but non-trivial extension of the Bose gas: different from the latter, the quantum entropic interactions of the string gas are driven by long wavelength fluctuations. I will only cite the result for the string gas and refer the interested reader to the reference[110] for further details.

The hard-core Bose gas is a gas of particles characterized by a kinetic scale E_F , while at the same time the long wavelength density-density correlator exhibits the algebraic decay characteristic for a harmonic crystal in 1+1D: $\langle n(x)n(0) \rangle \sim \cos(2k_F x)/x^2$. The concept of entropic interaction offers a simple explanation. At zero temperature the hard-core gas corresponds with the statistical physics problem of a gas of non-intersecting elastic lines embedded in 2D space-time[114], which are directed along the time direction. The space-like displacement of the i -th worldline is parametrized in terms of a field $\phi_i(\tau)$ (τ is imaginary time) and the partition function is,

$$\begin{aligned} Z &= \prod_{i=1}^N \int d\phi_i(\tau) e^{-\frac{S}{\hbar}}, \\ S &= \int d\tau \sum_i \frac{M}{2} (\partial_\tau \phi_i)^2, \end{aligned} \quad (6.2.1)$$

supplemented by the avoidance condition,

$$\phi_1 < \phi_2 < \dots < \phi_N. \quad (6.2.2)$$

The hard-core condition Eq.(6.2.2) renders this to be a highly non-trivial problem. Helfrich considered the related classical problem of a stack of linearized and directed extrinsic curvature membranes embedded in 3D space. Although this is a higher dimensional problem, the action depends on double derivatives instead of the single derivatives in Eq. (6.2.1),

$(\partial_\mu \phi)^2 \rightarrow (\partial_\tau^2 \phi)^2$, and it follows from powercounting that this problem is equivalent to the hard-core Bose gas in the present context. In order to determine the 'entropic' elastic modulus at long wavelength Helfrich introduced the following construction. Assume that the long wavelength modulus B_0 is finite. For the Bose gas this implies that the long wavelength action is that of a 1+1D harmonic solid,

$$S_{eff} = \frac{1}{2} \int d\tau \int dx \left[\rho (\partial_\tau \psi)^2 + B_0 (\partial_x \psi)^2 \right], \quad (6.2.3)$$

where $\psi(x, \tau)$ is a coarse grained long-wavelength displacement field, $\rho = M/d$ the mass density, and d the average interworldline distance ($n = 1/d$ is the density). Obviously, for finite B_0 fluctuations are suppressed relative to the case that B_0 vanishes and this cost of kinetic energy in the quantum problem (entropy in the classical problem) raises the free-energy. Define this 'free-energy of membrane joining' as

$$\Delta F(B_0) = F(B_0) - F(B_0 = 0). \quad (6.2.4)$$

At the same time, by general principle the 'true' long wavelength modulus B in the x direction has to satisfy (V is the volume),

$$B = d^2 \frac{\partial^2 (\Delta F(B_0)/V)}{\partial d^2}. \quad (6.2.5)$$

In case of the steric interactions, the only source of long wavelength rigidity in the space direction is the fluctuation contribution to ΔF . This means that $B_0 = B$ and B can be self-consistently determined from the differential equation, Eq. (6.2.5). In fact, the only ambiguity in this procedure is the choice for the short distance cut-off for the fluctuations in the x direction, which is expected to be proportional to the distance between the world-lines, $x_{min} = \eta d$. The shortcoming of the method is that mode-couplings are completely neglected and this is not quite correct since the outcomes do depend crucially on short wavelength fluctuations. However, it appears [116] that these effects can be absorbed in the non-universal 'fudge-factor' η , giving rise to changes in numerical prefactors without affecting the dependence of B on the dimensionful quantities in the problem.

The free energy difference for the Bose gas, Eq. (6.2.4), is easily computed from the Gaussian action Eq. (6.2.3) and expanding up to leading order in $\lambda = (\sqrt{B} \tau_0)/(\sqrt{\rho} d)$ (τ_0 is the cut-off time), it becomes small in the low density limit,

$$\frac{\Delta F}{V} = \frac{\pi \hbar}{4\eta^2} \sqrt{\frac{B}{M}} \frac{1}{d^{3/2}} + O(\lambda^2). \quad (6.2.6)$$

Inserting Eq. (6.2.6) on the r.h.s. of the self-consistency equation Eq. (6.2.5) and solving the differential equation up to leading order in λ yields,

$$B = \frac{9\pi^2}{\eta^4} \frac{\hbar^2}{M d^3}. \quad (6.2.7)$$

It is easily checked that this corresponds with the elasticity modulus appearing in the bosonized action of the hard-core boson problem, taking $\eta = \sqrt{6}$. Hence, the space-like rigidity of the bosc gas at long wavelength can be understood as a consequence of entropic interactions living in Euclidean space-time.

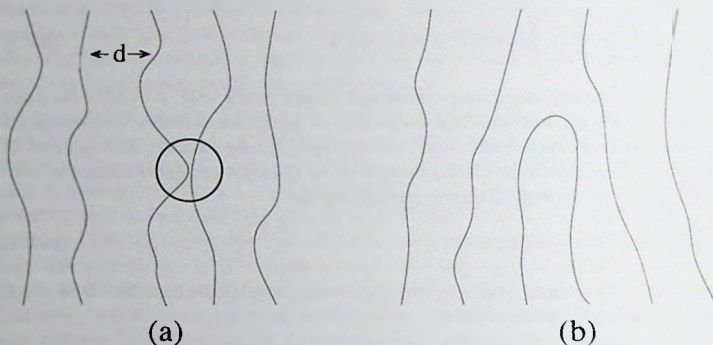


Figure 6-1. A typical space-like configuration in the directed string gas (a), including a collision of the type driving the 'quantum-entropic' interactions. In the string gas dislocations (b) do not proliferate, and it is therefore equivalent to the directed gas.

For the string gas problem, the string gas in 2+1D is related to the hard-core bosc gas in 1+1D: the latter can be viewed as the *compactified* version of the former. Imagine that the hard-core bosc gas lives actually in 2+1D where the additional dimension y is rolled up to a cylinder with a compactification radius R_y of order of the lattice constant a , while the bosons are spread out in elastic strings wrapped around the y -axis. Let R_y go to infinity. This has the effect that the embedding space becomes 2 + 1 dimensional, while the boson worldlines spread out in string worldsheets. This 'directed string-gas' is not yet the one of interest, since the worldsheets are not only directed along the imaginary time directions (as required by quantum mechanics) but also in the $x - y$ plane (Fig. 1a). The difficulty is that in the string gas dislocations can occur (Fig. 1b), and if these proliferate they will destroy the generic long range order of the directed string gas. However, two objections can be raised against a dislocation mediated quantum melting. The first objection involves a further specification: As pointed out in chapter 3, 'overhangs' like in Fig. 1b are events where transversal fluctuations are suppressed, relative to those around directed configurations. Therefore already a single string tends to acquire spontaneously a direction, if it is regularized on a *lattice* (like the stripes). The second argument is more general. It is a classic result[117, 113] that at any finite temperature dislocations proliferate in the string gas. However, in the presence of a finite range interaction of any strength the Kosterlitz-Thouless transition will occur at a finite temperature. Hence, by letting this interaction to become arbitrary weak a $T = 0$ transition can always be circumvented.

When dislocations can be excluded the directed string gas remains and this is just the decompactified Bose gas. In Euclidean space-time it corresponds with a sequentially ordered stack of elastic membranes. This allows the use of Helfrich methods and a similar, but otherwise non-trivial derivation for the induced elastic modulus can be done. Zaanen found that the induced modulus, up to leading order in the density, is given by:

$$B = Ad^2 e^{-\eta(\frac{5d}{\pi})^{1/3} \frac{1}{\mu^{1/3}}} \quad (6.2.8)$$

where A is an integration constant and μ is the 'coupling constant' for the string-gas,

$$\mu = \frac{\hbar}{\rho c d^2}. \quad (6.2.9)$$

This result demonstrates that in parallel with the hard-core Bose gas, the string gas is characterized by a fluctuation induced elastic modulus at long wavelength which will be small but finite even at low density. Eq. (6.2.8) describes the counter-intuitive fact that upon increasing the kinetic energy of a single string, the rigidity of this medium is actually increasing. The parameter μ is the dimensionless quantity measuring the importance of quantum fluctuations[32]. Since quantum dislocation melting is prohibited, the string gas is always a solid, and this solid becomes more rigid when the microscopic quantum fluctuations become more important. This might appear as less surprising when the (directed) string gas is viewed as a decompactified Bose gas. On the one hand, the larger internal dimensionality of the worldsheets as compared to the worldlines weakens the 'quantum-entropic' interactions, but the enlarged overall dimensionality causes the algebraic long range order of the 1+1D Bose gas to become the true long range order of the 2+1D string gas.

6.3 Hidden order in the stripe phase

The above connection between the physics in (1+1) dimensions and the physics of directed strings gas in (2+1) dimensions is in fact more deep. An interesting observation, due to Zaanen, reveals a deeper similarity between the (1+1) dimensional doped Hubbard chain and the (2+1) dimensional anti-phase stripe system in the antiferromagnetic background. This similarity or connection involve a hidden order that occurs in both cases. This hidden order involves a global topological operator besides a local operator.

Consider a doped Hubbard chain at large U , ($U \gg t$), with a low density of holes Eq. (1.2.1). Such a system is known to be a Luttinger liquid where spin and charge separate. The charge (ρ) and spin (\vec{S}) correlators behave as follows:

$$\langle \rho(x) \rho(x') \rangle \sim B_\rho \frac{\cos(2\varepsilon)(x - x')}{|x - x'|^{K_\rho}} \quad (6.3.1)$$

$$\langle \vec{S}(x) \vec{S}(x') \rangle \sim B_\sigma \frac{\cos(\varepsilon)(x - x')}{|x - x'|^{K_\sigma + K_\rho}} \quad (6.3.2)$$

at long distances. B_ρ and B_σ are non-universal amplitudes while the exponents $K_{\rho,\sigma}$ correspond with the stiffness of the free charge and spin fields, respectively. The wavevectors where the dominant correlations occur ($\varepsilon = 2k_F$ and $\varepsilon = 4k_F$ for spin and charge, respectively) are quite like to what is found in underdoped cuprates: $\varepsilon = x(\pi/a)$ (a is the lattice constant).

Calling this a liquid is actually a bit misleading. The power law behaviors revealed by Eqs. (6.3.1.6.3.2) in fact reflect order more than disorder. As emphasized by Haldane and many others, these correlators express *algebraic long range order*. The Luttinger liquid should be viewed basically as an ordered state, a one dimensional Wigner crystal which is at the same time an antiferromagnet. Since both condensates carry zero-modes (massless phonons and magnons) true long range order is impossible in 1+1D. As is well known, the virtual admixing of these modes in the ground state changes true long range order in the algebraic correlations revealed by equations (6.3.1.6.3.2).

It is convenient to associate the charge dynamics with the low density gas of holes. Two holes cannot occupy the same site, and should therefore be regarded as hard-core particles. As discussed in the previous section (6.2), by general principle, this hard core gas crystallizes into a massless 1+1D Wigner crystal. This explains Eq. (6.3.1): 2ε is nothing else than $2\pi/d$, where $d = a/x$ is the average interparticle distance, while K_ρ is the stiffness associated with the crystal. How to understand the spin correlator? When the hole moves, say, to the right the electron moves to the left, colliding with the electron which was already to the left of the hole before it moved. According to Schulz, the spins of these electrons are subjected to an antiferromagnetic exchange interaction. Hence, the spins surrounding the hole have an antiparallel relative orientation which is not different from what is found in the pure spin system. Alternatively, one can view such a configuration as a (missing) electron bound to an Ising-type domain wall in the staggered magnetization with a spin opposite to that of the (missing) electron: this is of course nothing else than the holon. The holons condense in the Wigner crystal, but since they are also Ising domain walls in the algebraic antiferromagnet they shift the ordering wavevector to the incommensurate 2ε while their Gaussian zero-point motions also fluctuate the spin system and Eq. (6.3.2) follows.

By spreading out ('decompactifying') this Luttinger liquid along an additional space direction, one obtains a 2+1D state which is remarkably close to a stripe phase. The holons spread out in lines of holes which are at the time Ising domain walls in the spin system. The algebraic charge- and spin order changes into true long range order. One can in fact fairly say that *the Luttinger liquid associated with a 1+1D doped Mott-insulator is nothing else than a stripe phase showing algebraic long range order*. Although the microscopic mechanism responsible for this phenomenon in 2+1D is still poorly understood, one finds it hard to accept that the similarity with the 1+1D Luttinger liquid is merely accidental.

Now a deeper connection is clear when one considers the Ogata and Shiba[121] solution of the Hubbard chain in the limit of strong interaction $U \gg t$. Without going into details, the Ogata-Shiba solution shows that holons are genuine entities on all scales, down to the lattice constant. In 1D the Hubbard model is exactly solvable using Bethe-Ansatz. Although the information on the spin dynamics reside in the amplitude of the wavefunc-

tion, the equation for the spin and charge rapidities are entangled in the general case. Ogata and Shiba observed, however, that in the large U limit these equations separate. The charge dynamics can be associated with the holes, which become equivalent to hard-core bosons, while the spin dynamics are in one-to-one relation with an effective Heisenberg chain. This effective chain is obtained by a *squeezing* operation of the original Hubbard chain: take a particular configuration of holes and consider the spin system left behind after taking out the holes and their corresponding sites as just a Heisenberg chain. Below we will show that a similar *squeezing* operation can be done for a system of stripes and the spin system left behind is related to the 2D Heisenberg system. To put this in mathematical terms, consider the following. Take an arbitrary point x_0 on the chain and define the following non-local (topological spin) operator,

$$\tilde{T}_{x_0, x} = e^{i\pi \sum_{l=x_0}^x (1-n_l)} (-1)^x \tilde{S}_x \quad (6.3.3)$$

where n_l measures the charge on site l (n_l has eigenvalues 0, 1 and 2 for an empty-, singly-, and doubly occupied site, respectively). Now consider the correlator,

$$O_{top}(|x - x'|, x_0) = \langle \Psi | \tilde{T}_{x_0, x} \tilde{T}_{x_0, x'} | \Psi \rangle \quad (6.3.4)$$

the meaning of the 'charge string operator' $\exp i\pi \sum_{l=x_0}^x (1 - n_l)$ is that it adds a minus sign every time that a hole is passed on the trajectory $x_0 - x$. One infers immediately that the charge string operator keeps track of the sign changes in between the points x and x' or *squeezing* this part of the chain and thereby cutting out the spin disorder caused by the motion of the Ising domain walls attached to the hole. In fact, it can be easily demonstrated by a simple calculation [118] that for the Ogata-Shiba case the following asymptotic form holds (modulo log corrections),

$$O_{top}(|x - x'|, x_0) = B_\sigma \frac{(n)}{|x - x'|^{K_\sigma}} \quad (6.3.5)$$

to be compared with the correlator of staggered spin eq. (6.3.2). Here $K_\sigma = 1$ (Heisenberg) and B_σ is the staggered spin amplitude associated with the Heisenberg chain.

The key point here is that the above correlation function is independent of the paths joining x_0 and x or x_0 and x' .

Now in the stripe system, the same "topological spin" operator can be defined,

$$\tilde{T}_{\vec{r}_0, \vec{r}} = e^{i\pi \sum_{\vec{r}' \in \mathcal{L}} (1-n_{\vec{r}'})} (-1)^{(x+y)} \tilde{S}_{\vec{r}} \quad (6.3.6)$$

where \mathcal{L} is a path joining point \vec{r}_0 and \vec{r} . The topological spin-spin correlator in the original spin now reads,

$$O_{top}(|\vec{r} - \vec{r}'|, \mathcal{C}) = \langle \Psi | (-1)^{(x+y)} \tilde{S}_{\vec{r}} e^{i\pi \sum_{\vec{r}'' \in \mathcal{C}} (1-n_{\vec{r}''})} (-1)^{(x'+y')} \tilde{S}_{\vec{r}'} | \Psi \rangle \quad (6.3.7)$$

where, now C is a path joining point \vec{x} and \vec{x}' .

The stripe phase, of the type considered in the previous section, where dislocations can be excluded, can be considered as (2+1) dimensional decompactification of the (1+1) dimensional Hubbard model in the Ogata-Shiba limit. Similar to the one dimensional case, in this phase the above "topological" correlation function is again independent of the path C . One can then, write;

$$O_{top.}(|\vec{r} - \vec{r}'|, |C|) = O_{top.}(|\vec{r} - \vec{r}'|) \quad (6.3.8)$$

where $|C|$ is the length of the path C

The independence of a correlator with respect to a length scale reveals true long range order. In this case this order is hidden because of its topological nature. In (1+1) dimension this hidden order is nothing else than a manifestation of the phenomenon of spin-charge separation.

In a situation where a small density of stripes dislocation is present or at non-zero, but low, temperature, the operator $\vec{O}_{top.}$ decays exponentially as a function of the length of the path C

$$O_{top.}(|\vec{r} - \vec{r}'|, |C|) \sim e^{\frac{-|C|}{\xi_{str}}} \quad (6.3.9)$$

where now ξ_{str} is a correlation length which is generally should be inversely proportional to the density of stripe dislocations at small densities.

This is unusual since this length scale is associated with a non-local ('topological') operator, while standard long range order is associated with local operators. However, this general type of order has been recognized before. The best understood precedent is the 'hidden order' associated with $S = 1$ ('Haldane') spin chains, as first recognized by den Nijs and Rommelse[47].

Similar to the Ogata-Shiba limit of the one dimensional Hubbard model, and at low stripes density, the stripes can be *squeezed* out. The spin system left behind is just a 2D Heisenberg spin system with an anisotropy in the coupling due to the charges or stripes as in chapter 5. The above correlation function of the topological spin will show the same behavior as the spin-spin correlation of the related 2D Heisenberg model.

Although the correlator is independent of the length of path C , it is still a function of the distance $|\vec{r} - \vec{r}'|$ between the two "topological spins". If it becomes independent of this length scale then the topological spin system will show long range order, or more precisely, the spin system left after *squeezing* the stripes, which from now on we will refer to as the topological spin system. This, in a sense, is an ordering of the original spin system, because even when the stripes are dynamically fluctuating the spin system possess a sense of staggering. This order is obviously hidden. In fact the direct staggered spin-spin correlation may reveal a disordered system while the topological spin is ordered.

Now consider a system in which the above hidden order is present, i.e. the correlator defined in Eq. (6.3.7) is independent of the path C . In such a system three correlators that may

reveal further long range order exist. Corresponding to each one an order parameter can be defined. These are the staggered spin-spin correlator given by:

$$O_{stag.}(|\vec{r} - \vec{r}'|) = \langle \Psi | (-1)^{(x+y)} \vec{S}_{\vec{r}} \vec{S}_{\vec{r}'} (-1)^{(x'+y')} | \Psi \rangle, \quad (6.3.10)$$

and its corresponding order parameter is the usual staggered magnetization;

$$\vec{M}_{stag} = \langle (-1)^{x+y} \vec{S}_{\vec{r}} \rangle. \quad (6.3.11)$$

The topological spin-spin correlator is given by Eq. (6.3.8) above. Corresponding to it one can define a topological spin order parameter as;

$$\vec{M}_{top} = \langle \vec{T}_{\vec{r}_0, \vec{r}} \rangle = \langle e^{i\pi \sum_{\vec{r}' \in L(1-\vec{n}_{\vec{r}})} (-1)^{(x+y)} \vec{S}_{\vec{r}}} \rangle. \quad (6.3.12)$$

And thirdly the charge-charge correlation;

$$O_{cha.}(|\vec{r} - \vec{r}'|) = \langle \Psi | n(\vec{r}) n(\vec{r}') | \Psi \rangle, \quad (6.3.13)$$

This correlator should reveal the stripes order and its corresponding order parameter is the value of the charge charge structural factor at the q -point at which the stripes ordering occurs.

$$\rho_{\vec{q}} = \sum_{\vec{r}, \vec{r}'} e^{i\vec{q} \cdot (\vec{r} - \vec{r}')} \langle \Psi | n(\vec{r}) n(\vec{r}') | \Psi \rangle. \quad (6.3.14)$$

When one of the correlator is independent of $|\vec{r} - \vec{r}'|$ and its order parameter acquire a non-zero value the corresponding system orders. And when it decays exponentially with $|\vec{r} - \vec{r}'|$ its corresponding order parameter will be zero: the system will be disordered.

Let us now discuss the nature of the possible order that may occur in a system of anti-phase stripes in an antiferromagnetic background. Firstly, the stripes or the charge can order, implying that $\rho_{\vec{q}}$ is non-zero at some q value. The spin system left will be a system of coupled spin ladders. This is the problem considered in the previous chapter 5. Depending on the charge induced anisotropy on the spin system and whether the spin ladders have even or odd legs, the topological spin correlator Eq. (6.3.8) may show long range order. If the topological spin orders, the staggered spin magnetization will show the alternating modulation seen in the experiment on the ordered stripe phase. The order parameter of the topological spin will have the same absolute value of the staggered spin magnetization, however, it will not be alternating.

When the stripes are disordered, the order parameter of the staggered magnetization will be zero and the direct staggered spin-spin correlation will not show long range order. However the hidden topological spin-spin correlator may still show long range order and its corresponding order parameter (6.3.12) will be a non-zero constant. In fact we will show below that this is the only possible case when the stripes are disordered. Here, we of course

mean the stripes are disordered because of their quantum fluctuations and not because of the presence of stripe dislocations. These are omitted as we assumed that we started from a system where the hidden order discussed above is present, which means stripe dislocations are not present. The reason for this is that the fluctuations of the stripe system induce ordering in the spin system. This order is reflected in the hidden topological spin-spin correlator. The direct staggered spin-spin correlator do not show long range order in this case because it carries information about the stripes system which is disordered. This is similar to the one dimensional case. The spin-spin correlator in eq. 6.3.2 carry information about the charges (through its dependence on k_ρ) whereas the topological one, eq. 6.3.5, does not. Therefore the fourth possibility where every thing is disordered can not exist in this case. It is only when stripes dislocations are allowed this fourth possibilities can exist. This is a central result of our study, that in a stripe phase where dislocations are not present there is a hidden spin order. Unfortunately, one can hardly think of an experimental way to probe the hidden ordering of the topological spin in a dynamically fluctuating stripe system.

This leaves us with only three possible scenarios,

- (1) Ordered stripes, ordered topological spin system \rightarrow ordered staggered spin, (however, the spin magnetization is alternating).
- (2) Ordered stripes, disordered topological spin system \rightarrow disordered staggered spin; i.e. zero spin magnetization.
- (3) Disordered stripes \rightarrow ordered topological spin system \rightarrow disordered staggered spin; i.e. zero spin magnetization.

6.4 A Model for dynamical stripes in an antiferromagnetic background

In this section we will consider a model for dynamically fluctuating stripes living in an antiferromagnetic spin background. As in the previous two sections the stripes will be considered as directed strings, however they are otherwise fully quantum mechanical. The above three possible scenarios of ordering will be clearly shown. The last possibility where the disordering of the stripes will induce ordering of the topological spin will be elaborated further. We will justify our claim that a phase where both the strings and the spins are disordered is not present, unless stripes dislocations are allowed.

From the previous section we learned that the direct staggered spin-spin correlator, which is the experimentally measurable quantity, carries information about both the spins and the charges. Furthermore, although the spin system may show long range order, in the sense of the hidden ordering of the topological spin, the direct staggered spin spin correlator may however still show a disorder system due to a disordered stripe system, scenario (3). This motivates one to search for a model where the *squeezing* of the stripes is part of the model, but however trying to retain the effect of the stripes on the spin system. In the model for static stripes, the stripes were considered to live on the bonds of the lattice while the spins

occupy the lattice sites. This is in fact an explicit *squeezing* operation. The stripes were removed together with their corresponding lattice sites. However to retain their effect on the spin system, as anti-phase boundary inducing anisotropy on the spins, they were put back in the bonds. The spin system considered is actually the topological one and not the direct spin system. This is clear because every missing site implicitly adds a (-1) factor to the spin-spin correlator. Because these missing sites correspond to removed charges, this is an implicit addition of the factor $e^{i\pi(1-n)}$ in the correlator.

The discussion in the previous section shows that the same implicit way of *squeezing* the stripes can be done even in the case of dynamically fluctuating stripes. We can now put the stripes back on the bonds. For every stripe configuration we can remove the stripes with their sites and put them back on bonds. The bonds form a lattice as well and the stripes can now fluctuate on the bonds lattice. Similar to the ordered stripe case the spin system left on the lattice sites after the *squeezing* operation is the topological one. The stripe system and the topological spins are still coupled. This is already seen in the static stripes case. The presence of the stripes induces anisotropy in the spin system. In the dynamical stripes case this coupling is even more than just the spin anisotropy. A stripe induces a spin anisotropy. That means it makes the exchange interaction in the bond between the two spins across them weaker. When these stripes fluctuate they carry this weaker bond with them. This means the influence of the stripes is not only to induce spin anisotropy but also to fluctuate the weaker bond inside the spin system. The spin system also influence the stripes. When the stripes fluctuate they break some of the spin bonds, this will cost exchange energy. This energy cost can be considered as a curvature energy on the stripes.

To be specific we will consider the following model of directed strings living in a spin- $\frac{1}{2}$ antiferromagnetic background. Consider the two-dimensional square lattice. The bonds connecting the lattice sites can be divided onto those bonds parallel to the x-axis and those parallel to the y-axis. Now we will consider the strings to be of the same variety of strings considered in chapter (3) and with the particles building up the strings to be living on the bonds parallel to the x-axis. Furthermore we will assume that the strings are directed. Therefore these particles can only hop along the x-axis, specifically to the nearest neighbor bond along the x-axis with a hopping parameter t . The particles are assumed to satisfy the hard core bosons condition. (As these particles are essentially living in one dimension they can also be assumed to be fermion). The spins (spin $\frac{1}{2}$) live on the lattice sites, interacting among themselves with nearest neighbor antiferromagnetic interaction. The exchange interaction is J if no string is present in the bond connecting them and $J' = \alpha J$ if a string's particle is present in the bond connecting the two spins. As in the previous chapter, the exchange interaction is weaker if a stripe is present between the spins. Therefore $1 \geq \alpha \geq 0$. (see figure 6-2). Since the strings live on bonds parallel to the x-axis, the spins along the y-axis interact with interaction energy J . However, when a kink is present on a string we notice that across the kink two spins which were not nearest neighbors in the original lattice, may become nearest neighbor after putting the stripes on the bonds. The interaction between these two spins should be zero. This happen along the y-axis only. Figure 6-2 gives a clear picture of the model we consider. From the above, it follows that the Hamiltonian

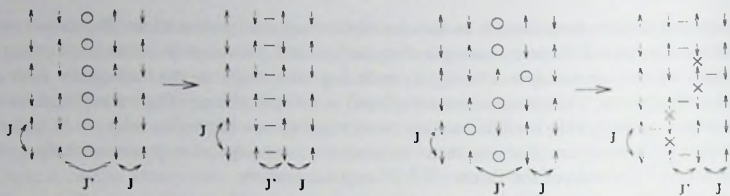


Figure 6-2. Description of the model of fluctuating stripes in the AF spin background. By squeezing the stripes one arrives at a spin-only model. The stripes are put back as strings living on bonds. Note that a kink (crosses) on a string breaks a spin bond along the y-axis and costs energy.

of the system can be written in as the following form:

$$\begin{aligned} \mathcal{H} = & \tau \sum_{l, (x', y)} \mathcal{P} \left(a_{l, (x', y)}^\dagger a_{l, (x', y)} + H.C \right) P^{-1} + J \sum_{(x, y)} \left(1 - \rho \sum_l n_{l, (x', y)} \right) \bar{S}_{(x, y)} \bar{S}_{(x+1, y)} \\ & + J \sum_{(x, y)} \left[1 - \sum_l \left(n_{l, (x', y)} n_{l, (x'-1, y+1)} + n_{l, (x'-1, y)} n_{l, (x', y+1)} \right) \right] \bar{S}_{(x, y)} \bar{S}_{(x, y+1)} \quad (6.4.1) \end{aligned}$$

where a is a bosonic operator obeying hard core conditions and $n_l = a_l^\dagger a_l$. P is a projection operator insuring that hole hoppings do not break the strings.

As emphasized above, the spin system living on the lattice sites is the topological spin system. The direct measurements of the spin-spin correlation in the above constructions measures the topological spin-spin correlations as given in equation 6.3.7. To measure the true staggered spin-spin correlator we have to undo the *squeezing* operation by taking care of the strings positions. This is done by adding extra sites whenever a string is encountered. It is clear that if the strings are disordered or fluctuating, this disorder will appear in the staggered spin-spin correlator while the topological spin-spin correlator will not feel the disorderedness of the strings, at least not directly.

The above model is essentially a strong coupling model for the stripes at low density similar to the Ogata-Shiba case of the 1d Hubbard model. The reason is that in the above constructions the minimum width of the spin domains between any two strings is one and can not be zero. In other words, the hard core condition now imposes that strings can not even be nearest neighbors. Below it will be shown that a strong repulsive force between strings arises when two strings are next nearest neighbors.

Our main aim is to study the model and justify our claim that the above three scenarios for the ordering are the only possibilities. This will be done by mapping out the zero temperature phase diagram of the model as a function of the strings hopping parameter τ and the charge-induced spin anisotropy $\alpha = 1 - \rho$. The nature of the different phases will be mapped out in detail as characterized by the string and spin (hidden) order.

6.5 The phase diagram

Motivated by the result of bond centered stripes in the previous chapter, we will consider the model at a stripe density of $\frac{1}{2}$. This means there is one particle for every two bonds on the bonds lattice. On average, the stripes leave between them a two leg ladder spin system. This filling is particularly interesting for the following reason. If the stripes order, forming a coupled two leg ladders spin system, the $t = 0$ result is now known from the previous chapter. The interesting point is that already two of the above three possibilities are demonstrated in this case. Below a finite critical α ($\alpha_c = 0.3$) both the topological spin system and the direct spin are disordered, while the stripes are ordered. Above α_c both the stripes are ordered and (hidden) spin system is ordered. The question is now what will happen when switching on the strings kinetic energy t .

Later on we will in fact argue that, by changing the density of the strings, the topology of the phase diagram will not change. Only the precise position of the transitions lines changes with the filling.

We studied the model numerically employing a combined Quantum Monte-Carlo algorithm for spins and the strings. The fact that the spins and the strings live essentially on separate lattices makes it possible to develop such a code. The spins are efficiently simulated using the loop cluster algorithm while for the strings we used world line algorithm. Since the quantum motion of the strings is effectively one dimensional, this world-line algorithm turned to be efficient enough for a quantitative study of the model. We also employed the Binder parameter technique to map out the phase diagram[119]. This parameter is the reduced fourth order cumulant defined as

$$B = 1 - \frac{\langle O^4 \rangle}{3\langle O^2 \rangle^2} \quad (6.5.1)$$

where O is the order parameter of the ordered phase. The Binder parameter behaves differently in the ordered and disordered state. In the ordered state $\langle O^4 \rangle = \langle O^2 \rangle^2$ and therefore $B = 2/3$ while in a disordered state, and for Gaussian fluctuations, $\langle O^4 \rangle = 3\langle O^2 \rangle^2$, and therefore $B = 0$. This property can be exploited to find the location of a phase transition or a cross over line between an ordered state and the disordered state characterized with severe Gaussian fluctuations[119].

The order parameter of the spin system is easily identified as the staggered magnetization of the spin lattice.

$$m = \frac{1}{N} \sum_{\vec{r}} (-1)^{x+y} \langle \vec{S}_{\vec{r}} \rangle. \quad (6.5.2)$$

As the stripes were shifted to live in the bonds lattice, this spin order parameter is actually the order parameter of the topological spin and gives information about the hidden order of the spin system.

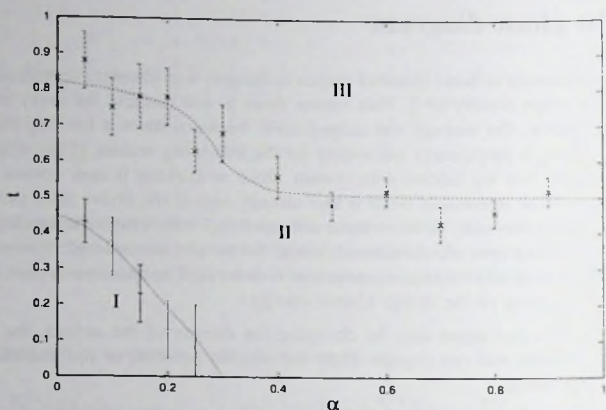


Figure 6-3. Phase diagram of the fluctuating stripes model at a stripes filling of $\frac{1}{2}$. The continuous lines are for the eye guide.

In the bond lattice, the ordered stripe phase correspond with strings running vertically and spaced one bond apart. A line perpendicular to the strings, correspond with a 1D half filled hard core bose system. This makes the following order parameter to be the relevant one for the stripe system in this case.

$$\rho_{st} = \langle (-1)^x (a_x^\dagger a_x - 1) \rangle. \quad (6.5.3)$$

Using the combined quantum Monte-Carlo algorithm with the Binder parameter technique applied for the above defined order parameters, we arrived at the following phase diagram shown in figure 6-3.

Three distinct phases are present. They in fact correspond to the three ordering possibilities discussed above. Phase I and II are just continuations of the " $t = 0$ " case. In both phases, the strings system is ordered. The strings are of the flat string type discussed in chapter 3, (see table 3-4). Because now t is non-zero, there are local quantum fluctuations consisting of kinks in individual strings. In phase I the spin system is disordered and there is no hidden spin order. This is similar to the system at $t = 0$. However, the two leg ladders are now not only coupled by the charge induced anisotropy but also by the exchange of weaker bonds. In phase II the spin system is ordered. The topological spin show the "hidden" long range order. The direct staggered spin-spin magnetization flip when ever one crosses a string. The line separating phase I and II is a line of true quantum phase transitions separating a disordered spin state and an ordered one. Every point on the line is now a quantum critical

point. The transition is driven not only by the spin anisotropy α but also by the strings fluctuations. At $\alpha = 0$ the transition is solely driven by the strings fluctuations.

In phase III and at the single string level, the strings are Gaussian. However the strings system solidify because of the "string gas" effect discussed at the first section of this chapter. One should note that this solidification is driven by the Gaussian fluctuations in the strings system. Because of these fluctuations we termed this phase as disordered. The line separating this phase and phase II is actually a crossover line. The stripes order parameter in phases II and I is significantly above zero. In this phase one has to go to a much lower density of stripes to see a finite value of the order parameter. The "topological" spin system shows the same hidden order present in Phase II, however because of the severe quantum fluctuations in the string system the direct staggered spin-spin correlation decays exponentially.

To get more insight about the nature of this phase, we analyze the following figures. In figure 6-4 we show a plot of the topological spin-spin correlation function (Eq. 6.3.7) at a point inside phase III ($\alpha = 0.9$ and $t = 1.5$). Because we are working at non-zero temperature, this has been normalized by the staggered spin-spin correlation function of the quantum Heisenberg model at the same temperature. One can fairly conclude that the topological spin system behaves as a quantum Heisenberg system. We also show the direct staggered spin-spin correlation function. This function falls exponentially to zero signaling a disordered behavior. The nature of the stripe system is best figured by examining the charge-charge structural factor (Eq. 6.5.3). The solidification of the stripes system due to the string gas effect should appear as a peak at the relevant q value. At the density we studied ($\frac{1}{2}$) this should occur at $(\pi, 0)$. However as mentioned above it is quite hard to detect this effect at such densities. By going to lower densities, a much more clear peak appears. In figure 6-5 we plot the structural factor for a (48×48) lattice with 12 strings, i.e. at a $1/4$ doping, at a point deep inside phase III ($\alpha = 0.05$, $t = 8.0$). One clearly notice a sharp peak at $(\frac{\pi}{2}, 0)$. The, higher, peak at $(0, 0)$ correspond to the homogeneous charge background. However the relative ratio of the two peaks gives a feeling for the quantum fluctuations in the system. One would expect that by going to lower densities the stripes have more room to fluctuate and therefore they should be more disordered. In fact the opposite occurs. It is shown in the first section that the solidification of the quantum strings gas is driven by the fluctuations. The more room the strings have to fluctuate the more the effect is present. By going to lower densities one increases the fluctuations, which will help solidify the string system. This is why for a density of $\frac{1}{2}$ it was quite hard to detect any solidifications of the system. At lower densities the effect is more clear.

6.6 Discussion of the Phase Diagram

The $\alpha \rightarrow 1$ limit is quite easy to understand. In this limit the spin system is obviously ordered. Here I mean the "topological" spin system. This system will possess long range order and the "topological" spin-spin correlation, Eq.(6.3.7), behave in the same way as the spin-spin correlations of the 2D Heisenberg model.

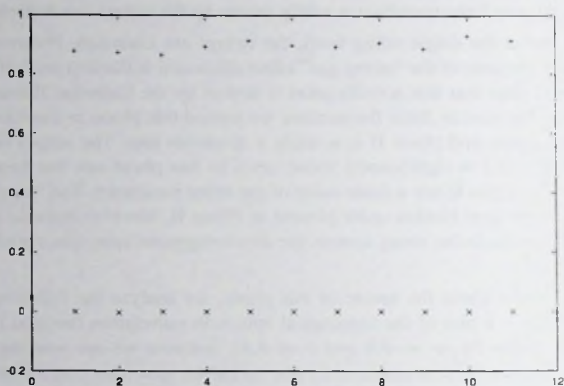


Figure 6-4. Plot of the Topological spin-spin correlation (pluses) and the direct staggered spin-spin correlation (crosses) for a 24×24 lattice at ($\alpha = 0.05$, $t = 2.0$).

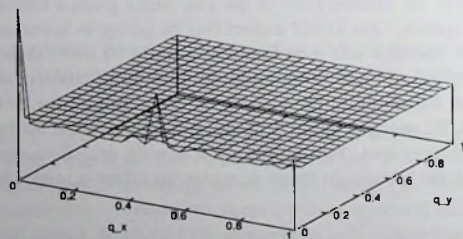


Figure 6-5. Plot of the charge-charge structural factor for a lattice of 48×48 at the point $\alpha = 0.05$ and $t = 8.0$ inside phase III. The average distance between the strings is 4.

For the string system, the crossover can be understood as a single string unbinding transition. A kink in the string will break a spin bond along the y-axis and this will cost an energy equal to the bond energy of the spin system, see figure 6-2. As the spin system is equivalent to the Heisenberg model, this energy can be estimated by considering the energy per bond in the pure Heisenberg model. The energy per site, e_0 , of the Heisenberg system is calculated by many groups and found to be [122],

$$e_0 = -6692(1)J \quad (6.6.1)$$

As the number of bonds is twice the number of sites, the energy per bond is half of this value and this will be the energy cost of one kink, \mathcal{K} , in the strings system

$$\mathcal{K} = 0.34J \quad (6.6.2)$$

From section 3.7 chapter 3 a transition from a flat phase to a Gaussian phase occurs when \mathcal{K} is equal $0.7t$. This allow us to estimate the t value at which this transition occur

$$t = \mathcal{K}/0.7 = 0.34J/0.7 = 0.49J. \quad (6.6.3)$$

This is the same value at which the crossover from an ordered strings system to a disordered system occurs. Below this value one has an ordered system of flat strings and above this value the strings are Gaussian.

As \mathcal{K} is coming from breaking a spin bond along the y-axis, along the y-axis the spin-spin interaction is equal to J for all α . Therefore \mathcal{K} does not change upon changing α . This explains that the cross over occurs at the same t value all the way from $\alpha = 1$ to approximately $\alpha = 0.3$. For $\alpha < 0.3$ the spin system is disordered therefore the above mechanism is not valid.

For the spin system, below the string transition, both the direct staggered spin-spin correlation and the "topological" one show long range order. However it is the topological one that is equivalent to the Heisenberg spin system. The "topological" spin-spin correlation behave in the same way as the spin-spin correlations of the 2D Heisenberg model. Above the strings transition the "topological" spin system is still ordered. However the direct staggered spin-spin correlation will follow the disordered strings system and therefore decays exponentially.

We now discuss the other limit, $\alpha \rightarrow 0$. Let us first look at the $t \rightarrow 0$ limit. In this case the strings become classical. One would then like to find the minimum energy configuration of the combined system. We simulated the above model at different stripe densities with the strings considered to be classical at a relatively low temperature. Focusing on the equilibrium configuration, we found a tendency for the strings to be straight (flat strings) with an even distance between them. In this case the distance between the strings is two. This means that the strings leave between them spin ladders with an even number of legs. This finding is consistent with the fact that even-leg spin ladders always develop a gap therefore driving a special stability as compared to odd-leg spin ladders. To put this on a solid basis,

for the case we are considering (density equal to $\frac{1}{2}$) we compared the ground state energy of a coupled two-leg ladders system with that of coupled 1 and 3-leg ladders. We found that the energy of the two-leg ladders system is always lower and specifically at $\alpha = 0$ the energy density of the 2-leg ladder system is of order $0.1J$ lower than the system of 1 and 3-leg ladder. This fact is true for all α less than 0.3. This finding is in fact more general. For any density of strings, the minimum energy configuration will always be flat strings leaving between them a spin system consisting of coupled even-legs spin ladders.

Another observation that further supports this conclusion is related to the force acting between two static flat stripes in a spinful background. When injecting two stripes in an antiferromagnetic spin system, an induced interaction arises due to the modification of the quantum zero point spin wave energy. This effect is analogue to the Casimir effect. At long distances the interaction energy per unit length of stripe is attractive and falls, generally, like $V(d) = d^{-1}$ where d is the distance between the two stripes [120]. However, when d is not large, this interaction energy behaves differently. It fluctuates between even and odd distances with minima at even d depending on α . The reason for this behavior is the existence of a gap in the even-leg ladder spin systems. We define the interaction energy between the two stripes as follows,

$$V(d) = E_2(d) + E_0(d) - 2 * E_1(d) \quad (6.6.4)$$

where E_n is the total energy of the system with n stripes. We have calculated this interaction energy for two α values, $\alpha = 0.08$ and $\alpha = 0.2$. In figure 6.6 we display our results for $V(d)$. Although these forces are small, however, in the thermodynamic limit and at $T = 0$ they will dominate and one can fairly conclude that the stripes will prefer to leave an even distance between them.

From the above we conclude that in the limit $t \rightarrow 0$, $\alpha \rightarrow 0$ and at any string density one has an ordered strings system consisting of flat strings. Moreover, these strings leave between them a system of coupled even-legs spin ladders. This spin system has a finite correlation length and therefore it is disordered. This means that both the direct staggered and the "topological" spin-spin correlation will not show long range order. Moving away from $\alpha = 0$ along the $t = 0$ line, one will ultimately hit a critical $\alpha = \alpha_c$ at which a quantum phase transition will take place. Beyond this critical value the spin system will show long range order. For the doping we are considering, this quantum phase transition occurs at the value $\alpha_c = 0.3$. As has been shown in the previous chapter (5)

By switching on t , quantum fluctuations will develop in the strings system. These fluctuations are in the form of kinks in the flat strings system. They will ultimately drive the topological spin system from a disordered phase to an ordered one. One can think of two ways that the fluctuations in the strings system causes the spin system to order. Firstly, these fluctuations will induce odd-leg rungs in the even-leg ladder system. At some moment these odd rungs will proliferate, kill the gap and drive the whole spin system to a gapless state similar to the coupled odd-leg ladders. These fluctuations will also fluctuate the weaker bond along the axis perpendicular to the strings, the x -axis. This will distribute the effect of the weaker bonds along the x -axis and at some moment the spin-spin interaction

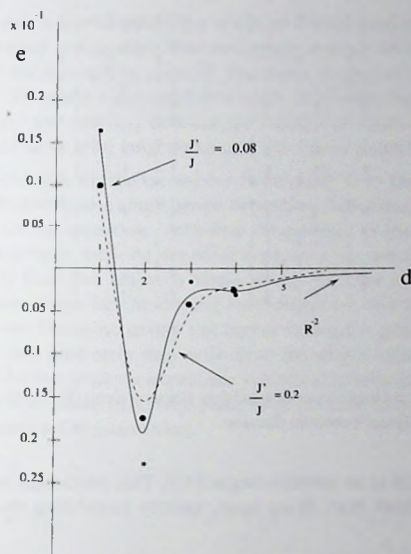


Figure 6-6. Induced interaction between two static flat stripes. d is the distance between the two stripes and e is the energy per unit length of stripe.

along this axis will switch from an alternate weak and strong bond to a more homogeneous interaction intermediate between J and αJ . This will change the nature of the whole spin system from coupled even-leg ladders system to an anisotropic Heisenberg model, or to coupled spin chains. Such a system show long range order at zero-temperature.[90].

The cross over from the ordered stripe system in phase II to the disordered one in phase III at this limit is more complicated. It can not be understood in terms of single string physics only. One may still argue that the spin system is actually ordered and a mechanism similar to the one working at the $\alpha \rightarrow 1$ limit should work here as well. This can not be true because of two reasons. Firstly the cross over seems to occur at a higher values of t and one need a rather large kink energy to account for this. This large energy can only come from the spin system. The only possible way is breaking the rungs inside the two leg ladder system. The kink energy is, however, quite small. It is of order of $O(0.01J)$. Therefore, it cannot explain the occurrence of the cross-over at such a relatively large value of t . Moreover, a linear confining potential interaction between kinks builds up, when two kinks try to run apart $V(l) = k.l$, where k is the kink energy and l is the distance between the two kinks. This linear potential is similar to the linear string interaction that occurs when

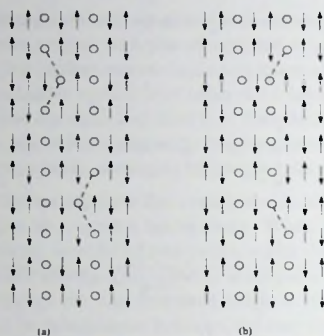


Figure 6-7. (a) Kinks in a coupled two-leg ladders stripe system. (b) When the kinks fly apart they induce odd rungs and a linear potential develop.

a single hole is injected in an antiferromagnet[13]. This interaction will pull the two kinks together and forbid them from flying apart, thereby prohibiting the proliferation of free kinks.

Therefore, a collective mechanism beyond single string physics should be taking place and is responsible for the disordering of the strings. The nature of this mechanism and how it disorders the strings system is still an open question.

It is clear that the disordering of the string system in Phase III is driven by the quantum fluctuations. However, before they are severe enough to disorder the strings system, these same quantum fluctuations are in fact responsible for driving the topological spin system from a disordered state to an order one. When the quantum fluctuations get more severe to the extend of disordering the strings system they should in fact help more to order the spin system. Therefore one can not have a phase where both the strings system and the topological spin are disordered. We again stress the fact that the direct spin spin correlation will show a disorder system because of its dependence on the disordered strings.

We end this section by showing that the topology of the phase diagram does not change by doping. From the discussion on the small t and $\alpha \rightarrow 0$ limit we concluded that at this limit and for any doping the stripes system consists of ordered strings of the flat type leaving between them a system of coupled even-leg spin ladders. These ladders may have different width. The system will choose the configuration with the lowest energy. For example at a $\frac{1}{3}$ doping the lowest energy configuration will be an alternate 2-4 leg ladders. Since even-leg spin ladders are gaped, the spin system as a whole will be gaped at this limit. Therefore both the topological spin and direct spin systems will show a disordered system. This is phase I. Upon increasing α one should hit a quantum critical point where the a transition to an ordered spin state should take place. This critical α is smaller for lower stripes densities.

This is obvious since at lower densities the width of the spin ladders will get larger and the gap of the spin system gets smaller. One then enters a phase where both the stripes and the spins are ordered and this will be phase II. The direct staggered spin will flip whenever one crosses a stripe. The same argument holds when increasing the kinetic energy of the stripes. By increasing t the coupling between the ladders increases and at some critical t the spin system should show long range order and one enters phase II.

For $\alpha > \alpha_c$, the mechanism for the cross-over from phase II to phase III is independent of the doping. It corresponds to a single stripe depinning transition. In fact the anisotropy does not play a role on the transition. Therefore the position of the cross-over should be independent of the doping as well. At the other limit, $\alpha < \alpha_c$, we note that the transition from phase I to phase II occurs before a single strings become Gaussian. The quantum fluctuations on the flat strings are the driving mechanism for this transition. This occurs at the single string level. Upon increasing t to higher values the quantum fluctuations will become more severe and ultimately they will drive the single string from the flat phase to a Gaussian string. At this level we expect the collective mechanism responsible for the transition from phase II to phase III to take place or at the least to occur some where after the single string becomes a Gaussian string.

the first two, but instead they will be stable, and their formation is not dependent on any particular initial conditions. In fact, it is not clear how the system will evolve in the long run, and it is not clear whether the system will reach a steady state or not. The only thing we can say is that the system will evolve in a way that is consistent with the laws of physics.

In the case of the third, the system will evolve in a way that is consistent with the laws of physics, but it will not reach a steady state. Instead, it will evolve in a way that is consistent with the laws of physics, but it will not reach a steady state. In fact, it is not clear how the system will evolve in the long run, and it is not clear whether the system will reach a steady state or not. The only thing we can say is that the system will evolve in a way that is consistent with the laws of physics.

Finally, we should note that the system will evolve in a way that is consistent with the laws of physics, but it will not reach a steady state. Instead, it will evolve in a way that is consistent with the laws of physics, but it will not reach a steady state. In fact, it is not clear how the system will evolve in the long run, and it is not clear whether the system will reach a steady state or not. The only thing we can say is that the system will evolve in a way that is consistent with the laws of physics.

The system will evolve in a way that is consistent with the laws of physics, but it will not reach a steady state. Instead, it will evolve in a way that is consistent with the laws of physics, but it will not reach a steady state. In fact, it is not clear how the system will evolve in the long run, and it is not clear whether the system will reach a steady state or not. The only thing we can say is that the system will evolve in a way that is consistent with the laws of physics.

The system will evolve in a way that is consistent with the laws of physics, but it will not reach a steady state. Instead, it will evolve in a way that is consistent with the laws of physics, but it will not reach a steady state. In fact, it is not clear how the system will evolve in the long run, and it is not clear whether the system will reach a steady state or not. The only thing we can say is that the system will evolve in a way that is consistent with the laws of physics.

The system will evolve in a way that is consistent with the laws of physics, but it will not reach a steady state. Instead, it will evolve in a way that is consistent with the laws of physics, but it will not reach a steady state. In fact, it is not clear how the system will evolve in the long run, and it is not clear whether the system will reach a steady state or not. The only thing we can say is that the system will evolve in a way that is consistent with the laws of physics.

Bibliography

- [1] V. J. Emery and S. A. Kivelson, Phys. Rev. Lett. **74**, 3253 (1995)
- [2] H. Ding *et al.*, cond-mat/9712100 (1997).¹
- [3] N. D. Mermin and H. Wagner, Phys. Rev. Lett. **17**, 1133 (1966).
- [4] B. Keimer *et al.*, Phys. Rev. B **46**, 14034 (1992).
- [5] F.D.M. Haldane, Phys. Lett. **93 A**, 464 (1983), Phys. Rev. Lett. **50**, 1153 (1983).
- [6] Henk Eskes, Some Unusual Aspects of Correlated Systems. PhD thesis, Groningen 1992.
- [7] S. Chakravarty, B. I. Halperin and D. R. Nelson, Phys. Rev. Lett. **60**, 1057 (1988); *ibid.* Phys. Rev. B **39**, 2344 (1989).
- [8] E. Fradkin, Field theories of condensed matter systems, Addison Wesley (1991), J. A. Hertz, Phys. Rev. B **14**, 1165 (1976).
- [9] J. Zaanen and O. Gunnarson, Phys. Rev. B **40**, 7391 (1989).
- [10] D. Poilblanc and T. M. Rice, Phys. Rev. B **39**, 9749 (1989); H. J. Schulz, Phys. Rev. Lett. **64**, 1445 (1990); M. Kato *et al.*, J. Phys. Soc. Jpn. **59**, 1047 (1990); M. Inui and P. B. Littlewood, Phys. Rev. B **44**, 4415 (1991); J.A. Vergés, F. Guinea and E. Louis, Phys. Rev. B **46**, 3562 (1992); T. Giamarchi and C. Lhuillier, Phys. Rev. B **43**, 12943 (1991); G. An and J. M. J. van Leeuwen, Phys. Rev. **44**, 9410 (1991); H.J.M. van Bemmelen *et al.*, Phys. Rev. Lett. **72**, 2442 (1994); J. Zaanen and P.B. Littlewood, Phys. Rev. B **50**, 7222 (1994).
- [11] J. M. Tranquada, D. J. Buttrey, V. Sachan, and J. E. Lorenzo, Phys. Rev. Lett. **73** 1003, (1994)
- [12] S. R. White, Phys. Rev. Lett. **69**, 2863 (1992); S. R. White, Phys. Rev. B **69**, 10345 (1993).
- [13] E. Dagotto, Rev. Mod. Phys. **66** No.3, 763, (1994).
- [14] E. Dagotto and A. Moreo, Phys. Rev. D **21** 865, (1985).
- [15] E. Gagliano *et al.*, Phys. Rev. B **34** 1677; **35** 5297(E) (1986).

¹'cond-mat' refers to the Los Alamos E-print archive: <http://xxx.lanl.gov/archive/cond-mat>.

- [16] M.H. Kalos and P.A. Whitlock, *Monte Carlo Method*. Vol 1. (Wiley 1986.)
- [17] H. F. Trotter, Proc. Ann. Math. Soc. 10 (1959) 545.
- [18] M. Suzuki, Commun. Math. Phys. 51 (1976) 183.
- [19] M. H. Kalos, ed., *Monte Carlo Methods in Quantum Problems*, Reidel, Boston 1982.
- [20] M. Suzuki, ed., *Quantum Monte Carlo Methods in Condensed Matter Physics*, World Scientific, (1993).
- [21] M. Barma and B. S. Shastry, Phys. Rev. B 18, 3351 (1978).
- [22] Henk Eskes, Osman yousif Osman, Rob Grimberg, Wim van Saarloos and Jan Zaanen Phys. Rev. B 58, 6963 (1998).
- [23] See, e.g., B. G. Levi, Physics Today 49 (6), 17 (1996) and references therein.
- [24] Y. Ando, G. S. Boebinger, A. Passner, T. Kimura and K. Kishio, Phys. Rev. Lett. 75, 4662 (1995); Y. Ando, G. S. Boebinger, A. Passner, N. L. Wang, C. Geiberl and F. Steglich, Phys. Rev. Lett. 77, 2065 (1996); Y. Ando, G. S. Boebinger, A. Passner, T. Kimura, M. Okuya, J. Shimoyama, K. Kishio, K. Tamasaku, N. Ichikawa and S. Uchida, Phys. Rev. Lett. 77, 5417 (1996).
- [25] J. M. Tranquada, B. J. Sternlieb, J. D. Axe, Y. Nakamura and S. Uchida, Nature 375 561 (1995); see also J. M. Tranquada, Physica B 241-243, 745 (1998).
- [26] J.M. Tranquada, J. D. Axe, N. Ichikawa, A. R. Moodenbaugh, Y. Yakamura and S. Uchida, Phys. Rev. Lett. 78, 338 (1997).
- [27] K. Yamada *et al.*, Physica C 282-287, 85 (1997).
- [28] K. Yamada *et al.*, *Doping dependence of spatially modulated dynamical spin correlations in superconducting $La_{2-x}Sr_xCuO_4$* , Tohoku Univ. preprint (unpublished 1997).
- [29] J. M. Tranquada, Physica C, 282-287, 166 (1997).
- [30] P. Dai, H. A. Mook and F. Dogan, Phys. Rev. Lett. 80 1738 (1998).
- [31] H. A. Mook and F. Dogan, Nature 401 145 (1999).
- [32] J. Zaanen, M.L. Horbach, and W. van Saarloos, Phys. Rev. B 53, 8671 (1996).
- [33] D. M. Ceperley, Rev. Mod. Phys. 67, 279 (1995).
- [34] H. Eskes, R. Grimberg, W. van Saarloos and J. Zaanen, Phys. Rev. B 54, 724 (1996).

- [35] C. Nayak and F. Wilczek, *Int. J. Mod. Phys.* **10**, 2125 (1996); *Phys. Rev. Lett.* **78**, 2465 (1997).
- [36] See, e.g., G. Forgacs, R. Lipowsky and Th. M. Nieuwenhuizen, in: *Phase transitions and critical phenomena* vol. 14, C. Domb and J. L. Lebowitz, eds. (Academic, New York, 1991), or *Structure and Dynamics of Membranes*, R. Lipowsky and E. Sackmann, eds. (North-Holland, Amsterdam, 1995).
- [37] U. Löw, V. J. Emery, K. Fabricius, and S. A. Kivelson, *Phys. Rev. Lett.* **72**, 1918 (1994); V. J. Emery and S. Kivelson, *Physica C* **209**, 597 (1993); S. A. Kivelson and V. J. Emery, *Synth. Met.* **80**, 151 (1996).
- [38] P. Prelovsek and X. Zotos, *Phys. Rev B* **47**, 5984 (1993); P. Prelovsek and I. Sega, *Phys. Rev B* **49**, 15241 (1994).
- [39] J. Zaanen and A.M. Oleš, *Ann. Physik* **5**, 224 (1996).
- [40] S. R. White and D. J. Scalapino, *Phys. Rev. Lett.* **80**, 1272 (1998).
- [41] V. J. Emery, S. A. Kivelson and O. Zachar, *Phys. Rev. B* **56**, 6120 (1997); A. H. Castro Neto, *Z. Phys. B*, **102** 185 (1997); *Phys. Rev. Lett.*, **78**, 3931 (1997); A. H. Castro Neto, C. de C. Chamon and C. Nayak, *ibid.*, **79**, 4629 (1997).
- [42] J. Zaanen, O. Y. Osman, H. Eskes and W. van Saarloos, *J. Low Temp. Phys.* **105**, 569 (1996).
- [43] Yu. A. Krotov, D.-H. Lee and A. V. Balatsky, *Phys. Rev. B* **56**, 8367 (1997).
- [44] J. Zaanen, O. Y. Osman, H. Eskes and W. van Saarloos, unpublished.
- [45] See, e.g., R. Rajaraman, *An Introduction to Solitons and Instantons in Quantum Field Theory* (North-Holland, Amsterdam, 1989)
- [46] M. den Nijs, in *Phase Transitions and Critical Phenomena*, Vol.12, Eds. C. Domb and J.L. Lebowitz, Academic Press, London, 1988.
- [47] M. den Nijs and K. Rommelse, *Phys. Rev. B* **40**, 4709 (1989).
- [48] V. Sachan *et al*, *Phys. Rev. B* **51**, 12742 (1995); K. Najima *et al*, *J. Phys. Soc. Jpn.* **66**, 809 (1997).
- [49] S. R. White and D. J. Scalapino, $d_{x^2-y^2}$ *pair domain walls*, cond-mat/9610104 (1996).
- [50] H.E. Viertiö and T.M. Rice, *J. Phys.: Condens. Matter* **6**, 7091 (1994).
- [51] A. J. Heeger, S. Kivelson, J. R. Schrieffer and W.-P. Su, *Rev. Mod. Phys.* **60**, 781 (1988).

- [52] S. A. Brazovskii, Zh. Eksp. Teor. Fiz. **78**, 677 (1980) [Sov. Phys. JETP **51**, 342 (1980)].
- [53] F. D. M. Haldane, Phys. Rev. Lett. **45**, 1358 (1980)
- [54] M. Suzuki, Progr. Theor. Phys. **56**, 1454 (1976).
- [55] J. D. Weeks, J. Chem. Phys. **67**, 3106 (1977); J. D. Weeks, Phys. Rev. Lett. **52**, 2160 (1984).
- [56] J. D. Weeks, in *Ordering in Strongly Fluctuating Condensed Matter Systems*, edited by T. Riste, Plenum, New York, 1980, p. 293.
- [57] H. van Beijeren and I. Nolten, in: *Structure and Dynamics of Surfaces II*, eds. W. Schommers and P. von Blanckenhagen (Springer, Berlin, 1987).
- [58] R. Botet, R. Jullien, and M. Kolb, Phys. Rev. B **28**, 3914 (1983).
- [59] U. Glaus and T. Schneider, Phys. Rev. B **30**, 215 (1984).
- [60] H. J. Schulz and T. Ziman, Phys. Rev. B **33**, 6545 (1986).
- [61] H. J. Schulz, Phys. Rev. B **34**, 6372 (1986).
- [62] These order parameters, as well as the string order parameter introduced below, are only nonzero once the height at an arbitrary point is specified. This can, e.g., be the guider point discussed in section V or the reference height h_0 introduced in Ref. [47].
- [63] F. D. M. Haldane, Phys. Rev. Lett. **50**, 1153 (1983).
- [64] I. Affleck, J. Phys. Condens. Matter **1** 3047 (1989).
- [65] I. Affleck, T. Kennedy, E. H. Lieb, and H. Tasaki, Phys. Rev. Lett. **59**, 799 (1987); Commun. Math. Phys. **115**, 477 (1988).
- [66] U. Schollwöck and T. Jolicœur, Europh. Lett. **30**, 493 (1995).
- [67] J. D. Johnson and B. M. McCoy, Phys. Rev. A **6**, 1613 (1972).
- [68] P. Nightingale, J. Appl. Phys. **53**, 7927 (1982).
- [69] M. N. Barber in *Phase Transitions and Critical Phenomena*, Vol. 8, Eds. C. Domb and J. L. Lebowitz, Academic Press, London, 1983.
- [70] K. Binder, Z. Phys. B - Condensed Matter **43**, 119 (1981).
- [71] S. N. Coppersmith, D. S. Fisher, B. I. Halperin, P. A. Lee and W. F. Brinkman, Phys. Rev. B **25**, 349 (1982).

- [72] J. M. Tranquada, D. J. Buttrey and V. Sachan, Phys. Rev. B **54**, 12318 (1996); Phys. Rev. B **55**, R6113 (1997); P. Wochner *et al.*, *ibid.* **57**, 1066 (1998).
- [73] M. E. Fisher and D. S. Fisher, Phys. Rev. B **25**, 3192 (1982).
- [74] In the high temperature limit, the string becomes a self-avoiding walk on a two-dimensional lattice. For such a walk of length N , the radius of gyration R_g grows as $R_g \sim N^\nu$ where $\nu = 0.6$ in $D=2$. This implies that the directedness defined in this paper should go to zero as $N^{\nu-1} = N^{-0.4}$ for $N \rightarrow \infty$ in the high temperature limit.
- [75] V. J. Emery, S. A. Kivelson, and O. Zachar, Phys. Rev. B **56**, 6120 (1997); Yu. A. Krotov, D.-H. Lee and A. V. Balatsky, Phys. Rev. B **56**, 8367 (1997); S. A. Kivelson, E. Fradkin and V. J. Emery, Nature **393**, 550 (1998); J. Zaanen, J. Phys. Chem. Sol. (in press, cond-mat, 9711009).
- [76] J. Voit, Rep. Prog. Phys. **57**, 977 (1994) and ref.'s therein.
- [77] H. Eskes *et al.*, Phys. Rev. B **54**, R724 (1996); *ibid.* cond-mat/9712316; C. Morais-Smith *et al.*, Phys. Rev. B **58**, 1 (1998).
- [78] C. Nayak and F. Wilczek, Phys. Rev. Lett. **78**, 2465 (1997).
- [79] F. D. M. Haldane, Phys. Rev. Lett. **45**, 1358 (1980); M. P. M. den Nijs, Phys. Rev. B **23**, 6111 (1981); V. J. Emery, Phys. Rev. Lett. **65**, 1076 (1990).
- [80] K. Penc and F. Mila, Phys. Rev. B **49**, 9670 (1994); K. Sano and Y. Ono, J. Phys. Soc. Jpn **63**, 1250 (1994).
- [81] S. A. Kivelson and J. R. Schrieffer, Phys. Rev. B **25**, 6447 (1982); J. R. Schrieffer, Proc. Int. School. Phys. Enrico Fermi LXXXIX, F. Bassani ed. (Elsevier, New York, 1985).
- [82] S. Chakravarty and P. W. Anderson, Phys. Rev. Lett. **72**, 3859 (1991).
- [83] A. Luther and V. J. Emery, Phys. Rev. Lett. **33**, 589 (1974).
- [84] A. Luther and I. Peschel, Phys. Rev. B **12**, 3908 (1975).
- [85] H. J. Schulz, in *Correlated Electron Systems*, ed. V. J. Emery (World Scientific, Singapore, 1993).
- [86] F. D. M. Haldane, Phys. Rev. Lett. **47**, 1840 (1981).
- [87] A.V. Chubukov, S. Sachdev, J. Ye, Phys. Rev. B **49**, 11919 (1994); A.V. Chubukov, S. Sachdev, A. Sokol, Phys. Rev. B **49**, 9052 (1994).
- [88] A. Sokol, D. Pines, Phys. Rev. Lett. **71**, 2813 (1993).

- [89] A. H. Castro Neto and Daniel Hone, Phys. Rev. Lett. **76**, 2165 (1996).
- [90] C. N. A. van Duin and J. Zaanen, Phys. Rev. Lett. **80**, 1513 (1998).
- [91] E. Dagotto and T. M. Rice, Science **271**, 618 (1996).
- [92] Z. Wang Phys. Rev. Lett. **78**, 126 (1997).
- [93] I. Affleck and B.I. Halperin, J. Phys. A **29**, 2627 (1996).
- [94] V. Kataev *et al*, Phys. Rev. B **55**, R3394 (1997).
- [95] G. Aeppli *et al*, Science **278**, 1432 (1997).
- [96] H.G. Evertz, G. Lana and M. Marcu, Phys. Rev. Lett. **70**, 875 (1993); H.G. Evertz and M. Marcu in "Quantum Monte Carlo Methods in Condensed Matter Physics" (ed. M. Suzuki, World Scientific, 1994).
- [97] U.J. Wiese and H.-P. Ying, Z. Phys. B **93**, 147 (1994); Phys. Lett. A **168**, 143 (1992).
- [98] B.B. Beard, R.J. Birgenau, M. Greven, U.J. Wiese cond-mat/9709110; S. Caracciolo *et al*, Phys. Rev. Lett. **75**, 1891 (1995); J.K. Kim Phys. Rev. Lett. **70**, 1735 (1993)
- [99] B.B. Beard and U.J. Wiese, Phys. Rev. Lett. **77**, 5130 (1996).
- [100] M. Greven, U.J. Wiese and R.J. Birgeneau, Phys. Rev. Lett. **77**, 1865 (1996).
- [101] P. Hasenfratz and F. Niedermayer, Phys. Lett. B **268**, 231 (1991); Z. Phys. B **92**, 91 (1993).
- [102] B. Frischmuth, B. Ammon and M. Troyer, Phys. Rev. B **54**, R1774 (1996); B. Frischmuth, S. Haas, G. Sierra, T. M. Rice, Phys. Rev. B **55** R3340 (1997)
- [103] M. Azzouz, B. Dumoulin, A. Benyoussef, Phys. Rev. B **55**, R11957 (1997).
- [104] S. Gopalan, T.M. Rice, and M. Sigrist, Phys. Rev. B **49**, 8901 (1994).
- [105] M. Imada, Y. Iino, J. Phys. Soc. Jpn **66**, 568 (1997).
- [106] A. W. Sandvik and D. J. Scalapino, Phys. Rev. B **51**, R9403 (1995).
- [107] M.S. Makivić, and H.-Q. Ding, Phys. Rev. B **43**, 3562 (1991).
- [108] D. Senechal, Phys. Rev. B **52**, 15319 (1995).
- [109] A.W. Sandvik, E. Dagotto, D.J. Scalapino, Phys. Rev. B **53**, R2934 (1996).
- [110] J. Zaanen, Phys. Rev. Lett. **84**, 753 (2000).

- [111] S. A. Kivelson, E. Fradkin and V. J. Emery, *Nature* **393**, 550 (1998).
- [112] N. Hasselmann *et al.*, *Phys. Rev. Lett.* **82**, 2135 (1999); Y. A. Dimashko *et al.*, *Phys. Rev. B* **60**, 88 (1999).
- [113] The classical, finite temperature version of this problem has been analyzed thoroughly in the past (see [114] and ref.'s therein) and considered in the context of stripes in [32].
- [114] S. N. Coppersmith *et al.*, *Phys. Rev. B* **25**, 349 (1982).
- [115] W. Helfrich, *Z. Naturforsch. A* **33**, 305 (1978); W. Helfrich and R. M. Servuss, *Nuovo Cimento D* **3**, 137 (1984).
- [116] W. Janke and H. Kleinert, *Phys. Rev. Lett.* **58**, 144 (1987); W. Janke, H. Kleinert and M. Meinhardt, *Phys. Lett. B* **217**, 525 (1989); see also H. Kleinert, *Phys. Lett. A* **257**, 269 (1999).
- [117] V. L. Pokrovsky and A. L. Talapov, *Phys. Rev. Lett.* **42**, 65 (1979).
- [118] J. Zaanen, Z. Nussinov and H. V. Kruis (unpublished).
- [119] K. Binder and D. W. Heermann, *Monte Carlo Simulation in Statistical Physics*, Springer Series in Solid- State Sciences 80.
- [120] L. P. Pryadko, S. A. Kivelson, D. W. Hone, *Phys. Rev. Lett.* **80**, 5651-5654 (1998).
- [121] M. Ogata and H. Shiba, *Phys. Rev. B* **41**, 2326 (1990).
- [122] T. Barnes, *Int. J. Mod. Phys. C2* (1991) 659. U. -J. Wiese and H. P. Ying *Z. Phys. B* **93**, 147 (1994).

Samenvatting

De titel van dit proefschrift is "Over stripe correlaties in Cuprate supergeleiders". De *cuprates* zijn quasi 2-dimensionale materialen die koperoxide bevatten. Ze zijn gelaagd en de koppeling tussen de vrijheidsgraden in de verschillende lagen is zeer zwak in vergelijking met die in de individuele lagen. De fysisch belangrijkste lagen kunnen gezien worden als vierkante roosters waarbij de elektronen de roosterpunten bezetten. Als de cuprates ongedoteerd zijn, zijn het spin- $\frac{1}{2}$ antiferromagnetische isolatoren. Door ze te doteren met gaten, dat wil zeggen door elektronen te verwijderen uit de lagen, gaan de materialen een gebied binnen dat bekend staat als een spinglas, waar de antiferromagnetische ordening zeer snel onderdrukt wordt. Door verder te doteren en de temperatuur te verlagen tot beneden een kritische temperatuur worden ze supergeleiders. Bij deze doteringconcentratie wordt ook een nieuwe fase waargenomen: de *stripe* fase. De gaten verzamelen zich in domeinwanden, snaar-achtige structuren vormend, die gat-vrije domeinen scheiden. In deze spindomeinen ordenen de spins zich antiferromagnetisch met tegengestelde oriëntatie over de gat-lijnen (de stripes).

Van deze stripe-fase wordt verondersteld dat ze zowel in competitie is als coëxisteert met de supergeleidende fase, in ieder geval tot en met de optimale dotering. Zowel statische als dynamische stripe correlaties zijn experimenteel waargenomen. De studie van deze stripe fase is het onderwerp van dit proefschrift. Een overzicht van bestaand experimenteel en theoretisch werk aan zowel het bestaan van deze stripe-fase als het mechanisme dat zorgt voor de stabiliteit ervan wordt in het introductie hoofdstuk gegeven.

Omdat stripes lijnachtige objecten zijn, kan men de ladings-sector van de elektronische toestand van de cuprates opvatten als een *kwantum stringvloeistof*. Om het probleem van vele wisselwerkende stripes aan te pakken, is het eerst noodzakelijk om uit te vinden wat de fysica van een enkele stripe in isolatie is. In hoofdstuk 3 wordt een kwantum roosterstring-model voor een enkele stripe geïntroduceerd. De spin achtergrond wordt hier verwaarloosd.

Gebruik makend van exacte diagonalisatie- en Quantum Monte-Carlo technieken wordt aangetoond dat bij het absolute nulpunt een symmetrie-breking plaatsheeft. Hoewel de string zich kwantum-mechanisch kan delocaliseren, blijkt dat de string in alle gevallen spontaan een *voorkeursrichting* in de ruimte ontwikkelt.

De belangrijkste reden hiervoor is dat knikken in de string kwantumtransport bemoeilijken, of vice versa, de kwantumbeweging van kinken rechtten de string (*het tuinslang effect*). Het gerichte-string probleem dat overblijft lijkt te zijn gerelateerd aan een goed begrepen oppervlakte statistisch fysisch model (het RSOS model) en tegelijkertijd aan een $S = 1$ XXZ kwantum spinketen met anisotropie op elke roosterplaats.

Een aantal door deze klasse van modellen beschreven fases, welke tot nu toe niet geïdentificeerd waren, werden gevonden. De fases vallen in drie hoofdcategorieën: klasieke, Gaussische en 'ongeordend vlakke' fases. De fases worden verder onderscheiden

door de oriëntatie van de string op het rooster. Behalve de vlakke string in de horizontale en diagonale richtingen, laat dit proefschrift zien dat ook de ongeordend-vlakke fase een zeer rijk gedrag vertoont. Naast de bekende fase met horizontale richting, welke geassocieerd is met de onsamendrukbare fase van het spin model, wordt een nieuwe categorie geïdentificeerd: de ongeordend vlakke fase, die afhankelijk van parameters, willekeurige richtingen in ruimte inneemt (de "slanted" fases).

Het kwantum roosterstring model is een model voor niet-metallische stripes. In hoofdstuk 4 wordt het probleem van een metallische string beschouwd. Dit is een één-dimensionaal metaal levend op een gedelocaliseerd traject in twee dimensies. Startend met specifieke aannames geïnspireerd door de cuprate stripes wordt er aangetoond dat de dynamica op lange golflengte van zo'n probleem een eenvoudige generalisatie is van een Luttinger vloeistof, waarbij de gebruikelijke theorie van spin-ladings scheiding moet worden uitgebreid met een derde sector van transversale string modes. Door een specifiek model te beschouwen wordt aangetoond dat het feit of een string metallisch is een zwakke invloed heeft op de string fluctuaties, hetgeen impliceert dat het geen belangrijke factor is voor het kwantumsmelten van de stripe-fase. Dit resultaat biedt een verklaring voor de ongevoeligheid van de statische stripe fase tegen dotering.

In hoofdstuk 5 wordt een model van statische stripes in een spin achtergrond beschouwd. Deze zijn of gecentreerd op de rooster-punten of gecentreerd op de rooster-bindingen. De spin-dynamica wordt bestudeerd en er wordt aangetoond dat voor de bindings-gecentreerde stripes veel van de spin fluctuaties zullen ontstaan in de spin sector. Een interessante kwantum fase-overgang vindt plaats bij een eindige ladings-geïnduceerde anisotropie. Voor rooster-punt gecentreerde stripes spelen de kwantum spinfluctuaties een centrale rol in het ontstaan van kwantum spinfluctuaties.

Een interessante vraag is wat er gebeurt als de ladings-stripes zelf kwantum-mechanisch gedelocaliseerd worden. Het probleem van wisselwerkende kwantumfluctuerende stripes, levend in een kwantum mechanische antiferromagnetische spin achtergrond wordt bekeken in het laatste hoofdstuk. Het stripe systeem komt overeen met een kwantum stringvloeistof en omdat de fluctuerende stripes anti-fase grenzen zijn voor het spin systeem, zullen ze ook het spin systeem laten fluctueren. Eerst wordt een overzicht van het probleem van een puur kwantum string gas zonder dislocaties gegeven. Gebruik makend van de connectie van dit probleem met het harde kern Bose gas probleem, wordt aangetoond dat het string systeem vast zal worden ten gevolge van de kwantum fluctuaties. Deze fluctuaties induceren op lange golflengte een elastische modulus, welke klein maar eindig zal zijn, en vanwege de twee-dimensionaliteit van het probleem zal een werkelijk lange afstands ordening ontstaan. Vervolgens wordt aangetoond dat dit verband tussen de stripe-fysica en één-dimensionale fysica veel dieper is. Het wordt aangetoond dat een verborgen spin ordening van het zelfde soort bestaat in zowel de grote U -Hubbard keten en een systeem van fluctuerende strings in een spin-volle achtergrond. De fysische reden van deze ordening is, dat als men alle gaten samen met hun roosterpunten uit de Hubbard keten haalt, of alle strings uit het stripe systeem, het "topologische" spin systeem dat achterblijft precies een 1-dimensionaal respectievelijk 2-dimensionaal Heisenberg systeem is. Gebruik makend van

deze verborgen ordening wordt aangetoond dat de fluctuaties van de stripes altijd ordening induceren in het topologische spin systeem, hoewel deze ordening verborgen is. Het fase-diagram van het probleem van fluctuerende strings in een spin-volle achtergrond wordt vervolgens volledig bepaald. Drie scenarios blijken te bestaan: Geordende stripes met een geordend topologisch spin systeem, geordende stripes met een ongeordend topologische spin systeem of ongeordende stripes met een geordend topologisch spin systeem.

List of publications

- Dynamical Stripe Correlations in Cuprate Superconductors,
Jan Zaanen, O. Y. Osman and Wim van Saarloos,
J. Low Temp. Phys. **105**, 596 (1996).
- Charged domain walls as quantum strings on a lattice,
Henk Eskes, O. Y. Osman, R. Grimberg, Wim van Saarloos and Jan Zaanen,
Phys. Rev. B **58**, 6963 (1998).
- Metallic stripes: separation of spin, charge and string fluctuation,
Jan Zaanen, O. Y. Osman and Wim van Saarloos,
Phys. Rev. B **58**, R11 868 (1998).
- Quantum magnetism in the stripe phase: bond- versus site order,
J. Tworzydło, O. Y. Osman, C.N.A. van Duin and J. Zaanen,
Phys. Rev. B **59**, 115 (1999).
- Spontaneous orientation of a quantum lattice string,
O. Y. Osman, Jan Zaanen and Wim van Saarloos,
Proc. of 2nd Intern. Conf. on Stripes and High T_c Superconductivity, Rome 1998,
J. of Superconductivity.
- Dynamical Stripes in an antiferromagnetic spin background,
O. Y. Osman and Jan Zaanen,
(in preparation for publication).

Curriculum vitae

Ik ben geboren te Khartoum (Sudan) op 24 maart 1966. In 1985 behaalde ik het eindexamen van de "Sudanese Secondary school" te Khartoum Noord. In november 1985 begon ik mijn studie natuurkunde aan de universiteit van Khartoum en behaalde aldaar in 1991 de Bachelor of Science graad met (First class honour). Mijn afstudeerproject ging over conceptueel ontwikkelingen in de theorie van licht. Van januari 1991 tot september 1992 werkte ik als "teaching assistant" bij de natuurkunde van de Universiteit van Khartoum. In October 1992 ging ik naar het International Centre for Theoretical Physics in Trieste, Italië, voor het volgen van een cursus (diploma course) in hoge-energie fysica en kosmologie. Het diploma (with honour) werd behaald in september 1993. Daarna was ik een jaar bij de Elementary Particle Physics groep van de International School for Advanced Studies (SISSA) in Trieste, Italië.

In december 1994 kwam ik naar Nederland. In de werkgroep gecondenseerde materie van het Instituut Lorentz voor theoretische fysica van de Universiteit Leiden verrichte ik, in samenwerking met Dr. Henk Eskes en met begeleiding door Dr. Jan Zaanen en Prof. dr. Wim van Saarloos onderzoek over het "Quantum Lattice String Model" voor het doctoraal examen natuurkunde dat ik in februari 1996 met goed gevolg aflegde. In maart 1996 trad ik in dienst van de Universiteit Leiden voor het doen van onderzoek over hetzelfde thema en met begeleiding door Dr. Jan Zaanen en prof. dr. Wim van Saarloos. Tijdens mijn studie volgde ik verschillende workshops en zomerscholen in Twente, Ameland, Trieste, Cambridge en in Leiden. Het onderzoek dat ik in deze periode verrichte is in dit proefschrift beschreven.

Sinds mei 2000 werk ik als software-ontwikkelaar bij het informatietechnologiebedrijf Collis in Leiden.

Acknowledgement

I am grateful to Dr. Marten Durieux for his continuous support and encouragement during my PhD work.

Stellingen

behorende bij het proefschrift

On Stripe Correlations in Cuprate Superconductors

1. Apart from some extreme classical limits, the general quantum lattice string model at zero temperature is a directed string, *the garden hose effect*.

Chapter 3, this thesis

2. The effective anisotropic quantum non-linear sigma models for the coupled 2-leg and 3-leg spin ladders systems are characterized by the following anisotropic spin-wave velocities:

$$\begin{aligned} c_x^2 &= \alpha c_0^2 \begin{cases} \frac{(3+\alpha)}{2(1+\alpha)} & \text{for } n_l = 2 \\ \frac{9(7+3\alpha)}{2(1+2\alpha)(13+2\alpha)} & \text{for } n_l = 3 \end{cases} \\ c_y^2 &= c_0^2 \begin{cases} \frac{(3+\alpha)}{4} & \text{for } n_l = 2 \\ \frac{3(7+3\alpha)}{2(13+2\alpha)} & \text{for } n_l = 3 \end{cases} \end{aligned}$$

respectively, where α is the spin anisotropy and c_0 is the spin-wave velocity in the isotropic limit.

Chapter 5, this thesis

3. A system of directed quantum strings is equivalent to a decompactified, in an extra dimension, algebraic Wigner crystal which is formed by the hard core bose gas system in 1+1 dimension. The strings system is now a true solid due to the extra dimension.

Chapter 6, this thesis

4. For a system of anti-phase, directed quantum strings living in an antiferromagnetic spin background, it is impossible to have both the strings and the topological spin system quantum disordered. The topological spin system is the spin system left after removing the strings together with their sites.

Chapter 6, this thesis

5. In the large U , 1+1-dimensional Hubbard model, the holes form an algebraically long range ordered Wigner crystal. By taking out the holes together with their corresponding sites, the remaining spin system is analogous to a Heisenberg chain.

M. Ogata and H. Shiba, Phys. Rev. B 41, 2326 (1990)

5. The renormalization group approach to dimensional crossover suggests that order occurs for infinitesimal higher dimensional coupling only if the renormalized coupling in the lower dimensional theory is smaller than the critical coupling in the higher dimensional theory.

Ian Affleck and Bertrand I. Halperin, J. Phys. A **29**, 2627 (1996)

7. A Landau mean-field analysis falls short as a description for the thermodynamic behavior of the stripe phase because of the importance of fluctuations.

C. N. A. van Duin and J. Zaanen, Phys. Rev. Lett. **80**, 1513 (1998)

8. The current civil war in Sudan, which is the longest in Africa, will come to a lasting end if the leaders of the different warring parties take the economic interest of the Sudanese people as their top priority.
9. Education and technology should be the main focus of the policy makers in the third world, in order to attain a sustained development.
10. Considering the current trends in the rate of change of the countries' population, the world population will reach a maximum of around 10 billion in the third decade of this century then drop to a minimum of around 4 billion at the end of the fifth decade before start rising again.

Osman Yousif Osman

4 October 2000